



HAL
open science

Design and applications of protein delivery systems in nanomedicine and tissue engineering

Joëlle Bizeau, Damien Mertz

► **To cite this version:**

Joëlle Bizeau, Damien Mertz. Design and applications of protein delivery systems in nanomedicine and tissue engineering. *Advances in Colloid and Interface Science*, 2021, 287, pp.102334. 10.1016/j.cis.2020.102334 . hal-03438338

HAL Id: hal-03438338

<https://hal.science/hal-03438338>

Submitted on 21 Nov 2021

HAL is a multi-disciplinary open access archive for the deposit and dissemination of scientific research documents, whether they are published or not. The documents may come from teaching and research institutions in France or abroad, or from public or private research centers.

L'archive ouverte pluridisciplinaire **HAL**, est destinée au dépôt et à la diffusion de documents scientifiques de niveau recherche, publiés ou non, émanant des établissements d'enseignement et de recherche français ou étrangers, des laboratoires publics ou privés.

Design and Applications of Protein Delivery Systems in Nanomedicine and Tissue Engineering

Joëlle Bizeau¹ and Damien Mertz¹

¹Institut de Physique et Chimie des Matériaux de Strasbourg (IPCMS), UMR-7504 CNRS-
Université de Strasbourg, 23 rue du Loëss, BP 34 67034, Strasbourg Cedex 2, France
Corresponding e-mail : damien.mertz@ipcms.unistra.fr

Abstract

Proteins are biological macromolecules involved in a wide range of biological functions, which makes them very appealing as therapeutics agents. Indeed, compared to small molecule drugs, their endogenous nature ensures their biocompatibility and biodegradability, they can be used in a large range of applications and present a higher specificity and activity. However, they suffer from unfolding, enzymatic degradation, short half-life and poor membrane permeability. To overcome such drawbacks, the development of protein delivery systems to protect, carry and deliver them in a controlled way have emerged importantly these last years. In this review, the formulation of a wide panel of protein delivery systems either in the form of polymer or inorganic nanoengineered colloids and scaffolds are presented and the protein loading and release mechanisms are addressed. A section is also dedicated to the detection of proteins and the characterization methods of their release. Then, the main protein delivery systems developed these last three years for anticancer, tissue engineering or diabetes applications are presented, as well as the major *in vivo* models used to test them. The last part of this review aims at presenting the perspectives of the field such as the use of protein-rich material or the sequestration of proteins. This part will also deal with less common applications and gene therapy as an indirect method to deliver protein.

Keywords

Protein therapeutics, Drug delivery systems, Nanoengineered carriers, Scaffolds, Growth factors, RNase, Insulin, Tissue Engineering, Cancer, Diabetes

Highlights

- A wide range of delivery systems was recently developed to control protein release
- Delivery systems consist typically of polymer or inorganic colloids and scaffolds
- Various experimental and theoretical methods allow to characterize the protein release

- 39 • Main applications of these systems are cancer, tissue engineering and
40 diabetes

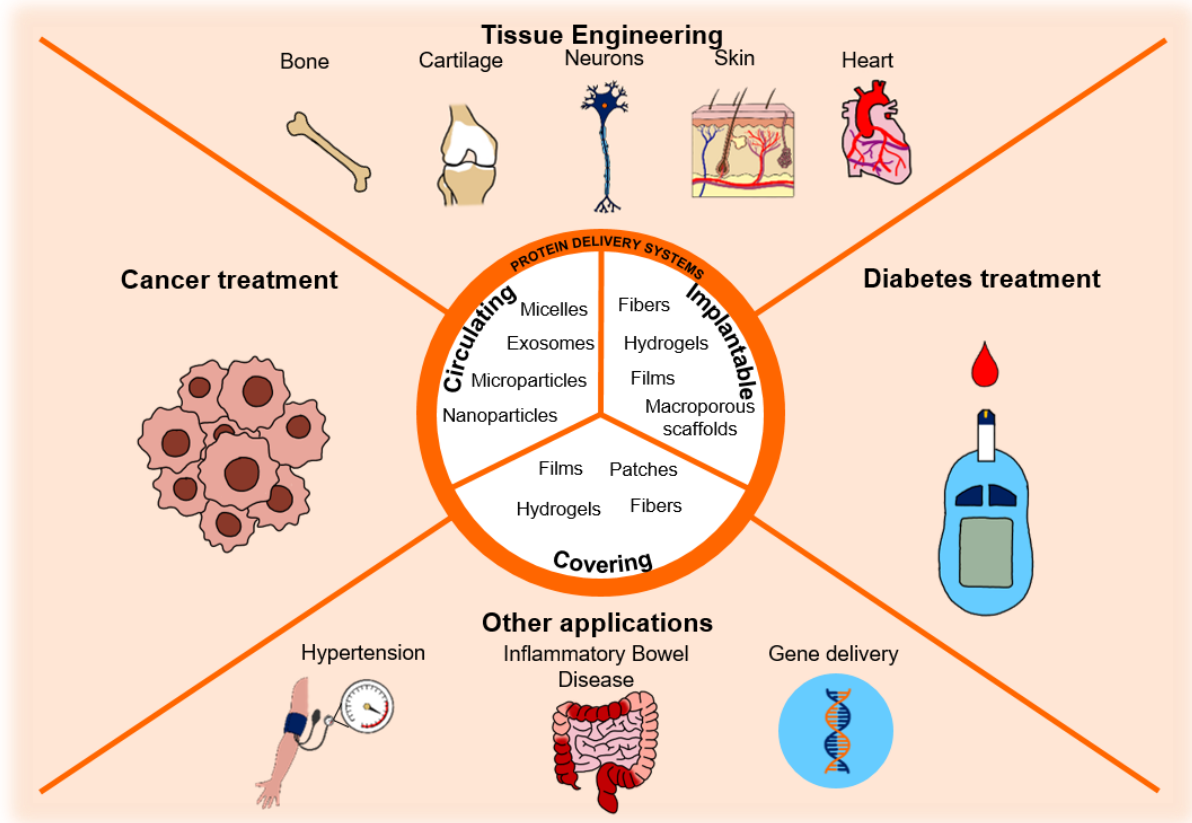
41 I Introduction

42 Proteins are biomacromolecules existing in a very broad range of biological
43 processes and displaying remarkable functions such as biocatalysis, high affinity
44 molecular recognition, activation/inhibition of cell pathways [1], which makes them
45 very interesting therapeutic agents. Indeed, they present a unique therapeutic
46 richness compared to small molecule drugs, with higher spectra of specificity and
47 activity [2]. Thus, they have been studied for decades in various applications: for
48 instance, ribonuclease A (RNase A) has been studied for the treatment of cancer,
49 growth factors are widely used for tissue engineering and insulin is still the molecule
50 of choice to treat diabetes. Another advantage of using proteins as therapeutic
51 agents rather than other molecules is their endogenous nature which makes them
52 biocompatible and biodegradable. It is also important to notice that their degradation
53 products are already known and eliminated by the body, which also has the
54 advantage to limit importantly any potential toxicity of the treatment.

55 However, proteins are fragile conformational macromolecular structures,
56 susceptible to unfolding and to enzymatic degradation and they present a short half-
57 life. Combined with poor membrane permeability limiting their cellular internalization,
58 it necessitates frequent administrations [1,2]. To overcome these challenges, protein
59 delivery systems have been developed these last years to protect, carry and release
60 therapeutic proteins in a sufficient dose and only at specific sites without altering their
61 bioactivity. These systems can be formulated in a wide range of dimensions, from
62 nanocolloid to macroscopic scaffold sizes, with tailored shapes and physicochemical
63 features and they can be designed to control the protein release thanks to local or
64 external stimuli. Such control is essential to bring a longer efficiency of the treatment
65 but also to avoid a burst release leading to the loss of the majority of the cargo and to
66 a locally high concentration of protein which can potentially induce detrimental effects
67 [3,4]. If this control usually aims at providing a continuous release, it is interesting to
68 notice that some research works are also performed to design delivery systems
69 responding to external fields (light, magnetic field) endowed with a pulsatile release,
70 aiming at triggering in time and location adjusted amounts of drug released in the
71 body [5,6].

72 In this review article, we detail the recent design and applications of protein
73 delivery systems in nanomedicine and tissue engineering, which has been very few
74 reviewed these last years, by providing an up-date of various impacting works (non-
75 exhaustive list) achieved these last years in this area. In the first section of this
76 review, the fabrication techniques of the different protein delivery systems are
77 presented: microparticles (MPs), nanoparticles (NPs), hydrogels (HGs), fibers, films,
78 patches and macroporous scaffolds (MacPSs). This section also describes the
79 various loading and release possibilities by giving insights into the release
80 mechanism from drug delivery systems including natural diffusion, hydrolytic erosion
81 or local biochemical stimuli (pH, redox, enzymes). In a second section, the
82 characterization techniques and mathematical models commonly used to detect and
83 quantify proteins and to study the release mechanism are presented. Then, the three

84 following sections present the protein delivery systems split into three categories:
 85 circulating, implantable and covering systems that are mainly used for anticancer,
 86 tissue engineering and diabetes applications. The *in vivo* models used to evaluate
 87 the efficiency of these systems, as well as the main experimental results, are
 88 presented in a dedicated section while the last one will present emerging designs of
 89 proteins delivery systems. The **Figure 1** gives a global view into the kind of delivery
 90 systems presented in this review as well as their most common applications.



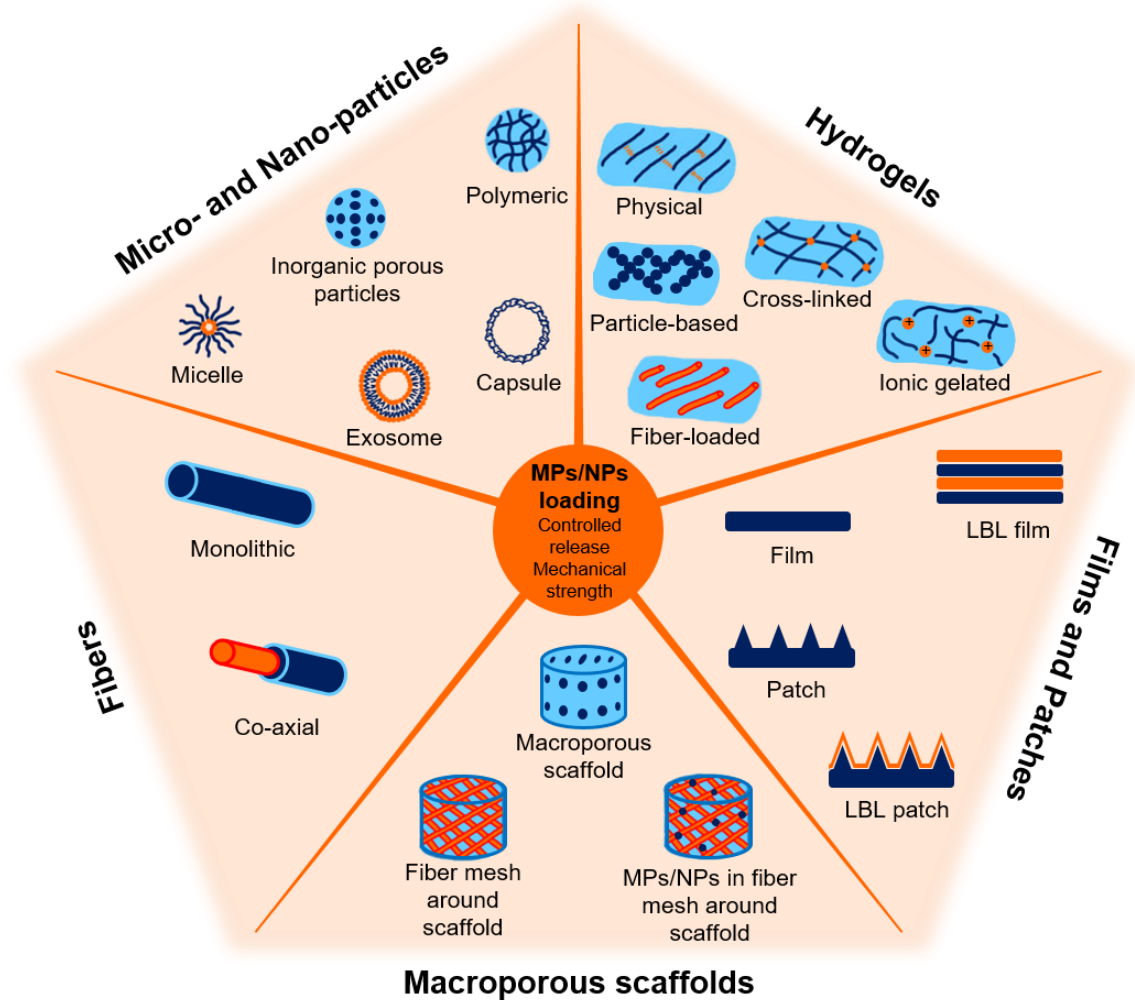
91
 92
 93

Figure 1: Overview of the different protein delivery devices and their applications

II Formulation and physico-chemistry

II.1 Fabrication techniques

94
95
96 Protein delivery systems are designed with range of dimensions and shapes –MPs
97 orNPs, HGs, films or patches, fibers, MacPSs – as represented in **Figure 2**.
98 Whatever the chosen formulation, it is also possible to load a macroscopic scaffold
99 with MPs or NPs to improve its mechanical strength or to trigger drug release by local
100 or external stimuli when using stimuli responsive MPs/NPs. In this section, the
101 common fabrication techniques are reviewed for the different delivery devices.



102

103

Figure 2: Overview of the different protein delivery devices

104 II.1.1 Micro- and nano- particles

105 MPs and NPs are promising tools to deliver proteins as they have the adequate
106 size to be internalized by cells and can then directly deliver proteins to the
107 intracellular environment. Besides, these systems are highly tunable by chemical or
108 physical processes. They can be made with organic or inorganic materials, in the
109 form of plain particles or capsules, or even in more complex assemblies such as
110 micelles or exosomes.

111

112

113 II.1.1.1 Emulsification

114 The emulsion solvent evaporation is a simple and rapid fabrication method
115 allowing the synthesis of MPs and NPs. The basic principle of an emulsion is to form
116 droplets by mixing a first phase in a second immiscible one and then to eliminate the
117 solvent. An emulsifier, such as polysorbate, can be added to the preparation to
118 stabilize the emulsion. Even if this technique is very common to obtain poly(lactic-co-
119 glycolic acid) (PLGA) [7] or chitosan (CHI) [8] particles, it can also be extended to
120 many biological macromolecules as building blocks. For example, Rinker *et al.*
121 reported the synthesis of heparin MPs by mixing an aqueous solution of heparin in
122 corn oil, which is the classic water-in-oil emulsion technique [9]. More interestingly,
123 they used it again to entrap these heparin MPs in bigger MPs mainly composed of
124 poly(ethylene glycol) (PEG). Conversely, oil-in-water emulsion is also used to obtain
125 particles. Recently, this technique has been reported to be useful to obtain Eudragit
126 S100 polymer hollow MPs with pH-sensitive pores [10]. One big advantage of this
127 technique is the easy loading of drugs by simply blending it in the adequate phase.
128 For example, Galliani *et al.* reported the synthesis of PLGA/poly(ethylene imine)
129 (PEI) NPs loaded with cross-linked aggregates (CLAs) made of bovine serum
130 albumin (BSA) or cross-linked enzymes aggregates (CLEAs) made of superoxide
131 dismutase (SOD). These CLAs or CLEAs were mixed with PLGA and PEI to obtain
132 the oil phase that was further added dropwise to a poly(vinyl alcohol) (PVA) aqueous
133 solution to obtain the NPs [11].

134 Single emulsion can be used as it is or in combination with other processes such
135 as cross-linking [8,12] or external gelation [13]. Cross-linking CHI MPs is widely used
136 with the nature and amount of cross-linker being important parameters to control.
137 Recently, a study reported the chain length influence of dicarboxylic acid linkers on
138 the properties of CHI MPs [8]. The results showed that the increase of the carbon
139 chain length induces an increase in size, swelling ratio, erosion, encapsulation
140 efficiency and loading capacity. For the release, the increase of the chain length
141 increased the initial burst release and cumulative release of BSA, which is in
142 agreement with the higher swelling ratio and erosion associated with the
143 corresponding carbon chain length. Cross-linking has also been used to obtain
144 polypeptide-based gel particles to combine the features of NPs and HGs [12]. A wide
145 range of gel particles has been synthesized using water-in-oil emulsion further cross-
146 linked with genipin, a much less toxic cross-linker as compared to the conventional
147 glutaraldehyde. Upon their characteristics, the study notably showed the efficient
148 encapsulation of BSA, myoglobin and lectoferrin and most importantly, it was
149 reported that their bioactivity was retained. The use of a disulfide cross-linking agent
150 showed the possibility to release BSA in the presence of glutathione, a naturally
151 reducing agent of the cytoplasm. Single emulsion can also be used in combination
152 with polymerization. As an example, Zhang *et al.* used the reverse emulsion
153 polymerization technique to obtain hydroxypropyl- β -cyclodextrin microspheres [14].
154 More precisely, they emulsified the hydroxypropyl- β -cyclodextrin which then
155 polymerized to form the microspheres.

156 Double emulsion technique is also operated to obtain MPs and NPs with the
157 water-in-oil-in-water being the most used procedure and PLGA being the most
158 commonly used polymer. A recent study aimed at tailoring PLGA MPs to obtain a
159 controlled delayed release of the cytokine CCL25, a chemoattractant of
160 mesenchymal stem cells (MSCs), by playing on the polymer molecular weight,
161 chemical functionalization, emulsion type and amount of BSA excipient [15]. Another
162 study reported the combination of lipids and PLGA to encapsulate and release

163 lysozyme, showing a better encapsulation efficiency and reduction of burst release of
164 this enzyme with a higher content of PLGA [16]. This technique has also been used
165 to integrate superparamagnetic iron oxide NPs (SPIONs) in the PLGA shell in core-
166 shell particles encapsulating BSA [17]. The goal of this study was to exploit the
167 superparamagnetic properties of SPIONs to obtain a better cellular uptake and
168 immune response. This double emulsion process has been modified by Chen *et al.*
169 as solid-in-oil-in-water process to encapsulate BSA-loaded lecithin NPs in PLGA MPs
170 [7]. The term “solid” used here refers to the anhydrous reverse micelle made of BSA
171 surrounded by lecithin.

172 As said before, the advantages of the emulsion technique are its easy handling
173 and the possibility to load the therapeutics by blending it within the phase of interest.
174 Unfortunately, this can lead to denaturation because the therapeutics can be in
175 contact with an unfavourable phase or can be damaged by the mechanical stress
176 induced by the emulsion creation process (vortex, sonication) [10].

177

178 *II.1.1.2 Polymer self-assembly*

179 Another well-known technique to obtain MPs and NPs is the self-assembly based
180 on intra- or intermolecular interactions. In such formulations, the protein can be
181 trapped in the self-assembled system due to interactions with the polymer material or
182 the protein is one of the material that self-assembles to form the delivery system. Lv
183 *et al.* used this technique in a recent study where they reported the synthesis of a
184 library of dendrimers functionalized with fluoroalkyls and fluoroaromatics. The
185 objective was to obtain an efficient fluorodendrimer able to self-assemble via
186 fluorophilic effect, to entrap proteins through ionic interaction and to deliver it to the
187 cytosol [18]. More recently, a study reported the use of the self-assembling technique
188 to obtain metal-organic frameworks (MOFs) by mixing zinc ion with imidazole-2-
189 carboxaldehyde and proteins. The study notably showed the effective intracellular
190 delivery of two enzymes involved in genetic material reactions: RNase A and
191 genome-editing Cas9 nuclease [19].

192 The cross-linking can also be part of the self-assembling process as in the ionic
193 gelation process. This technique is widely used to obtain CHI particles. Briefly, the
194 cationic form of CHI is mixed with anionic cross-linker, the most common one being
195 tripolyphosphate (TPP), and the ionic complexation leads to CHI gelation and
196 precipitation in particle form. Thus, the cross-linking of CHI by cationic/anionic
197 interaction is the self-assembling phenomenon leading to the formation of CHI
198 particles. CHI can be used as it is [20] or after functionalization, as reported by Song
199 *et al.* who synthesized carboxymethyl- β -cyclodextrin grafted CHI NPs (CMCD-g-CHI)
200 [21]. Another example of ionic gelation is the synthesis of gellan gum MPs with
201 aluminium ions [22].

202 Finally, self-assembly is the driving mechanism to obtain micelles which consists
203 in the spatial arrangement of amphiphilic species into a core-shell system where the
204 hydrophobic parts segregate within the core and the hydrophilic parts locate in the
205 shell. Meng *et al.* reported the synthesis of Pluronic F127 (PF127)/D- α -tocopheryl
206 polyethylene glycol succinate (TPGS) micelle by thin-film hydration to specifically
207 deliver proteins to the brain [23]. In another study, Gao *et al.* reported the
208 stabilization of recombinant human growth hormone (rhGH) by sugar glass NPs
209 obtained from inverse micelles [24].

210

211 *II.1.1.3 Extrusion and spraying*

212 Extrusion is a general technique in which the precursor solution is forced to go
213 through a nozzle whose cross-section dictates the dimensions of the final material.
214 This process has been used to obtain CHI/polyphosphoric acid (PPA) beads to
215 encapsulate several proteins including BSA, insulin, casein hydrolysate and whey
216 protein isolate (WPI) [25].

217 Spray drying is the extrusion way allowing the fabrication of drug powders. It
218 consists of mixing the interesting therapeutics with an excipient and to spray it
219 through an atomizer into a chamber where it will be dried by hot gas and precipitated
220 into nanopowder. Several factors influence the final product such as the composition
221 of initial solution and its temperature at several points of the process [26]. Wu *et al.*
222 specifically studied the effect of excipients on the encapsulation and release
223 properties of solid/lipid MPs obtained by spray drying. Insulin-phospholipid were then
224 formulated with several excipients: glycerol monostearate, distearate, tribehenate
225 and tristearate. The results showed that the spray drying process does not impact
226 insulin conformation and that triglycerides with long chain reduces the burst release
227 in a significant way compared to PLGA [26]. A possibility to play on the solvent is the
228 use of supercritical fluid-assisted spray drying (SASD), and notably supercritical CO₂
229 (scCO₂)-assisted spray drying, as it is supposed to reduce organic solvent quantities
230 and temperatures. This technique has been used to synthesize PLGA particles
231 containing BSA and L-leucine, which role was to enhance the dispersion of the
232 powder, for vaccine delivery to the lung [27].

233 The electrospraying process, also known as electrodynamic spraying, is another
234 spraying method where a high electrical potential is applied to the atomizer, leading
235 to the formation of charged droplets that dry before reaching the collector. This
236 technique does not require chemical modifications and allows high encapsulation
237 efficiency, notably of sensitive molecules such as proteins as it does not expose them
238 to unfavourable solvents or shear stress as required in emulsions. As an example,
239 Chen *et al.* operated coaxial electrospraying to obtain murabutide and ovalbumin
240 (OVA)-loaded acetalated dextran MPs with several degradation profiles [28].

241

242 *II.1.1.4 Microfluidics*

243 Microfluidics is a pioneering technique to fabricate micro- and nano-materials
244 presenting several advantages. The mixing is notably changed compared to
245 conventional reactors as it is faster and more intensive, which leads to increased
246 reaction kinetics and allows fast screening of experimental conditions. Besides, the
247 surface-to-volume ratio can be tuned by changing the microchannel size and shape
248 and the operations can be automatized, which reduces variations between
249 experiments [29]. It can then be used to obtain inorganic particles as well as
250 polymeric particles. For example, Hao *et al.* used this technique to synthesize hollow
251 spherical silica with sponge-like pores with a system containing two inlets [29] while
252 Foster *et al.* reported the use of microfluidics-based polymerization to obtain PEG
253 microgels [30]. More recently, Yu *et al.* designed a four inlets microfluidics systems to
254 synthesize PEI/CHI-coated alginate MPs [31]. The first two inlets were used to form
255 water/protein core-alginate shell MPs, with CaCO₃ present in the alginate phase. The
256 third inlet contained only a mineral oil to drag the particles while the fourth inlet
257 contained the same mineral oil mixed with acetic acid. The acetic acid released the
258 calcium ions from CaCO₃, leading to the internal gelation of the alginate shell. The
259 particles were then collected in a calcium chloride (CaCl₂) solution to have an
260 external gelation of the alginate. The advantage of having the four inlets was then to

261 have a high control of the particle size and to introduce an internal gelation of
262 alginate prior to the external gelation, the combination of both improving the stability
263 of the particles.

264

265

II.1.1.5 Synthesis and functionalization of inorganic colloids

266

267

268

269

270

271

272

273

274

275

276

277

278

279

280

281

282

283

284

285

286

287

288

289

290

291

292

293

294

295

296

297

298

299

300

301

302

303

304

305

306

307

Mesoporous silica nanoparticles (MSNs) are widely used in biomedical applications. The silica synthesis was historically reported by Stöber *et al.* in 1968 [32], also known as the sol-gel process while the introduction of mesopores was pioneered in the 1990's by Mobil Corporation laboratories. The sol-gel reaction consists in the hydrolysis and condensation of a silica source, mostly tetraethoxysilane (TEOS), in the presence of a catalyst in a water/ethanol/ammonia mixture. More precisely, this process leads to the formation of silica particles, and the pores are obtained by the addition of a surfactant such as cetyltrimethylammonium bromide (CTAB) [33]. The reaction is influenced by the composition of the solvent mixture, the surfactant used and the temperature. The process can also be adapted in order to obtain different shape. For example, Deng *et al.* reported the synthesis of silica nanotubes using the emulsion linear-merging growth technique [34]. More precisely, they operated the reaction in 1-pentanol, exploiting the formation and assembly of water droplets to obtain the nanotube shape. An additional feature of this work is that the authors could obtain an asymmetric chemical surface by using different silane molecules for the reaction. The use of a specific organosilane for the synthesis to add a chemical function to silica material has also been reported by Shao *et al.* [35]. Of course, the chemical functionality can also be added after the synthesis [36]. These last years in our groups, we have notably deeply investigated the potential of isobutyramide binders grafted on silica surface [37,38] to non-covalently immobilize various types of proteins films for drug delivery [39] and bioimaging [40,41]. It is also noteworthy that mesoporous particles can be used as material without chemical modification. For example, Wang *et al.* used MSNs as a building block to obtain supraparticles and used it as a BDNF delivery system for hearing loss therapy [42].

CaCO₃ MPs also attracted attention in biomedical applications due to several properties and notably the easy synthesis. Indeed, these particles can be obtained by simple co-precipitation of CaCl₂ and sodium carbonate (Na₂CO₃) [43]. The use of scCO₂ has also been developed, bringing better control of the MPs size [44].

Another technique to formulate mineral particles is ion etching. More precisely, it can be used as perforation etching to form porous particles [45,46] or as ion etching, as reported by Bae *et al.*, who used calcium ion etching to enlarge pores in cubic MSNs [47].

Finally, metallic or metal oxide particles are other kinds of particles presenting interesting properties for the delivery of drugs such as proteins. For example, iron oxide NPs were synthesized by annealing temperature directly inside the pores of MSNs to add a magnetic responsive property to the protein delivery system [33]. In another study, arginine-functionalized gold NPs were synthesized by phase-exchange reaction before being mixed with E-tagged protein to form nano-assemblies [48].

II.1.1.6 Template assisted method

308 Another common technique to obtain particles and capsules is the use of a
309 sacrificial template. The well-known technique to obtain capsules is the layer-by-layer
310 (LBL) assembly, where several layers of polymers are deposited around a template
311 thanks to intermolecular interactions. The strength of the assembly can be based
312 only on the force of the interactions, can be reinforced by cross-linking and
313 additionally tailored to be responsive to a local stimulus. This idea has been operated
314 by Yang *et al.* who added a thiol function to hyaluronic acid (HA) and CHI before
315 using them as LBL materials. The layers were then cross-linked by oxidation of the
316 thiol groups by horseradish peroxidase (HRP), leading to the formation of disulphide
317 bonds which are redox-responsive [43]. In this case, the sacrificial template was
318 CaCO_3 MPs, a material of choice to be used as template to formulate protein-loaded
319 particles or even protein particles as developed since decades by D.V. Volodkin *et al.*
320 [49,50].

321 Silica particles are also a very common sacrificial template. For example, Tan *et al.*
322 used mesoporous silica to synthesized poly(L-glutamic acid) (PGA) particles [51].
323 In this case, the PGA material infiltrated in the mesoporous silica before removal of
324 the template, resulting in the obtention of porous particles. The isobutyramide
325 functionalization of silica developed in our group has also been used to produce
326 nano/micro protein capsules for different applications: drug delivery [52], biocatalysis
327 [53] and siRNA delivery [54].

328 An interesting study also reported the use of proteins as a core template for the
329 surrounding assembly of polymers, forming a kind of shell that was further cross-
330 linked [55]. This approach is similar to the layer-by-layer self-assembly technique,
331 This template can be removed to obtain hollow capsules. Similarly, the on calcium
332 carbonate (CaCO_3) MPs sacrificial template..

333

334 *II.1.1.7 Cell exosome production*

335 Cell production is the technique used to obtain exosomes, as they are nanosized
336 extracellular vesicles and are produced by most of the cells. Usually, the cell line is
337 transfected with the desired plasmid to produce exosome with specific
338 functionalization. For example, HEK293T cells have been transfected with a plasmid
339 encoding for PH20 hyaluronidase [56] in a study and with signal regulatory protein α
340 (SIRP α) plasmid in another one [57]. The PH20 hyaluronidase and SIRP α were then
341 included in the structure of the exosome.

342 *II.1.2 Hydrogels*

343 HGs are three-dimensional hydrophilic networks able to absorb a large amount of
344 water. They are also highly tunable, notably on the viscoelastic point of view, making
345 them very interesting in tissue engineering as they can be formulated to have the
346 same mechanical properties of the damaged tissue. In this section, the different HG
347 cross-linking strategies will be described.

348 *II.1.2.1 Self-polymerized hydrogels*

349 Self-polymerized HGs refer to HGs that are formed through polymerization of
350 monomers or macromonomers with the creation of chemical cross-linking points. This
351 technique has for example been used by Lima *et al.* who modified alginate with
352 glycidyl methacrylate for further radical copolymerization with sodium acrylate and N-
353 vinyl-pyrrolidone [58]. The technique can also be used with a pre-formed polymer as

354 developed by the group of Wei Dong. This group used salectan as one of the building
355 blocks of HGs and polymerized 2-(dimethylamino) ethyl methacrylate (DMAEMA) in a
356 solution containing salectan to obtain a salectan/PDMAEMA interpenetrating HG [59]
357 or grafted 2-acrylamido-2-methyl-1-propanesulfonic acid (AMPS) directly to salectan
358 to polymerize it and obtain salectan-g-PAMPS HG [60].

359

360 *II.1.2.2 Covalent cross-linking of pre-formed polymers*

361 Here, the polymers are already formed and the cross-linking is induced. Two
362 possibilities appear: the addition of a cross-linker or the self-cross-linking of the
363 polymer. The work of Olthof *et al.* illustrates the first possibility as they used UV
364 irradiation of a mixture of oligo[(polyethylene glycol) fumarate]/ N-vinyl pyrrolidinone/
365 bis[2-(methacryloyloxy) ethyl] phosphate to obtain chemical cross-linking [61]. The
366 main drawback of this technique is the possible toxicity and the reactivity of the
367 chemical cross-linker. The second possibility can be illustrated by the work of
368 McAvan *et al.*, who used the deprotection of cysteine at the end of each arm of a 4-
369 armed PEG to form intermolecular disulfide bonds by exposition of the thiol groups
370 [62]. In addition, Ma *et al.* reported the use of Schiff base reaction to obtain HA/ γ -
371 PGA HG [63] and Koshy *et al.* the use of the inverse electron demand Diels-Alder
372 reaction to have the spontaneous cross-linking between alginate-norbornene and
373 alginate-tetrazine [64].

374

375

II.1.2.3 Physical hydrogels

376 Physical HGs are cross-linked by physical interactions, such as hydrogen bonding
377 [65,66], hydrophobic [67], electrostatic [65], van der Waals or even π - [66]
378 interactions. This physical cross-linking can occur spontaneously or can be induced
379 by the change of environmental conditions, the most common one being the change
380 in temperature. This is the common conditions used to obtain whey protein HGs, as
381 the heating partially denatures the protein, leading to exposure of non-polar moieties
382 and then to the aggregation of the protein in the form of HG [68]. More recently, the
383 use of thermoresponsive particles that self-assemble into HG upon hydrophobic
384 interaction through heating has also been reported [69]. Another possibility to induce
385 physical cross-linking is a change of light intensity. For example, Wang *et al.* used
386 the ability of the C-terminal adenosylcobalamin binding domain (CarHC) of CarH
387 protein to tetramerize in the dark when binding to adenosylcobalamin (AdoB₁₂) to
388 obtain an HG [70]. When exposed to light, the tetramer is disrupted and thus the HG
389 formulation loses its integrity.

390

391

II.1.2.4 Ionic gelation

392 Finally, HGs can be obtained through ionic gelation, which here means that the
393 cross-linker is an ion. This technique is the one already described to obtain some CHI
394 particle. It has been used by Hettiaratchi *et al.* to obtain alginate HG cross-linked with
395 calcium sulfate [71] and also by Lokhande *et al.* to obtain κ -carrageenan HG cross-
396 linked with potassium ions [72].

397

II.1.3 Fibers

398 Fibers are interesting drug delivery devices (DDS) notably in tissue engineering as
399 their interconnected porous structure can mimic the fibrous one of extracellular matrix

400 (ECM) or even of neurons. They also have a high surface area and the ability to load
401 several types of drugs and, more importantly, biological molecules.

402
403

403 *II.1.3.1 Single electrospinning*

404 Electrospinning is the most widely used technique to produce fibers due to many
405 advantages such as the simplicity, the cost-effectiveness and the adaptability to a
406 wide range of polymers either natural or synthetic [20,73]. In this fabrication
407 technique, an electrical potential is applied to a polymer solution by forcing it to move
408 through a charged needle. The electrostatic force between the charged needle and
409 the grounded collector leads to the formation of a jet called a Taylor cone, and this jet
410 dries before reaching the collector, forming a fiber [74]. The parameters influencing
411 the results are mainly the polymer properties (molecular weight, conductivity,
412 viscosity), the voltage, the distance between the needle and the collector, and the
413 size of the needle. This technique can be used with a single polymer solution [20] or
414 with a mixture of polymers [73]. The fibers can then be used as they are or treated
415 after synthesis. For example, oxygen plasma treatment can be used to increase the
416 hydrophilicity of the fibers or to functionalize it with chemical functions [20,75].

417 The shape of the collector is another interesting parameter to change. Most of the
418 time, fibers are collected on a grounded plate or a cylinder, but it is also possible to
419 collect them between two negatively charged plates or piers (spheres). This is
420 reported as the two-pole air gap electrospinning [76,77]. This way of synthesis
421 allows, for example, the fabrication of nerve conduit with the fibers aligned in the
422 same direction of the conduit, which can help to direct axons growth [77].

423 Although electrospinning is easy to handle, it has a major disadvantage: it
424 generally necessitates the use of an organic solvent to dissolve the polymer, which is
425 not a good environment for sensitive molecules such as proteins [46].

426
427

427 *II.1.3.2 Coaxial electrospinning*

428 Coaxial electrospinning allows the synthesis of core-sheath fibers. Even though it
429 is more difficult to operate, it brings some advantages compared to single
430 electrospinning: first of all, it allows the use of different solvents, such as hydrophobic
431 and hydrophilic, allowing the loading of a wide range of molecules. Then, when a
432 therapeutic is loaded in the core fiber, the sheath can protect it from the environment,
433 allowing the loading of sensitive molecules. This kind of fiber is very interesting as it
434 impacts the release profile of the drug loaded in the core, but it also allows the
435 loading of different drug in the core and the sheath with different release kinetics
436 [78,79]. As for monolithic fibers, core-sheath fibers can be functionalized after
437 synthesis, as reported by Wang *et al.* who treated the fibers with cold atmospheric
438 plasma to increase the pore size and the hydrophilicity to improve cell attachment
439 and proliferation [80].

440 The integration of particles in such fibers has been reported in different ways: they
441 have been blended in the core solution [79] or they have been electrospayed on the
442 fibers during the coaxial electrospinning process [81].

443
444

444 *II.1.3.3 Other techniques*

445 A quite new method to synthesize fibers is the rotary jet spinning. This technique
446 uses high-speed rotation to obtain aligned fibers. More precisely, the polymer is
447 injected to a reservoir fixed on the shaft of a motor. When the motor is rotating, the
448 polymer is extruded through a hole in the reservoir by centrifugal force, leading to the

449 formation of a jet from which the solvent evaporates, forming a fiber. The properties
450 of the fibers can then be controlled by the properties of the polymer solution itself, the
451 diameter of the hole and the rotation speed [74,82]. As an example, this technique
452 has notably been used to synthesize soy protein/cellulose nanofibers [82]. Compared
453 to electrospinning, this technique has the advantage to not need an electrical field,
454 which removes a stress applied to the polymer and its cargo [74].

455 Finally, fibers can also be synthesized by spray nebulization, as reported by
456 Zuidema *et al.* to avoid the electrical field needed for electrospinning and the
457 resulting stress induced to the loaded therapeutics [46].

458 459 II.1.4 Films and microneedle patches

460 Films are thin layers of material and are very interesting in the field of transdermal
461 delivery as they can replace classical subcutaneous injections and notably reduce
462 pain. Microneedles (MNs) patches are in the same family but present an array of
463 micron-sized needles able to penetrate the epidermis with low depth, reducing pain
464 and damages to the subcutaneous tissue.

465 466 II.1.4.1 Layer-by-layer assembly

467 The LBL process is a very suitable technique to incorporate proteins in a drug
468 delivery film as it is operated in soft conditions and on any template, whatever the
469 size, shape, porosity or surface chemistry, notably allowing a very high tunability of
470 the system [83–85]. The operation principle is to alternatively adsorb two materials on
471 a surface thanks to complementary interactions. Most of the time, two polymers are
472 adsorbed on a surface by alternative immersion in the polymer solutions. Regarding
473 these interactions, if electrostatic ones are the most common, the integrity of the
474 assembly can be due to other non-covalent (H-bond, van der Waals, hydrophobic),
475 covalent or even, bio-specific bonds [86,87].

476 Regarding materials, and especially in the scope of this review, proteins can also
477 be used as a layer type of the system without any modification [85,88,89] or after
478 functionalization, as reported by Zhao *et al.* who PEGylated salmon calcitonin
479 (PEGsc) before use with tannic acid to obtain hydrogen-bonded LBL film [87]. In
480 addition, they can be used in combination with another polymer, as developed by
481 Straeten *et al.* Indeed, they reported the use of protein-polyelectrolyte complex, more
482 precisely lysozyme-poly(styrene sulfonate) (PSS) complex, as building block to
483 synthesize an LBL film in combination with poly(allylamine hydrochloride) (PAH)
484 [83,84].

485 Regarding the fabrication technique, adsorption by dipping method is almost the
486 only one used, but inkjet-printing has also been reported with some advantages: it is
487 a non-contact technique, meaning that the therapeutic is not in contact with the
488 second material solvent or surfactant. Besides, it brings a high control of the coating
489 through the formation of the droplets and this brings an economical feature as it can
490 reduce the quantities of expensive therapeutics needed [89].

491 The LBL easily allows the tunability of the film properties, notably by the strength
492 of the interactions, by the number of layers and by the possible cross-linking between
493 layers [86].

494 495 II.1.4.2 Solvent evaporation

496 Solvent evaporation is a very easy way to prepare films. The desired solution is
497 simply poured on a surface, or even in a mold to have a specific shape, and dried

498 [90–92]. This is mainly reported as the solvent casting method [91] but can also be
499 referred as the dry phase-inversion when the main component is a polymer, as this
500 means that the polymer solution turns into a gel phase by solvent evaporation [92].

501

502

II.1.4.3 Molding

503

504

505

506

507

508

509

510

511

512

513

514

515

516

517

518

519

II.1.4.4 Other techniques

520

521

522

523

524

525

526

527

528

529

530

531

532

533

II.1.5 Macroporous scaffolds

534

535

536

537

538

II.1.5.1 Freeze-drying

539

540

541

542

543

544

545

546

Freeze-drying, also known as lyophilisation, is the most used technique to fabricate MacPSs. The principle is to freeze the material and then to eliminate the solvent by sublimation, which is the direct transition from solid state to gas state. Quite obviously, the procedure is influenced by the pressure and temperature in the freeze-drying chamber. The freeze-drying of materials can be done in a mold [100,101] or not and with only one polymer material [102–105] or several [100,101,106,107]. The incorporation of particles can easily be done on this kind of scaffold [100,101,105–107], but the integration of fibers has also been reported [104].

547 Here again, freeze-drying can be combined with other techniques used in device
548 fabrication. Cross-linking is notably used to reinforce the final scaffold, and it can be
549 done before the freeze-drying treatment [102,106] or after it [104,108]. Other
550 interesting combinations have been reported. For example, Li *et al.* fabricated a
551 device by freezing alternate layers of silk fibroin solution and silk fibroin MPs through
552 an LBL process before freeze-drying [105]. Another example is the one reported by
553 Wang *et al.* In their work, they first prepared a gelatin scaffold by freeze-drying and
554 cross-linking with glutaraldehyde. The scaffold was then functionalized with bacterial
555 cellulose by incubation in bacterial culture and with heparin via EDC/NHS reaction
556 [108].

557

558 *II.1.5.2 Template assisted method*

559 Template assisted method refers to a technique in which a template is used to
560 give a specific structure to the scaffold and is then removed, leading to the other
561 designation: template-leaching technique. The template can be of any type as long
562 as they can be removed without affecting the fabricated scaffold. A very common
563 type of template is spheres to obtain highly porous scaffold. For example, the use of
564 sugar spheres has been reported to fabricate a hydroxyapatite (HAP) scaffold [14] by
565 extruding the HAP solution to a cylindrical mold containing the sugar spheres. The
566 resulting scaffold were then immersed in water and the sugar spheres were slowly
567 dissolved while the HAP sol gelled. The use of paraffin spheres has also been
568 reported to obtain a 3D gelatin nanofibrous scaffold by combining thermally induced
569 phase separation (TIPS) and this template-leaching technique [109]. In this case, the
570 spheres were removed by immersion in hexane. The template can be more complex,
571 as reported by Bastami *et al.* who used a polyurethane (PU) foam as template, cut in
572 a cubic shape with two orthogonal canals in the interior, to obtain a β -tricalcium
573 phosphate (β -TCP) scaffold [110].

574

575 *II.1.5.3 3D printing*

576 Finally, 3D printing is also used to fabricate MacPSs as it allows good control of
577 the structure and good reproducibility. The synthesis of protein delivery devices made
578 of poly(lactic acid) (PLA) [111] or polycaprolactone (PCL) [112] using this technique
579 has been reported. Here again, the use of a mixture of material is also possible. As
580 an example, J. Lee and G. Kim reported the synthesis and characterization of
581 α -TCP/collagen (COL) scaffolds made by low-temperature printing and room-
582 temperature printing [113].

583

584 **II.2 Loading of protein and control of the release**

585 *II.2.1 Integration of proteins in the system*

586 The loading of proteins in a delivery system can be done by three techniques:
587 blending, adsorption or covalent immobilization.

588 The blending technique consists of mixing the protein with the raw material
589 constituting the scaffold (polymer, molecules, sol-gel precursor etc..) and then to
590 formulate this material in the desired shape. If this technique is easy, it necessitates
591 however having a good solubility of the protein in the material and a main drawback
592 is the possible denaturation of the protein due to the fabrication process. For
593 instance, the electrical stress induced by electrospinning when fabricating fibers is
594 reported to induce such effect [46].

595 The adsorption technique is also very easy to operate. It only consists of
596 incubating the DDS in the protein solution or to pipette the protein solution onto the
597 system, and to let it diffuse and being adsorbed by the DDS. The main drawback
598 linked to this technique is that the adsorption is a physical phenomenon which can be
599 too weak to retain a large amount of proteins. In addition, burst release is often
600 observed due to the desorption of proteins present at the surface of the DDS, which
601 can induce locally high drug concentration and lead to side effects.

602 Finally, the immobilization process consists of the covalent linking of the protein to
603 the material. This allows a very good anchor of the protein but it has also its
604 drawbacks. It is necessary needed that the protein is not denaturated by the covalent
605 immobilization which can potentially lead to a conformational change, or that the
606 biological function (enzymatic, receptor, etc...) site is still available and active.
607 Besides, this technique may lead to a few anchored proteins due to a low grafting
608 yield or even low percentage of available reactive sites on the material.

609 A representation of these loading technique is given in **Figure 3**.

610

611 II.2.2 Release of proteins

611

612 II.2.2.1 Generalities

612

613 Several mechanisms can be involved in the release of drugs from a delivery
614 system, alone or in combination. The first one is the desorption of drugs from the
615 surface, leading to a burst release. A possible solution to avoid this uncontrolled
616 release is to add standardized washings to the fabrication protocol to remove the
617 poorly bound proteins and only keep the strongly bound ones. The main drawback of
618 this technique is the reduction of the loading capacity, and the possible difficulty to
619 release the cargo. The challenge is then to design a delivery system that could
620 release the proteins in a controlled and efficient way due to specific stimuli. The
621 second mechanism is the diffusion of the drug through the matrix, which can be
622 helped by the swelling of this matrix, as it introduces more solvent inside the device.
623 The third one is the natural erosion of the system. Indeed, implantable systems are
624 often designed to degrade with a specific speed to let the place to new tissue. This
625 degradation rate leads to controlled delivery of the entrapped therapeutic. This
626 erosion can occur naturally or be driven by a sensitivity of the system to specific
627 conditions such as pH, Reactive Oxygen Species (ROS) concentration, glucose
628 concentration, etc... referred here as local stimuli. And the final one is the
629 degradation of the system due to external stimuli such as light (visible or near-
630 infrared (NIR)), magnetic field or even mechanical stimuli [114].

631 These general mechanisms are represented in **Figure 3**.

632

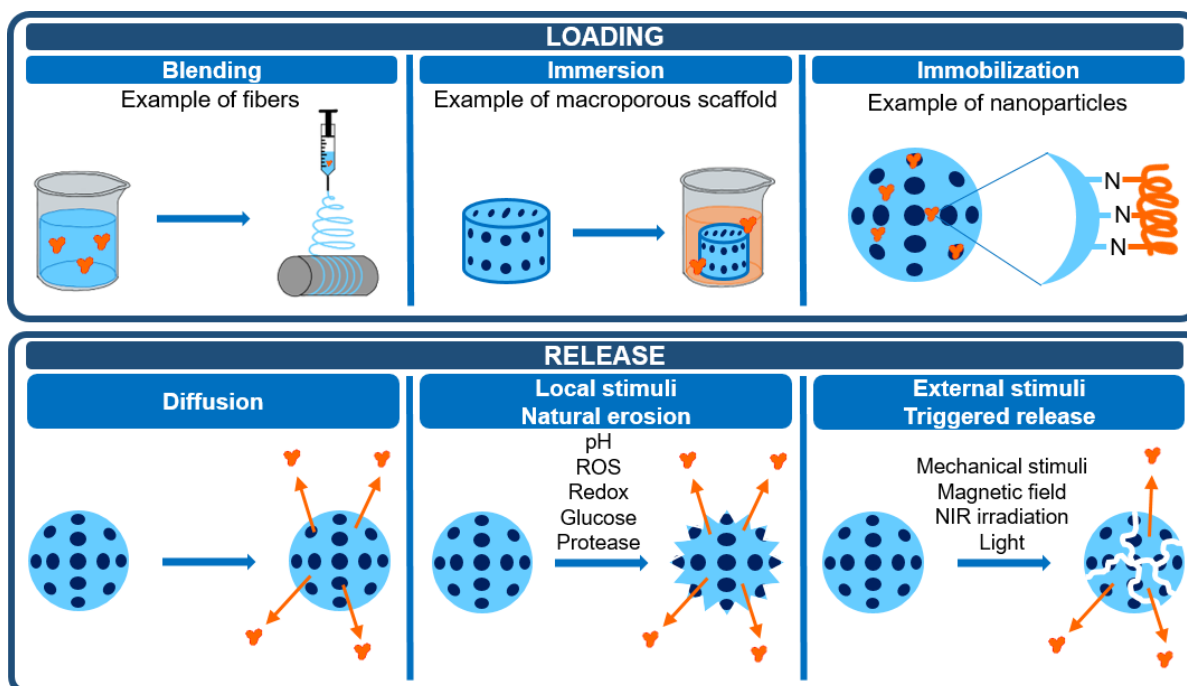


Figure 3: Protein loading and release methods

633
634

635
636

II.2.2.2 Local stimuli

637 Local stimuli are due to the natural change of physiological conditions, such as the
638 difference of the pH value in gastric fluid and intestinal fluid, to give only one
639 example. If pH is the most commonly used stimuli, it is not the only one: redox, ROS,
640 glucose and protease sensitivity are also used to design delivery devices. We detail
641 these local stimuli in the next paragraphs.

642
643

i) pH

644 The most common used local stimulus is the pH, which effect can be non-
645 destructive or destructive. The non-destructive effect implies that the change of pH
646 induces a change of interactions, which itself can induce a swelling/shrinking of the
647 system. Several MPs systems have been developed using this change of interaction,
648 notably for delivery through the intestine pathway, such as acetylated CHI/pectin MPs
649 [115], alginate/CHI MPs [116] or even gellan gum MPs coated with retrograded
650 starch and pectin [22]. In this last case, the authors showed very low release in acidic
651 media and explained that it comes from the protonation of the carboxyl group of
652 gellan gum. This protonation promotes electrostatic interactions between the
653 polymers, making the organization tighter and then preventing insulin release. The
654 pH sensitivity has also been used by the group of Wei Dong, who introduced pH-
655 sensitivity to salectan-based HGs by adding PDMAEMA or PAMPS. The PDMAEMA
656 notably brought pH-, ionic strength- and temperature-dependent swelling/shrinking
657 [59] while the PAMPS only induced pH-sensitivity, which played on electrostatic
658 interactions and so on swelling behaviour [60]. For the destructive effect, this means
659 that bonds are cleaved or that the change of pH leads to the degradation of the
660 system. For example, in Tian *et al.* work, the acidic pH cleaves the imine bond
661 between primary amine of BSA and aldehyde function grafted to the dendritic MSNs
662 [36]. In contrast, amino acid-modified CHI nanocapsules (NCs) and anionic
663 carboxymethyl starch/cationic quaternary ammonium starch NCs were decomposed
664 at pH 5.5 and 6.8 respectively [117,118]. The disruption of films has also been

665 reported. For example, He *et al.* reported the synthesis of an LBL film-coated MNs
666 patch with charge-invertible micelle as first layer. When pH is increased, the micelle
667 charge is inverted and the rest of the film is delivered from the MNs patch [88]. More
668 recently, Straeten *et al.* reported the disruption of an LBL film due to a change of
669 interaction when pH is changed. The film is composed of PAH as weak polycation
670 and a complex PSS/lysozyme, with PSS being a strong polyanion. When pH is
671 decreased under the pKa of PAH, the interaction between PSS and PAH becomes
672 stronger and the film is disrupted, releasing lysozyme [84].

673

674 *ii) Redox and ROS*

675 Most of the time, the redox-responsivity is induced in the system by a disulfide
676 bond. This can be added by the cross-linker itself [12] or by the addition of thiol
677 groups to the material to obtain a disulfide cross-linking [43,62]. This was the strategy
678 adopted by Yang *et al.* who thiolated CHI and HA prior to using them to fabricate LBL
679 NCs. The disulfide cross-linking then occurred through the action of HRP [43]. This
680 redox sensitivity can also be introduced by diselenide bonds as reported by Shao *et al.*,
681 who used bis[3-(triethoxysilyl)propyl]diselenide (BTESePD) as silica source to
682 add the diselenide bonds in MSNs [35]. Interestingly, this diselenide bond also
683 presents ROS-sensitivity, compared to disulphide bond that is only Redox-
684 responsive.

685 ROS, such as hydrogen peroxide H_2O_2 , hydroxyl radical $\bullet OH$ or even SOD $\bullet O_2^-$,
686 can be overproduced in some conditions like inflammation. Designing a ROS-
687 responsive system then totally makes sense to treat some diseases. The diselenide
688 bond-containing MSNs described above is one design example of ROS-sensitivity.
689 Another example, which combines this ROS-responsivity to glucose-responsivity, is
690 the one reported by Tong *et al.* They designed a tri-block copolymer made with PEG,
691 poly(phenylboronic acid) as glucose-sensitive block and poly(phenylboronic acid
692 pinacol ester) as H_2O_2 -sensitive block. They used this triblock copolymer to form
693 insulin and glucose oxidase (GOx)-loaded NPs. In presence of glucose, the glucose-
694 sensitive part of the copolymer starts releasing the cargos. The GOx then interacts
695 with glucose, producing H_2O_2 that reacts with the H_2O_2 -responsive block of the
696 polymer, enhancing the release [95]. The glucose-responsivity, which can be
697 combined with ROS-responsivity as presented here or with other stimuli such as pH
698 [119], is notably very used to treat diabetes.

699

700 *iii) Protease enzyme*

701 The last common stimulus inducing the degradation of delivery systems is the
702 presence of proteases [30,44,118,120,121]. This sensibility to protease can come
703 from the nature of the material, like the sensitivity of COL toward collagenase, or from
704 specific functionality added to the material. For example, Zhang *et al.* showed that
705 their starch-based NCs could be degraded under action of pH change in simulated
706 gastric, intestinal and colon fluid (SGF, SIF and SCF respectively) but also under
707 pancreatic α -amylase degradation in SIF [118]. Regarding the addition of
708 functionality, Foster *et al.* specifically added protease degradable peptide as cross-
709 linker to their MPs and modulated the degradation rate by modulating the ratio
710 between degradable and non-degradable cross-link [30] while Ramalapa *et al.* added
711 a thrombin sensitive site in their protein cargo to obtain thrombin-mediated release
712 [44].

713

714 Of course, other kinds of stimuli can be exploited such as ionic strength [59,97],
715 temperature [59] or even more specific ones such as adenosine triphosphate (ATP)
716 [19], bacterial alkaline phosphatase (BAP), sodium hydrosulfite ($\text{Na}_2\text{S}_2\text{O}_4$) [66] or
717 complementary DNA [96].

718

719

719 *II.2.2.3 External stimuli*

720 An external stimulus can also be used to induce the protein delivery, such as light
721 (visible or NIR), magnetic field or even mechanical stimulus. The next paragraphs will
722 present some examples of these stimuli.

723

724 *i) Light*

725 In this case, the exposure of the system to light is the cause of the release. For
726 example, Wang *et al.* synthesized a light sensitive HG based on the light sensitivity of
727 CarHc tetramer [70]. More precisely, they functionalized elastin-like polymers (ELPs)
728 with CarHc, a protein binding domain, able to form tetramers in presence of AdoB₁₂ if
729 the solution is in the dark, leading to the formation of an HG with cross-linking points:
730 the tetramers. When the obtained HG is exposed to light, the tetramer is disrupted,
731 which degrade the HG. In this case, the light only leads to the degradation of the HG,
732 but it can have multiple purposes as in the work reported by He *et al.* [122]. The
733 system described is composed of a nanocomplex of phenylboronic acid-modified
734 RNase A (RNBC) and ketal cross-linked PEI coated with hematoporphyrin-
735 conjugated HA. When the system is exposed to light, the irradiation of
736 hematoporphyrin leads to a high level of H_2O_2 which kills cancer cells. In addition,
737 this high H_2O_2 level cleaves the phenylboronic acid-RNase A bond, delivering the
738 protein which can also kill cancer cells. Thus the exposure of light has two
739 consequences: the production of H_2O_2 and the release of RNaseA.

740 In the same kind of field, NIR irradiation can also be used as a stimulus. It has for
741 example been reported as stimulus in a transdermal delivery system. The system
742 described is a polysaccharide HG film loaded with gold nanorods. Due to the
743 photothermal characteristic of these nanorods, the NIR irradiation of the system leads
744 to an increase in temperature and then to an enhancement of the transdermal
745 delivery of protein [123]. Tuncaboylu *et al.* also used this stimulus in their work. They
746 designed a shape-memory tube made of PCL loaded with IR-26-dye. The NIR
747 irradiation of the tube leads to temperature increase and so to the shrinking of the
748 tube, delivering the protein loaded inside the tube [124].

749

750 *ii) Magnetic field*

751 Another kind of external stimulus is the application of a magnetic field. This non-
752 invasive technique, which allows deeper penetration than NIR irradiation, has been
753 widely used to induce magnetic hyperthermia to kill cancer cells, but also as a
754 stimulus to release several types of drugs [125]. It has for example been used by
755 Omar *et al.* to control the release of mTFP-ferritin from silica-iron oxide NPs as a
756 proof of concept for the delivery of large proteins [33]. The suggested release
757 mechanism was that the application of the magnetic field leads to temperature
758 increase, disrupting the electrostatic interaction between the protein and the NPs.

759

760 *iii) Mechanical stress/action*

761 The last kind of external stimulus presented here is still not very developed:
762 mechanical stimulus. Even if not very used, it is easily applicable, notably in

763 mechanically active tissue such as cardiac tissue or cartilage tissue where it is
764 omnipresent [126,127]. As an example of reported systems, Xu *et al.* designed a
765 bioinspired ceramic composite sponge made of HAP and natural cornstarch and
766 tested its delivery properties under strain using bromophenol blue, BSA and fibroblast
767 [127]. In another hand, Zhang *et al.* reported the use of a piezoelectric-dielectric
768 composite film to release proteins. A piezoelectric material has the ability to convert
769 mechanical energy into electrical energy. The system developed converts the
770 mechanical stimulus such as press or massage into electrical energy, polarizing the
771 film and inducing shrinking or swelling of the layers, leading to an accelerated protein
772 delivery [126]. Furthermore, aside the protein delivery, the reversible enzyme
773 exhibition/embedding from LBL polymer films submitted to applied mechanical forces
774 was also developed for applications towards mechanically controlled biocatalytic
775 systems [128,129].

776
777

778

779 **III. Assessment of the protein release**

780 The characterization of the loading and release capacities of a designed protein
781 delivery device is mandatory to present a complete characterization of the system.
782 Thus, this section aims at reviewing the detection and characterization of proteins
783 loading and release and at presenting the common mathematical models used to
784 characterize the release. It is interesting to notice that there are two possibilities to
785 quantify the loaded amount of protein: indirect quantification by measuring the
786 unloaded amount of protein, the most commonly used, or destruction of the delivery
787 device to recover the loaded amount of protein.

788 **III.1 Characterization of the proteins: dosage, structure and imaging**

789 **III.1.1 UV-visible absorbance**

790 *III.1.1.1 Absorbance*

791 UltraViolet-visible absorbance is the measurement of the quantity of light absorbed
792 by a solution in the wavelength range of 200-800 nm. It is very easy to use and it
793 allows the quantification of proteins in a solution thanks to the Beer-Lambert law:

$$A = \varepsilon * l * c$$

794 where A is the absorbance of the solution, ε is the molar extinction coefficient in
795 $L \cdot mol^{-1} \cdot cm^{-1}$, l is the optical path length in cm and c is the concentration of the
796 absorbing molecule in $mol \cdot L^{-1}$.

797 Absorbance has been reported as quantifying technique for a lot of proteins: BSA
798 (around 280 nm) [27,36,58], WPI (200-320 nm) [25], casein hydrolysate (200-320
799 nm) [25], OVA (280 nm) [31], mTFP-ferritin [33], RNase A (280 nm) [35], black carrot
800 extract (530 nm, due to anthocyanins) [68], vancomycin chloride (280 nm) [73],
801 lysozyme (295 nm) [83], insulin (276 nm) [95], GOx (450 nm) [95]. The peak at 280
802 nm is due to the aromatic ring in two amino acids: tryptophan and tyrosine. It is also
803 possible to use the absorbance due to the peptide bond. This bond absorbs strongly
804 at 190 nm, but for technical reasons, the absorbance is usually measured around
805 205 nm [130]. Unfortunately, the absorption phenomenon is sensitive to its
806 environment and thus, the absorbance value can largely vary between two proteins
807 even if they have the same molecular weight.

808 *III.1.1.2 Bradford assay*

810 The Bradford assay has first been reported by Marion M. Bradford in 1976 [131]
811 and has widely been used since this moment to quantify proteins [132]. This assay
812 relies on the absorbance maximum shift of the Coomassie Blue G250 dye: the free
813 molecule is in a cationic red form with a maximum absorbance at 470 nm. When
814 binding to a protein, the molecule is in its anionic bleu form and the absorbance peak
815 is then at 595 nm. The complexation, due to electrostatic and hydrophobic
816 interactions [133], occurs more specifically with arginine and lysine residues of
817 proteins but it can also occur with histidine, tryptophan, tyrosine and phenylalanine
818 due to their aromatic residues. This quantification method is very interesting as is not
819 too sensitive to the presence of reagents or biological sample components other than
820 proteins. However, the presence of detergents has to be controlled to avoid
821 interferences [132]. The detection limits can vary from a commercial kit to another but
822 are usually ranging from 100 to
823 $1,500 \mu g \cdot mL^{-1}$. It has to be noticed that the detection limits can be different when the
824 protocol is adapted to be used with microplates. It is very used to quantify BSA

825 [8,13,43,47] and insulin [13,59,60,93], but it is also used with other proteins such as
826 chymotrypsin, myoglobin, HRP [13], immunoglobulin G (IgG) and OVA [47].

827 *III.1.1.3 Bicinchoninic Acid assay*

828 The BiCinchoninic Acid assay (BCA assay) has first been reported by Smith *et al.*
829 in 1985 [134]. The principle is to incubate the protein solution with Cu^{2+} in alkaline
830 solution to have the reduction of Cu^{2+} in Cu^+ by the peptide bonds of proteins, which
831 is a temperature-dependent reaction. Then, Cu^+ is chelated by two BCA molecules,
832 forming a purple complex having a maximum absorbance at 562 nm. The
833 advantages of this process is that it occurs in a single step and that it is not that
834 sensitive towards detergents, denaturing agents and other compounds that could be
835 present in the sample [135]. As for the Bradford assay, the detection limits can vary
836 from a kit to another but are usually ranging from 0.5 to 20 $\mu\text{g}\cdot\text{mL}^{-1}$, with a possible
837 modification when using microplates to perform the test. This technique has also
838 been used for a wide variety of proteins: BSA [97,124], lysozyme [46,124], OVA, IgG
839 [124], rhGH [24], human chitin binding domain-modified beta-lactamase (ChBD-BlaP)
840 [44], PH20 hyaluronidase [56], SIRP α [57], cytochrome C [97], enhanced green
841 fluorescent protein (eGFP) [116], GOx [119], HA-modified RNase A [136], E7-bone
842 morphogenetic protein 2 (BMP2) [137] and rhBMP2 [138].

843

844 *III.1.2 Fluorimetry*

845 *III.1.2.1 Intrinsic fluorescence*

846 Fluorescence is an interesting property to operate to quantify proteins as it is very
847 easy to handle. Intrinsic fluorescence of proteins notably allows a direct
848 quantification, and this has been used for example to quantify GFP [19] and mCherry
849 [70]. The major drawback is the potential environmental sensitivity of the
850 fluorescence moiety. As an example, intrinsic fluorescence of BSA is due to two
851 tryptophan residues, Trp-212 and Trp-134. However, the fluorescence of these
852 residues is influenced by their environment [139]. Thus, it is tricky to use this property
853 to quantify BSA in solution, but it is very interesting to characterize the interaction
854 with other components. Fluorescence quenching of BSA has for example been used
855 to study the interaction of BSA with tuftsin [140], wogonin [141], glutathione [142] and
856 more recently with lipidic NPs by applying the Stern-Volmer model [139]. It has also
857 been used by Cacicedo *et al.* to show the interaction between Levo and HSA, which
858 impacts the Levo release from bacterial cellulose film [98].

859

860 *III.1.2.2 Fluorescent labelling*

861 To avoid any modification of the intrinsic fluorescence due to the environment or
862 protein conformational change, it is common to covalently attach a fluorescent label
863 to proteins and then measure the fluorescence due to this moiety. The most common
864 label is fluorescein isothiocyanate (FITC) and it has been linked to a wide variety of
865 proteins such as BSA [18,72], insulin [105], HRP [90], RNBC [122], OVA [123] and
866 Concanavalin A (ConA) [143]. Advantages of this dye are an easy grafting and a low
867 cost, however FITC is known to be highly sensitive to experimental parameters such
868 as pH or photobleaching. Hence, other more stable labelling molecules have also
869 been used on several proteins such as cyanine 5 on BSA, erythropoietin [69], RNBC
870 [122], hepatocyte growth factor dimeric fragment (HGFdf) [144] and tumor necrosis
871 factor-related apoptosis inducing ligand TRAIL [145], vivostag S750 on BMP2 [71],

872 Texas red [85] and fluorescein [86] on OVA, rhodamine on hirudin [145] and
873 AlexaFluor on IgG [30].

874 *III.1.2.3 Fluorescamine assay*

875 Fluorescamine has first been used by Udenfriend *et al.* in 1972 for the detection of
876 primary amines in the picomole range [146]. Fluorescamine is a non-fluorescent
877 molecule but reacts very rapidly (hundreds of milliseconds) with primary amines to
878 form a fluorescent molecule, while the excess reacts with water to form a non-
879 fluorescent molecule (after some seconds). So this method is very interesting due to
880 the specific reaction with primary amines in proteins and peptides, its fast reaction
881 time and sensitivity [146]. In addition, a commercial protocols allows the use of only 2
882 μL of solution with a sensitivity ranging from 8 to 500 $\mu\text{g}\cdot\text{mL}^{-1}$ [147]. The assay has
883 been used by Chen *et al.* to characterize the loading of murabutide and OVA in
884 acetalated dextran MPs as well as BSA release from these MPs [28] and J. Lee and
885 G. Kim to characterize the release of BSA from α -TCP/COL scaffold [113].

886

887 *III.1.3 Highly specific and sensitive assays*

888 *III.1.3.1 ELISA*

889 Enzyme-Linked ImmunSor bent Assay has been developed by E. Engvall and P.
890 Perlmann in 1971 [148]. ELISA uses the specific binding of antigen and antibodies
891 and the formation of colour due to enzymatic reaction. It involves several steps: first
892 the capture of the antigen we want to detect and quantify, second the addition of a
893 specific antibody tagged with an enzyme, third the addition of a substrate that will
894 give a colour product by reacting with the enzyme, fourth the analysis of the colour
895 intensity. Three main types of ELISA exist: direct ELISA, indirect ELISA and
896 sandwich ELISA.

897 i) In direct ELISA, the antigen is adsorbed on the plate and an enzyme-tagged
898 primary antibody is then linked to it before the substrate is added to obtain the colour.
899 This technique is the simplest ELISA protocol but presents important disadvantages
900 such as the possible modification of the primary antibody immunoreactivity due to its
901 functionalization with an enzyme.

902 ii) The indirect ELISA protocol involves two antibodies: the antigen is adsorbed on
903 the plate surface, the primary antibody is linked to it and then an enzyme-tagged
904 secondary antibody specific to the primary antibody is added. The final steps, which
905 are the addition of a substrate and analysis of the signal, are similar. Even if this
906 technique has the disadvantages of adding a step in the protocol and of not
907 suppressing the risk of cross-reactivity, it presents many advantages such the wide
908 variety of secondary antibodies and the possibility to use different detection methods.

909 iii) Finally, in the sandwich ELISA, the plate used to adsorb the enzyme is coated
910 with an antibody. The antigen is adsorbed on this antibody before the same steps
911 than for an indirect ELISA are applied. Thus, the antigen is sandwiched between the
912 antibody coated on the plate and a primary antibody. As for indirect ELISA, it is
913 possible to use several detection methods. In addition, this protocol is highly
914 sensitive, as it can detect as low as some $\text{pg}\cdot\text{mL}^{-1}$ of protein (protein type
915 dependant), and highly specific but more optimization is required to operate it
916 [149,150].

917 In the domain of protein delivery device, ELISA is mainly used to detect sensitive
918 proteins such as BMP2 [103,109], stromal cell-derived factor 1 (SDF-1) [14,104],
919 chemokine CCL25 [15], neurotrophin-3 [76], vascular endothelial growth factor
920 (VEGF) [100,108], transforming growth factor- β (TGF- β) [20,113], basic fibroblast

921 growth factor (bFGF) [89], β -nerve growth factor (β -NGF) [92]... It is also used for
922 less sensitive proteins such as insulin [93,94], lysozyme [67] and OVA [92].

923

924 *III.1.3.2 Radiolabeling*

925 Radiolabeling consists of adding a radioactive label to proteins to detect and
926 quantify them. As the ELISA technique, it provides a high specificity and a high
927 sensitivity of the detection. The radiolabeling of proteins with ^{125}I and the use of a
928 gamma counter is the most used technique. Authors reported the quantification of
929 BMP2 [61], rhBMP2 [151], VEGF, FGF2 [152], BSA and ConA [143] using this
930 radiolabeling. In all these studies, the radioactivity decay was used to determine the
931 protein loading or *in vitro* release but *in vivo* release was also determined using ^{125}I -
932 radiolabelled proteins. For example, D.B. Raina *et al.* used single photon emission
933 computed tomography to image their implanted system in rats and then used the
934 signal to quantify the release [151]. In another study, Kuttappan *et al.* chose to excise
935 the skin where their implanted their DDS and then to quantify the release using a
936 gamma counter [152]. Farris *et al.* also reported the labelling of pEGFP-LUC with ^{32}P
937 α -dATP and the use of a scintillation counter to quantify the loading of this plasmid
938 DNA [153]. In this case, the radiolabeling of the protein was used because the
939 material constituting the DDS was autofluorescent.

940

941 *III.1.4 Separative techniques*

942 *III.1.4.2 High-Performance Liquid Chromatography*

943 High-Performance Liquid Chromatography, or High Performance Liquid
944 Chromatography (HPLC) is based on the difference of affinity (polar/apolar) between
945 the solutes present in the mobile phase and the stationary phase in the column. It
946 leads to the separation of the solutes and then to their detection and also
947 quantification if the protocol is designed to do so. In the domain of protein delivery
948 devices, it is mainly used with a UV detector to detect the protein and then quantify
949 them. This has been used to quantify insulin [26,99,101,115], BSA [154], lysozyme
950 [16], antihypertensive peptide [91,155], Exendin-4 (Ex4) [119], P28 peptide [156],
951 and PEGsc [87]. Reversed-phase HPLC can also be used. In this case, the
952 stationary phase is non polar while the mobile phase is polar. This has been used to
953 detect insulin [22] and liraglutide [157] for example.

954

955 *III.1.4.3 SDS PAGE*

956 SDS PAGE, the acronym for sodium dodecyl sulfate polyacrylamide gel
957 electrophoresis, is based on the different migration of proteins in a gel under an
958 electrical field due to their molecular weight. The principle is first to denature proteins
959 in presence of SDS. This is a detergent that breaks the weak interactions assuring
960 the protein assembly, so leading to a complete unfolding, and bringing a net negative
961 charge to the proteins. Then, the samples are deposited in wells present at the top of
962 the polyacrylamide gel and an electrical field is applied. The proteins migrate through
963 the gel thanks to the negative charge. The migration rate and distance depend on the
964 cross-linking density of the gel and of the protein molecular weight: the smaller the
965 protein, the faster the migration rate and the longer the distance. A solution
966 containing protein markers with known molecular weights allows the identification of
967 the molecular weights of the separated proteins. This technique is mainly used to
968 detect proteins in complex systems thanks to this molecular weight-dependent
969 migration, but it can also be operated to quantify them when known concentrations of

970 the protein are deposited on the gel with the sample to analyze. In this case, after
971 staining, the gel is imaged and the color intensity of all bands is analyzed with a
972 software. This technique has been used by Dutta *et al.* to evaluate the release of
973 lysozyme, RNase A and cytochrome C from polymeric particles [55] and by
974 Shigemitsu *et al.* to evaluate the release of IgG, ConA and myoglobin from a
975 supramolecular HG [66].

976
977

III.1.4.4 Western blot

978 Western blot is a technique aiming at detecting, identifying and quantifying
979 proteins in complex samples such as cellular samples. It involves three main steps:
980 separation, transfer to a membrane and revelation. The separation step is most often
981 an SDS PAGE, involving all the same preparation and electrophoresis steps. Then,
982 the proteins are transferred to a membrane, like nitrocellulose, by placing the gel
983 close to the membrane. This “assembly” is then placed between blotting papers and
984 an electrical field is applied, leading to the migration of proteins from the gel to the
985 membrane. This step allows the transfer of the gel result in more solid support. The
986 revelation is then done first by blocking all the non-specific sites of the membrane
987 with BSA or milk proteins, for example, and then an indirect ELISA is operated to
988 detect specific proteins. The result gives bands with different intensities related to the
989 protein concentration. At the end of the process, the membrane gives three
990 information: the presence or absence of the protein in the sample due to the absence
991 or presence of the band, the molecular weight of the protein due to the proteins
992 markers applied during the SDS PAGE step, and the concentration of the protein due
993 to the band intensity. It has for example been used to quantify the release of proteins
994 from bacterial inclusion body (BIB) [158], the encapsulation efficiency of neuregulin-1
995 (Nrg-1) from COL/poly(D-lysine) (PDL)-coated PLGA MPs [159], the OVA expression
996 from RAW264.7 cells after DA3/pOVA transfection [160] and the expression of
997 VEGF, notably with a transfer to a polyvinylidene difluoride (PVDF) membrane [161].

998
999

III.1.5 Imaging techniques

III.1.5.1 Fluorescence microscopy

1000 Fluorescence microscopy is simply the use of the fluorescent property of a
1001 molecule or material for its observation with an optical microscope. The fluorescent
1002 labelling of proteins is often used to bring this fluorescence property. This technique
1003 can be used to evaluate the loading of proteins in a scaffold or its repartition within
1004 the scaffold [105,119,143,162,163] but it is also used to check *in vitro* cellular uptake
1005 [29] or even *in vivo* or *ex vivo* repartition of a protein drug in tissues or organs
1006 [71,145].

1007
1008
1009

III.1.5.2 Confocal laser scanning microscopy

1010 The confocal microscope has been described and patented by M. Minsky in 1957
1011 [164]. This type of microscope used the fluorescence of the sample. As the source of
1012 light is mainly a laser, it is then called confocal laser scanning microscopy (CLSM).
1013 The principle is that the light source is directed to a specific point, which allows the
1014 acquisition of an image point-by-point by a scanning process. An important
1015 advantage of CLSM is that it is possible to control the depth of the field in the sample,
1016 which allows obtaining a three-dimensional image of the sample by combining the
1017 images of several planes. This imaging technique is very used to observe the cellular
1018 uptake of fluorescently-labelled proteins *in vitro* and *in vivo* after the recuperation of

1019 the tissues and staining of cells [18,19,28,43,48,55,122,136,145,165]. But this has
1020 also been used to observe protein distribution in delivery devices [26,86,166,167] or
1021 in tissue after application of the delivery device. For example, Liu *et al.* used it to
1022 image FITC-insulin in skin after application of PVP MNs patch containing FITC-insulin
1023 loaded-CaCO₃ MPs [94] and Marciello *et al.* to visualize the FITC-insulin penetration
1024 into porcine vaginal mucosa after application of a sponge-like scaffold containing
1025 FITC-insulin-loaded CHI NPs [101].

1026

1027 **III.1.6 Protein integrity**

1028 **III.1.6.1 Circular dichroism**

1029 It is important to remember that the treatments applied to proteins to load them
1030 into delivery devices and then to release them may impact their integrity and activity.
1031 Most of the time, the preservation of their activity is assessed by checking their
1032 bioactivity through a specific test. For example, the bioactivity of BMP2 is assessed
1033 by measuring the alkaline phosphatase (ALP) activity as BMP2 enhances it. But to
1034 specifically check the protein integrity, so its conformation, the most common
1035 technique is circular dichroism (CD). CD is based on the fact that an optically active
1036 molecule will not absorb the right-hand and the left-hand circular polarized light in the
1037 same way. In proteins, there are several chromophores: the peptide bond, the
1038 aromatic amino acid side chain and the disulfide bond, which makes CD a very
1039 suitable technique to analyze proteins and more importantly, to obtain information on
1040 their conformation [168]. In protein delivery device domain, it is very used to compare
1041 the conformation of the native protein and the released protein from any device to
1042 check that the integrity has not been impacted by the loading and release processes.
1043 This has for example been used on eGFP [19], cytochrome C [55], BSA [43], OVA
1044 [85], PEGsc [87], insulin [101], FITC-insulin [105], Ex4 [119], hirudin and TRAIL [145].

1045

1046 **III.1.6.2 CryoTEM**

1047 Cryogenic transmission electron microscopy (CryoTEM) is the observation by TEM
1048 of samples kept at cryogenic temperatures. It notably allows the imaging of systems
1049 in their native form in solution. Thus, it is a very interesting technique to observe
1050 systems such as lipid-based NPs [139,169], liposomes [170–172] or even lipoplexes
1051 [173]. For example, Colombani *et al.* used CryoTEM to observe the impact of the
1052 composition of lipoplexes, made of cationic liposomes and DNA, and of solvent on
1053 the lipoplexes structure [173]. Of course, it can also be used to observe polymeric
1054 NPs as reported by Dutta *et al.* who used this technique to observe CytochromeC-
1055 polymer nano-assemblies [55].

1056

1057 **III.2. Modelization of drug release kinetics**

1058 Drug release kinetics is the application of mathematical models to the data
1059 obtained from the study of drug release. This section aims at describing the most
1060 used mathematical models and at giving some example of use.

1061 **III.2.1 Presentation of the mathematical models**

1062 **III.2.1.1 Zero-order model**

1063 The zero-order release model describes a constant release which means that the
1064 same amount of drug is released per unit of time, and this release process is
1065 independent of drug concentration. The equation is:

$$M_t = M_0 + K_0 * t$$

1066 where M_t is the amount of drug dissolved at time t , M_0 the amount of drug dissolved
1067 when $t=0$, so usually 0, and K_0 is the zero-order constant release. The curve to plot
1068 when using this model is the percentage cumulative drug released (%CDR) in
1069 function of time and this curve has to be linear. This model can be used to describe
1070 several types of systems such as transdermal delivery systems, matrix tablets with
1071 low soluble drugs or coated systems [174].

1072

1073 *III.2.1.2 First-order model*

1074 The first-order model describes systems for which the release is dependent on the
1075 amount of drug remaining in the system, with a diminution of the drug released dose
1076 per unit of time. The equation describing this model is:

$$\log M_t = \log M_0 + \frac{K_1 * t}{2.303}$$

1077 where K_1 is the first-order release constant. The curve to plot is $\log(M_t)$ in function of
1078 time, which gives a linear curve. The systems for which the release can be described
1079 by this equation are usually porous matrices containing hydrosoluble drugs [174].

1080

1081 *III.2.1.3 Higuchi model*

1082 The Higuchi model is based on Fick's law and describes the diffusion of water-
1083 soluble drugs and low water-soluble drug out of semi-solid and solid matrices. The
1084 simplified equation of this model is:

$$M_t = K_H * \sqrt{t}$$

1085 where K_H is the Higuchi dissolution constant. The curve to plot is the %CDR in
1086 function of the square root of time, which gives a linear curve [174].

1087

1088 *III.2.1.4 Korsmeyer-Peppas model*

1089 The Korsmeyer-Peppas model has first been reported in 1983 by these authors to
1090 describe the release of drugs from hydrophilic polymeric matrices. The equation of
1091 this model is:

$$\frac{M_t}{M_\infty} = K * t^n$$

1092 where M_t is the amount of drug released at time t , M_∞ is the amount of drug released
1093 at infinite time, which is the total amount of drug loaded in the system, and so M_t/M_∞
1094 represents the fraction of drug released at time t , K is the kinetic constant and n is the
1095 release exponent. This exponent can be determined only with $M_t/M_\infty < 0.6$ and
1096 represents the release mechanism. If $n=0.5$, the release mechanism is the Fickian
1097 diffusion (only diffusion-controlled release), if $0.5 < n < 1.0$, it is an anomalous non-
1098 Fickian diffusion (mix of erosion-controlled release and diffusion-controlled release), if
1099 $n=1.0$ it is a zero-order release (Case II transport), and if $n > 1.0$, it is a super Case II
1100 transport mechanism [175]. The curve to plot for this model is $\log(\%CDR)$ in function
1101 of $\log(t)$.

1102 The Case II transport, or Case II diffusion denomination has been introduced by T.
1103 Alfrey *et al.* in 1966 to describe a specific type of non-Fickian diffusion [176]. The
1104 concept is that, when the solvent penetrates the polymer system, a sharp boundary is
1105 created between the swollen region and the un-swollen region, and that this
1106 boundary moves with time in a linear way. So it comes from the relaxation of the
1107 polymer due to the movement of molecule in the system [177].

1108

1109 *III.2.1.5 Ritger-Peppas model*

1110 The Ritger-Peppas model has been reported by these authors in 1987 after
 1111 experiments conducted on non-swellable [178] and swellable matrices [179] such as
 1112 spheres, cylinders, discs, slabs and sheets. The general equation is the same than
 1113 for the Korsmeyer-Peppas, and the determination of the n value has also to be done
 1114 only for $M_t/M_\infty < 0.6$, but the mechanism associated to the n value is different and
 1115 reported in **Table 1**. The curve to plot is also $\log(\%CDR)$ in function of $\log(t)$.

1116 **Table 1:** Release exponent and associated release mechanism for several types of matrices

Release exponent n value			Drug release mechanism
Thin film	Cylinder	Sphere	
Non-swellable matrices			
0.50	0.45	0.43	Fickian diffusion
$0.50 < n < 1.00$	$0.45 < n < 1.00$	$0.43 < n < 1.00$	Anomalous non-Fickian transport
1.0	1.0	1.0	Zero-order (Case II transport)
Swellable matrices			
0.5	0.45	0.43	Fickian diffusion
$0.5 < n < 1.0$	$0.45 < n < 0.89$	$0.43 < n < 0.85$	Anomalous non-Fickian transport
1.0	0.89	0.85	Case II transport

1117
 1118 *III.2.1.6 Peppas-Sahlin model*

1119 The Peppas-Sahlin model has first been reported by these authors in 1989 [180]
 1120 and refers to the following equation:

$$\frac{M_t}{M_\infty} = K_d * t^m + K_r * t^{2*m}$$

1121 where K_d is the diffusion constant, K_r is the relaxation constant and m is the purely
 1122 Fickian diffusion coefficient for a controlled delivery device with any geometrical
 1123 shape. The K_d constant represents the contribution of Fickian diffusion and the K_r
 1124 constant represents the contribution of the relaxation in the release mechanism. The
 1125 values and mechanisms to be considered for m are the ones reported in Table 1 for
 1126 swellable matrices. The authors gave a methodology to analyse the release study
 1127 results:

- 1128 1. Calculate the value of the aspect ratio=diameter/thickness of the device.
- 1129 2. Determine m: if aspect ratio<0.1, m=0.45 and if aspect ratio>100, m=0.50. If m
 1130 is in between, use their article as a reference to determine m.
- 1131 3. Fit the first 60 % of the experimental data to the Peppas-Sahlin equation.
- 1132 4. Calculate K_d and K_r .
- 1133 5. Use the following equation to determine the percentage of Fickian diffusion to
 1134 the release mechanism F:

$$F = \frac{1}{1 + \frac{K_r}{K_d} * t^m}$$

1135 Although this model is more complex, it allows a finer characterization of the
 1136 release mechanism.

1137
 1138 *III.2.2 How to use mathematical models?*

1139 Usually, the experimental data are fitted to the expected mathematical model, or
 1140 the most relevant one or even a selection of several models. The best fit is then
 1141 determined using the correlation coefficient. **Table 2** regroups some studies using
 1142 mathematical models to describe their delivery device.

1143 **Table 2:** Some example of mathematical models used on protein delivery devices

System	Material	Protein/ therapeutic moieity	Mathematical model tested	Ref
MPs	Reverse micelle lecithin NPs in PLGA MPS	BSA	Zero-order, modified Ritger-Peppas	[7]
MPs	Gellan gum coated with retrograded starch and pectin	Insulin	First order, Higuchi, Korsmeyer-Peppas	[22]
MPs	CHI/alginate	Vancomycin chloride	Ritger-Peppas, Higuchi, Peppas-Sahlin, zero-order, first order	[114]
HG	HA, γ -PGA	FITC-BSA	Zero-order, first order, Higuchi, Korsmeyer-Peppas, modified Korsmeyer-Peppas, Peppas-Sahlin, modified Peppas-Sahlin	[63]
HG	TEMPO-oxidized cellulose nanofibers and cationic gar gum	BSA	Ritger-Peppas	[65]
HG	WPI, xanthan, pectin, gum tragacanth	Black carrot extract	Fick's second law as reported by Crank <i>et al.</i>	[68]
Fiber	Sodium alginate, soy protein isolate, PEO	Vancomycin chloride	Ritger-Peppas	[73]
Fiber	CHI NPs-loaded PVA core – sodium alginate, POE sheath	BSA	Higuchi, Ritger-Peppas	[79]
Fiber	PCL-HAPn core-PCL or PVAc sheath, PLGA NPs simultaneous electrospaying	BMP2, HAPn	Korsmeyer-Peppas, Peppas-Sahlin	[81]
LBL film	PEGsc, tannic acid	PEGsc	Zero-order	[87]
MacPS	CHI NPs-loaded COL HG placed in canals in porous TCP scaffold	rhBMP2	Zero-order, Higuchi	[110]

1144 MPs microparticles; NPs nanoparticles; PLGA poly(lactic-co-glycolic acid); BSA bovine serum albumin; CHI chitosan; HG
1145 hydrogel; HA hyaluronic acid; γ -PGA poly(γ -glutamic acid); FITC-BSA fluorescein isothiocyanate-BSA; TEMPO 2,2,6,6-
1146 tetramethylpiperidine-1-oxyl; WPI whey protein isolate; PEO poly(ethylene oxide); PVA poly(vinyl alcohol); PCL
1147 polycaprolactone; HAPn hydroxyapatite nanorods; PVAc poly(vinyl acetate); LBL layer-by-layer; PEGsc PEGylated salmon
1148 calcitonin, COL collagen; TCP tricalcium phosphate

1149

1150 IV Circulating systems

1151 Circulating systems refer to protein delivery systems able to circulate in the body
1152 fluids to reach their target. They are developed for several decades for the treatment
1153 of cancer due to their ability to penetrate tumour cells and are also a good alternative
1154 to subcutaneous injection of insulin when designed for oral delivery. Some circulating
1155 systems have also been proposed for tissue engineering even if implantable systems
1156 are more common.

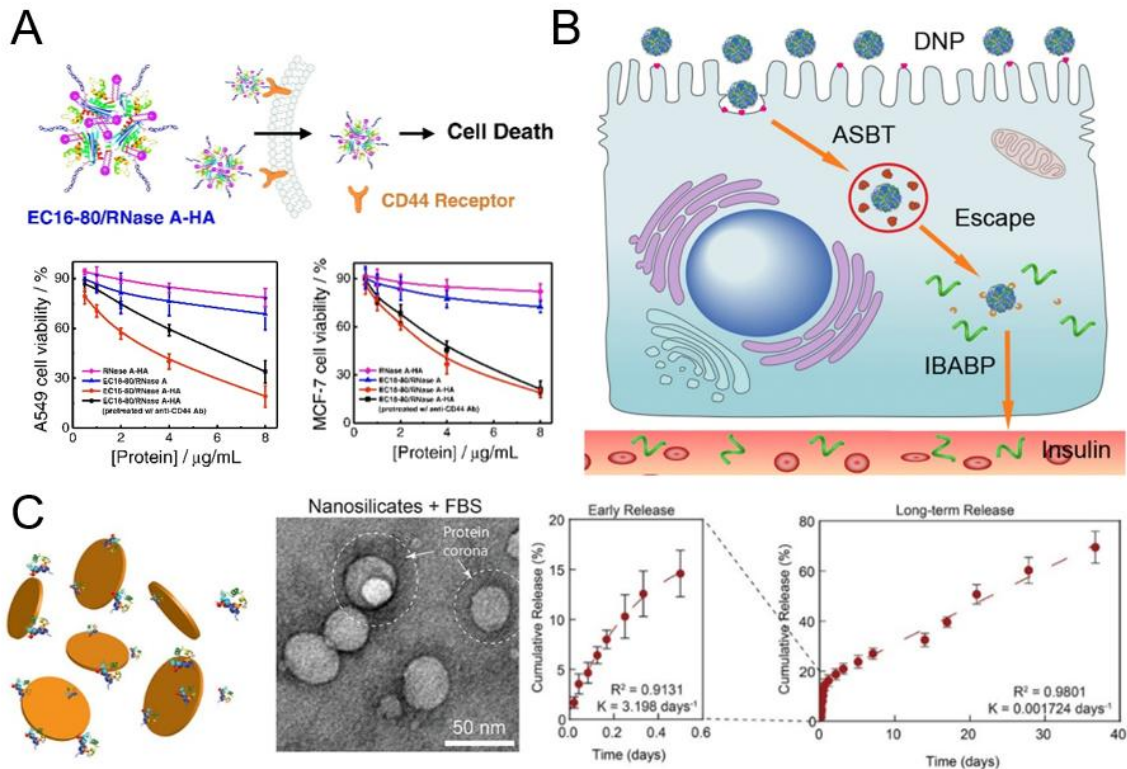
1157 IV.1 Cancer treatment

1158 IV.1.1 RNase delivery

1159 Among the possible proteins studied to treat cancer, RNase A is interesting as it
1160 enters the cytosol and cleaves the intracellular RNA, preventing the synthesis of
1161 proteins and thus leading to cell death [181]. Several systems have then been
1162 developed to maximise the intracellular delivery of RNase A. For example, a study
1163 reported the covalent coupling of RNase A with HA to obtain two effects [136]. First,
1164 the increase of the RNase A negative charge, helping the complexation with the
1165 cationic lipid-like molecule EC16-80 to form protein/lipid-like NPs. Second, the
1166 targeting of cancer cells as HA can specifically bind to CD44 receptor, which is
1167 overexpressed in many solid tumours. The EC16-80/RNase A-HA had the best cell
1168 internalization result in A549 (lung) and MCF-7 (breast) cancer cell lines, exhibiting
1169 high and low CD44 expression respectively. An additional experiment showed the
1170 necessity of having the HA-CD44 binding to have cellular uptake and so, to have
1171 RNase A intracellular delivery and efficacy. These results are represented in **Figure**
1172 **4A**.

1173 In another study, the specific cell internalization was assured by the coating of
1174 NPs with cancer cell membrane. In this case, the selective cellular uptake was
1175 induced by the cancer cell membrane type used to coat the NPs [35].

1176 He *et al.* also proposed an RNase A delivery system by caging this protein. As
1177 explained above in the external stimuli section, the system consists of the caging of
1178 RNase A by modifying it with H₂O₂-cleavable phenylboronic acid (RNBC). The RNBC
1179 was then encapsulated in KPEI NCs coated with hematoporphyrin-HA. The study
1180 showed that the use of HA allowed the high internalization of the system by cancer
1181 cell lines highly expressing CD44. Furthermore, the authors demonstrated the
1182 synergistic activity of the system against cancer cells: the light exposure of the
1183 system leads to the production of ROS, which induces the release of RNase A, and
1184 both leads to cancer cell death [122].



1185

1186 **Figure 4:** A. RNase A-HA/lipid-like NPs cell internalization via HA-CD44 interaction and efficiency on A459 and
 1187 NCF-7 cancerous cell lines (adapted from article [136]). B. Schematic illustration of the bile acid pathways
 1188 exploited by deoxycholic acid-modified nanoparticles to deliver insulin intracellularly (reproduced from article
 1189 [182]). C. Interaction between nanosilicate and proteins, percent binding efficiency and protein release (adapted
 1190 from article [183]).

1191

1192 IV.1.2 Caspase-3 delivery

1193 Of course, RNase A is not the only interesting protein for cancer treatment. For
 1194 example, Wu *et al.* developed a system for the co-delivery of paclitaxel (PTX) and
 1195 recombinant human caspase-3 (Casp-3) [117]. Casp-3 is a crucial protein for the
 1196 induction of apoptosis as it is able to cleave key structural proteins, leading to several
 1197 phenomenon causing apoptosis such as DNA fragmentation, chromatin
 1198 condensation and membrane bleeding [184]. The described system consists of
 1199 linoleic acid droplet encapsulated in an amino-acid-modified CHI NC. The authors
 1200 first optimized the system by functionalizing CHI with L-arginine, L-lysine or L-
 1201 phenylalanine and finally chose the L-arginine due to the higher stability of the
 1202 system. The PTX was then loaded inside the linoleic acid droplet and the Casp-3 was
 1203 adsorbed on the NC surface. The *in vitro* tests showed a higher percentage of
 1204 apoptotic cells in the samples treated with Arg-CHI-NCs-PTX/Casp-3 (53.2 %)
 1205 compared to samples treated with Arg-CHI-NCs-PTX (43.7 %) and Arg-CHI-NCs-
 1206 Casp-3 (20.0 %).

1207

1208

1209 IV.1.3 Anticancer protein delivery mediated by exosomes

1210 Exosomes are also systems of interest for protein delivery systems as the protein
 1211 can directly be integrated into the exosome building block by transfecting cells with
 1212 adequate plasmid. For example, PH20 hyaluronidase-exosome (PH20-ExSM) has
 1213 been produced by HEK293T cells [56]. HA can contribute to the tumorigenesis by
 interaction with different receptors, such as CD44, and by accumulation in tumours,

1214 which has notably been associated with tumour migration and chemoradioresistance.
1215 Thus, this system was expected to enhance tumour penetration via HA degradation,
1216 leading to enhanced tumour growth inhibition. The HA degradation capacity of the
1217 system has been assessed by checking the HA depletion in PC3 cells: the relative
1218 length clearly decreased in a PH20 dose-dependent manner (maximum decrease
1219 from 100% to ~ 20 %).

1220 In another study, the use of exosome has been studied for immunotherapy, which
1221 is the stimulation of the immune system to cure a disease. More precisely, the
1222 delivery of SIRP α from exosome or ferritin nanocage has been studied for the
1223 blockage of CD47 activity, which is the inhibition of phagocytosis of tumour cells.
1224 Here again, HEK293T cells were used to produce SIRP α -ExSM [57]. A first *in vitro*
1225 experiment showed that the CD47 binding affinity on HT29 human colon
1226 adenocarcinoma cells was 5-fold higher for SIRP α -ExSM compared to SIRP α -ferritin
1227 nanocage (SIRP α -FN). In addition, the phagocytosis index of these HT29 cells was ~
1228 22.5 % for SIRP α -ExSM and ~ 6 % for SIRP α -FN. Altogether, these results showed
1229 that the SIRP α -ExSM was more efficient than SIRP α -FN to bind to CD47 in HT29,
1230 leading to an increase of the HT29 cells phagocytosis by inhibiting the CD47-
1231 mediated “don’t eat me” signal.

1232

1233 IV.2 Diabetes treatment

1234 Insulin is almost the only protein used to treat diabetes type I with some
1235 exceptions. A quite common polymer material used to design new insulin delivery
1236 systems, and delivery systems in general, is CHI. Indeed, this biopolymer affords
1237 several advantages such as biodegradability and biocompatibility and importantly,
1238 also because it can self-assemble via electrostatic interactions with oppositely
1239 charged ions or molecules such as polysaccharides, proteins or nucleic acid. Of
1240 course, it can also be chemically modified before use.

1241

1242 IV.2.1 CHI as DDS material

1243 For example, Maciel *et al.* reported the synthesis of MPs and NPs made of pectin
1244 and acetylated CHI playing on the acetylation degree (15.0 and 28.8 %) and the
1245 pectin /modified CHI ratio to act on the charge ratio [115]. After complete
1246 characterization, the release of insulin from MPs and NPs with both acetylation
1247 degrees but a unique charge ratio was evaluated in SGF (pH=1.2) and SIF (pH=6.8).
1248 The results showed no impact of the acetylation degree on the release process,
1249 which is pH-dependent: the cumulative amount of released insulin reached a
1250 maximum of 13 % in SGF and 89 % in SIF. Another study reported the modification
1251 of CHI with deoxycholic acid and then the synthesis of NPs by mixing the modified
1252 CHI, insulin and γ -PGA [182]. The authors notably studied all the insulin delivery
1253 mechanism, more precisely how it goes from the gastric system to the blood
1254 circulatory system, illustrated in Erreur ! Source du renvoi introuvable. **B**. The NPs
1255 were first internalized through apical sodium-dependent bile acid transporter (ASBT)-
1256 mediated endocytosis. Then, the endolysosomal escape of the NPs occurred leading
1257 to the crossing of the intracellular barrier. And finally, the trafficking and release of
1258 insulin were guided by the interaction between the NPs and ileal bile acid-binding
1259 protein (IBABP).

1260 These two systems were developed for oral administration of insulin, a very
1261 interesting administration route to replace the classical subcutaneous injection.

1262

1263 IV.2.2 Other biopolymers for insulin delivery

1264 Oral administration of insulin was also the objective in other studies, such as the
1265 one conducted by Meneguín *et al.* [22]. These authors synthesized gellan gum MPs
1266 coated with retrograded starch and pectin in order to enhance the insulin protection
1267 against enzymatic degradation and thus to enhance its delivery. The results showed
1268 high protection against trypsin and α -chymotrypsin with up to 80 % of insulin
1269 remaining intact when loaded inside the MPs compared to 3 % when delivered in the
1270 free form. Besides, the authors showed that the insulin permeability on Caco-2 cells
1271 was enhanced when delivered from MPs with a permeability rate between 42 and 67
1272 % compared to free insulin for which it was 25 %. More recently, Wang *et al.* used
1273 another strategy to obtain a good oral insulin delivery [170]. They designed an
1274 insulin-loaded cationic liposome on which they adsorbed BSA to obtain a protein
1275 corona around the liposome. The resulting PcCL system, for protein corona cationic
1276 liposome, showed a very good mucus-penetrating ability and also a very good
1277 cellular uptake in presence of trypsin. Indeed, the trypsin was necessary to gradually
1278 degrade the BSA corona and then allow the cellular uptake of the remaining cationic
1279 liposome.

1280

1281

IV.3 Tissue engineering

1282

IV.3.1 Bone and cartilage tissue

1283

1284

1285

1286

1287

1288

1289

1290

1291

1292

1293

1294

1295

1296

1297

BMP2 is the protein drug of choice when designing a DDS for bone tissue engineering due to its osteogenesis property. Even if implantable systems are more developed to deliver this protein as it will be described in part V, some circulating systems have been reported in the literature. For example, a study reported the use of heparin NPs-loaded PEG MPs to deliver rhBMP2 after loading it by two methods: the “pre-fabrication loading” or “post-fabrication loading” which consists of loading the heparin NPs before PEG MPs formation or loading the final heparin NP/PEG MP system respectively, both done through adsorption [9]. This study showed that the pre-fabrication loading induced a similar C2C12 cell ALP activity while post-fabrication loading induced 7-fold higher ALP activity compared to free rhBMP2. As both systems presented very low protein release, the ALP activity measurement showed that the PEG-based part of the system was able to sequester proteins and then to deliver them to induce a cellular response. This sequestration ability has also been shown for SDF-1 α as proof of concept for proteins with different molecular weight.

1298

1299

1300

1301

1302

1303

1304

1305

Other simplest systems have been developed, such as MPs fabricated with human COL I-based recombinant protein [120]. The authors studied the impact of several parameters on the protein release ability, such as degree of chemical cross-linking, use of dehydrothermal cross-linking (dehydration by high temperature) and the size of the MPs. For example, the initial burst release was decreased from 23 % to 17 % when increasing the chemical cross-linking. When using dehydrothermal cross-linking, this initial burst release represented 11 % of loaded protein. The measure of ALP activity in C2C12-BreLUC cells ensured the bioactivity of the released rhBMP2.

1306

1307

1308

1309

1310

1311

1312

Another reported simple system is disk-shaped nanosilicate, as illustrated in Erreur ! Source du renvoi introuvable.C [183]. This system has been studied for the loading and release of rhBMP2 and TGF- β 3 individually. The efficient differentiation of hMSCs in osteoblast cells by treatment with nanosilicate/rhBMP2 was checked by evaluating the expression of osteocalcin (OCN), as it is an osteospecific marker, and the production of COL1A1 and mineralized matrix. Regarding the treatment of hMSCs with nanosilicate/ TGF- β 3, their chondrogenic differentiation has been

1313 showed with the production of cartilage-like matrix by notably checking the amount of
1314 sulphated glycosaminoglycans (GAGs).

1315
1316

IV.3.2 Nerve tissue

1317 PLGA MPs have been used to obtain protein drug delivery MPs. For example,
1318 Santhosh *et al.* optimized the PLGA MPs size and porosity to obtain an optimal
1319 release profile of rhNrg-1 β 1 peptide for the treatment of spinal cord injury (SCI) [185].
1320 The goal was to deliver rhNrg-1 β 1 to promote the differentiation of neural precursors
1321 cells (NPCs) into myelinating oligodendrocytes as well as their survival, which could
1322 lead to cellular replacement and then to SCI repair. The *in vitro* study conducted on
1323 adult NPCs showed the successful differentiation of NPCs to oligodendrocytes. An *in*
1324 *vitro* study has also been performed on primary mixed astrocytes and microglia
1325 culture, as they play a key role in the central nervous system protection [186], to
1326 show that the treatment does not activate them and thus does not lead to
1327 neuroinflammation and glial scar formation.

1328 In another study, Zeng *et al.* synthesized multiple PLGA core- CHI single shell
1329 MPs for the delivery of glial cell line-derived neurotrophic factor (GDNF) as it is able
1330 to regenerate peripheral nerves [187]. The modulation of CHI concentration allowed
1331 the reduction of the initial burst release compared to PLGA MPs and also the
1332 neutralization of PLGA degradation product acidity. Besides, *in vitro* experiments
1333 showed the preservation of GDNF bioactivity after release by assessing the neuronal
1334 differentiation of PC12 cells.

1335 Mixed micelles made of PF127 and TPGS were also proposed for specifically
1336 deliver proteins across the blood brain barrier (BBB) [23]. An *in vitro* model of BBB
1337 using brain capillary endothelial cells (BCECs) was used to evaluate the cellular
1338 uptake of Rhodamine123 (Rho123) used as a model, notably due to its fluorescence.
1339 The CLSM analysis showed a clear enhancement of cellular uptake when using
1340 PF127/TPGS mixed micelles compared to free Rho123 and even PF127 micelles.

1341
1342

IV.3.3 Cardiac tissue

1343 PLGA particles were also used for the regeneration of cardiac tissue after
1344 myocardial infarction (MI). For example, PLGA-PEG NPs have been proposed for the
1345 delivery of liraglutide [157]. Even if this protein was developed as a treatment for
1346 diabetes type II, it has multiple therapeutic effects for cardiac regeneration such as
1347 inhibition of myocardial apoptosis, attenuation of infarct size, promotion of
1348 angiogenesis and improvement of cardiac performance. The bioactivity of the
1349 released liraglutide was assessed *in vitro* by checking the phosphorylation level of
1350 AKT protein kinase in a culture of neonatal ventricular myocytes. The results showed
1351 no significant difference of AKT phosphorylation between the groups treated with
1352 liraglutide-loaded NPs and free liraglutide, showing that the bioactivity of the protein
1353 was retained.

1354 In another study, PLGA MPs were loaded with Nrg-1 and coated with COL/PDL
1355 before adipose-derived stem cells (ADSCs) have been adhered on the MPs surface
1356 [159]. The goal was to combine the cardiac regeneration effect of both ADSCs, by
1357 their secretion of growth factors such as VEGF and HGF, and Nrg-1, by its promotion
1358 of angiogenesis, cardiomyocyte proliferation and cell survival. The MPs presented an
1359 encapsulation efficiency of 65 \pm 2 % and the released Nrg-1 was still bioactive as
1360 demonstrated by the proliferation of H9c2 cells.

1361
1362

IV.4 Gastrointestinal delivery

1363 Gastrointestinal delivery is interesting to deliver proteins with enriched food to
 1364 prevent some diseases or to treat diseases like inflammatory bowel disease (IBD).
 1365 However, it is difficult to achieve due to several barriers such as enzymatic
 1366 degradation and change of pH in the gastrointestinal tract.

1367 To overcome these barriers and obtain an oral delivery system for protein delivery
 1368 to colon, Zhang *et al.* modified cassava starch with chloroacetic acid and 3-chloro-2-
 1369 hydroxy-propyl-trimethyl ammonium chloride to obtain anionic carboxymethyl starch
 1370 (CMS) and cationic quaternary ammonium starch (QAS) respectively [118]. Then,
 1371 they use these new materials to produce LBL NCs and played on the degree of
 1372 substitution and molecular weight of CMS to obtain several NCs. The release ability
 1373 of these MPs was then tested with BSA in SGF, SIF and SCF (pH=7.2). The results
 1374 showed that the NCs obtained with a lower degree of substitution and molecular
 1375 weight were the best NCs for colon delivery.

1376 CHI/PPA beads were also developed for such application and tested for BSA,
 1377 WPI, insulin and casein hydrolysate encapsulation and release [25]. The authors
 1378 could obtain very high encapsulation efficiency, more than 95 %, for all proteins
 1379 except casein hydrolysate. The release studies showed good potential for delivery in
 1380 the intestine as insulin and WPI were well retained in SGF and then delivered in SIF.
 1381 More recently, Ling *et al.* studied alginate/CHI MPs for the intestinal release of
 1382 bacterial effector protein AvrA/eGFP NPs for IBD treatment, as AvrA has anti-
 1383 inflammatory and anti-apoptotic activity [116]. *In vitro* studies showed the MP ability
 1384 to protect protein NPs in SGF and to release them in SIF as well as the cellular
 1385 uptake of ~65 % of released protein NPs by HeLa cells.

1386

1387 IV.5 Vaccine delivery

1388 Vaccine delivery is also an application for which MPs and NPs can be used. For
 1389 example, Tavares *et al.* synthesized PLGA MPs in the form of dry powder for
 1390 pulmonary vaccine delivery [27]. Their study aimed at evaluating the effect of BSA
 1391 and L-leucine on the MPs characteristics, with BSA being a model antigen and L-
 1392 leucine a dispersibility enhancer for the SASD process. *In vitro* studies conducted on
 1393 A549 cells showed no cytotoxicity of the system.

1394 More recently, Chatzikleantous *et al.* studied the use of cationic liposomes made
 1395 of 1, 2-distearoyl-sn-glycero-3-phosphocholine (DSPC), cholesterol and
 1396 dimethyldioctadecylammonium bromide (DDA) to deliver a GBS67-CpGODN
 1397 complex [172]. GBS67 is a recognized antigen of Group B *Streptococcus* (GBS)
 1398 bacteria, which activity can lead to serious infections in pregnant woman and
 1399 newborn. GBS67 has notably been investigated as potential vaccine candidate
 1400 against GBS [188]. CpG oligodeoxynucleotide (CpGODN) is a Toll like receptor 9
 1401 (TLR9) agonist and its action leads to rapid immune responses that can inhibit or limit
 1402 infections. The aim of the study was to obtain a new vaccine by covalently linking
 1403 GBS67 and CpGODN prior to absorption on a liposome. The conjugation of both
 1404 proteins led to a higher immune response compared to individual ones and more
 1405 importantly a higher immune response with lower proteins doses.

1406 The

1407 **Table 3** sums up some interesting circulating systems and their main *in vitro*
 1408 results.

1409

1410 **Table 3:** Interesting *in vitro* results obtained with circulating systems

System/	Material	Protein /	Therapeutic ability	<i>In vitro</i> cell	Main result	Ref
---------	----------	-----------	---------------------	----------------------	-------------	-----

Application		therapeutic moiety		line model		
NPs Cancer	Cancer cell membrane coated MSNs containing diselenide bonds	RNase A	Cleaves RNA	Hec HeLa cells, Raw 264.7, Hbc MCF-7, MEF	Selective cellular uptake	[35]
NCs Cancer	Amino acid-functionalized CHI	Casp-3 PTX	Casp-3: apoptosis of tumor cells PTX: chemotherapeutic agent	Hcc HeLa cells	Highest apoptosis with the co-delivery	[117]
ExSM Cancer	PH20-modified exosome from HEK293T cells	Hyaluronidase PH20 DOX	PH20: Hyaluronan degradation DOX: anti-cancer	PC3 cells	Reduction of HA production by cells	[56]
MPs Diabetes	Retrograded start/pectin-coated Gellan gum MPs	Insulin	Hypoglycemic effect	Caco-2 cells Caco-2 cells monolayer	Insulin permeability on cells increased	[22]
NPs Bone tissue eng.	Disk-shaped nanosilicate	rhBMP2 or TGF-β3	rhBMP2: osteogenesis TGF-β3: chondrogenesis	hMSCs	Osteogenic or chondrogenic differentiation	[183]
MPs Nerve tissue eng.	PLGA particles in a single CHI MP	GDNF	Peripheral nerves regeneration	PC12 cells	Neuronal differentiation	[187]
Micelle Nerve tissue eng.	PF127 and TPGS	Rho123	Model molecule	BCECs	Enhanced cellular uptake in an <i>in vitro</i> model of BBB	[23]
MPs Cardiac tissue eng.	Adipose-derived SCs on PLGA/COL/ PDL MPs	Nrg-1	Angiogenesis, cardiomyocyte proliferation	H9c2 cells	Released Nrg-1 is bioactive	[159]

1411 NPs nanoparticles; MSNs mesoporous silica nanoparticles; RNase A ribonuclease A; RNA ribonucleic acid; Hec HeLa cells
1412 human epithelial carcinoma HeLa cells; Raw 264.7 murine macrophages cells Raw 264.7; Hbc MCF-7 human breast cancer cell
1413 MCF-7; MEF mouse embryonic fibroblast; NCs nanocapsules, CHI chitosan; Casp-3 caspase-3; PTX paclitaxel; Hcc HeLa cells
1414 human cervical cancer HeLa cells; ExSM exosome; DOX doxorubicin; PC3 cells human PC3 prostate cancer cells; HA
1415 hyaluronic acid; MPs microparticles; Caco-2 cells Caco-2 human colon cancer cells; eng. Engineering; rhBMP2 recombinant
1416 human bone morphogenetic protein 2; TGF-β3 transforming growth factor-β3; hMSCs human mesenchymal stem cells; PLGA
1417 poly(lactic-co-glycolic acid); GDNF glial cell line derived neurotrophic factor; PC12 cells Rat pheochromocytome; PF127
1418 Pluronic ® F127; TPGS D-α-tocopheryl polyethylene glycol succinate; Rho123 Rhodamine 123; BCECs brain capillary
1419 endothelial cells; BBB Blood Brain Barrier; SCs stem cells; COL Collagen; PDL poly-D-lysine, Nrg-1 Neuregulin-1
1420
1421

1422
1423
1424
1425
1426
1427
1428

1429
1430
1431
1432
1433
1434
1435
1436
1437
1438
1439
1440
1441
1442
1443
1444
1445
1446
1447
1448
1449
1450
1451
1452
1453
1454
1455
1456
1457
1458
1459
1460
1461
1462
1463
1464
1465
1466
1467
1468
1469
1470

V Implantable matrices

Implantable matrices are mainly developed for tissue engineering, as they can be designed to mimic the tissue characteristics and thus to improve cell adhesion, migration and proliferation. Even if a huge amount of works focuses on bone tissue engineering, implantable matrices are also suitable for the regeneration of cartilage, nerve and cardiac tissues. Interestingly, implantable matrices have also emerged for the treatment of diabetes and cancer.

V.1 Bone tissue engineering

V.1.1 Macroporous scaffolds

MacPSs have been widely developed for bone tissue engineering, in response to the need of a material that could replace autologous bone graft. Indeed, this latter has several disadvantages such as the limit of donor source or the risk of rejection. As MacPSs are solids and present a porous structure, they can support cell migration and proliferation, making them very interesting in this field. As said previously, BMP2 is the therapeutic protein of choice for such application due to its ability to promote osteogenesis. The systems developed to deliver BMP2 can be separated in two categories: the first one consists of only one formulation type which can be made of organic, inorganic or a mixture organic/inorganic materials. The second category consists of the combination of several formulations such as the integration of nanostructures (MPs, NPs) into a scaffold. These ones are called nanocomposites here.

V.1.1.1 Single formulation: organic and inorganic material, alone or in combination

Organic MacPSs mainly consists of COL sponges. They have been studied for the release of BMP2, alone or with other drugs/proteins such as alendronate which promotes osteogenic cells differentiation and supresses osteoclasts [102], or osteoprotegerin which inhibits osteoclast maturation, leading to the inhibition of new bone resorption [189]. It has also been used to compare the efficiency of BMP2 and BMP9 for bone regeneration [190]. Another organic MacPSs reported recently consisted of polydopamine-coated 3D printed PLA scaffold [111]. BMP2 was then loaded on the coated surface via adsorption and the obtained MacPSs could release it, allowing proliferation and osteogenesis differentiation of hMSCs.

For inorganic-based MacPSs, Cao *et al.* proposed to use commercial α -TCP scaffold for the loading and release of a BMP2 peptide via E7 domain [137]. The E7 domain, a natural part of bone sialoprotein, was covalently linked to the BMP2 peptide KIPKASSVPTELSAISTLYL and allowed the loading via its binding to Ca^{2+} on the scaffold. Lin *et al.*, on their side, reported the synthesis of mesoporous bioactive glass scaffold for the co-delivery of BMP2 and chemokine interleukine-8 (IL-8), due to its ability to recruit stem cells [191]. The scaffold allowed the burst release of IL-8, adsorbed on the PEG-coated surface, and the sustained release of BMP2, loaded inside the mesopores.

Layered or sandwiched composite MacPSs, meaning that the final delivery system consists of a mixture of such organic and inorganic materials, have also been developed. For example, Cai *et al.* reported an HAP-COL scaffold able to release BMP2, leading to the adhesion, proliferation and differentiation of rat bone marrow-derived MSCs [103]. Another example is the formulation of a mixture of gelatin, HAP and calcium sulphate in the form of cryogel for the delivery of BMP2 and zoledronic acid, another inhibitor of new bone resorption by the killing of osteoclast [151].

1471 The case where nanostructures are formulated into another phase, to form
1472 nanocomposites MacPSs is developed more in details in the next paragraph.

1473

1474 *V.1.1.2 Nanocomposites: nanostructures integrated in a scaffold*

1475 A very common way to obtain such nanocomposite MacPSs is to embed MPs/NPs
1476 particles in the scaffold or on the scaffold. Here also, we can classify the delivery
1477 systems depending on the organic/inorganic nature of the material.

1478 For example, Wang *et al.* synthesized a scaffold made of CHI, agarose and gelatin
1479 in which they loaded CHI/heparin NPs for the delivery of BMP2 and SDF-1, which is
1480 a full organic-based scaffold [106]. Full inorganic-based scaffolds can also be done,
1481 as reported by Cui *et al.* who loaded P28 peptide in enlarged pores hollow MSNs
1482 before embedding them in true bone ceramics. This system showed its ability to
1483 promote MC3T3-E1 cells proliferation and osteogenic differentiation *in vitro* due to
1484 the osteogenic activity of the BMP2 related P28 peptide [156]. Of course, the use of
1485 organic and inorganic material together is common. For example, Yao *et al.* proposed
1486 the encapsulation of BMP2 in MSNs embedded in gelatin 3D nanofibrous scaffold
1487 further coated with deferoxamine-modified CHI [109]. This allowed the delivery of
1488 deferoxamine in addition to BMP2, a molecule able to activate the hypoxia-inducible
1489 factor- α and to trigger angiogenesis. The scaffold and BMP2 release are notably
1490 illustrated in Erreur ! Source du renvoi introuvable. **A**.

1491 The integration of the particles can be more complex. For example, Hettiaratchi *et*
1492 *al.* embedded heparin MPs in PCL nanofibers that were formulated as a mesh further
1493 placed around a COL sponge [192].

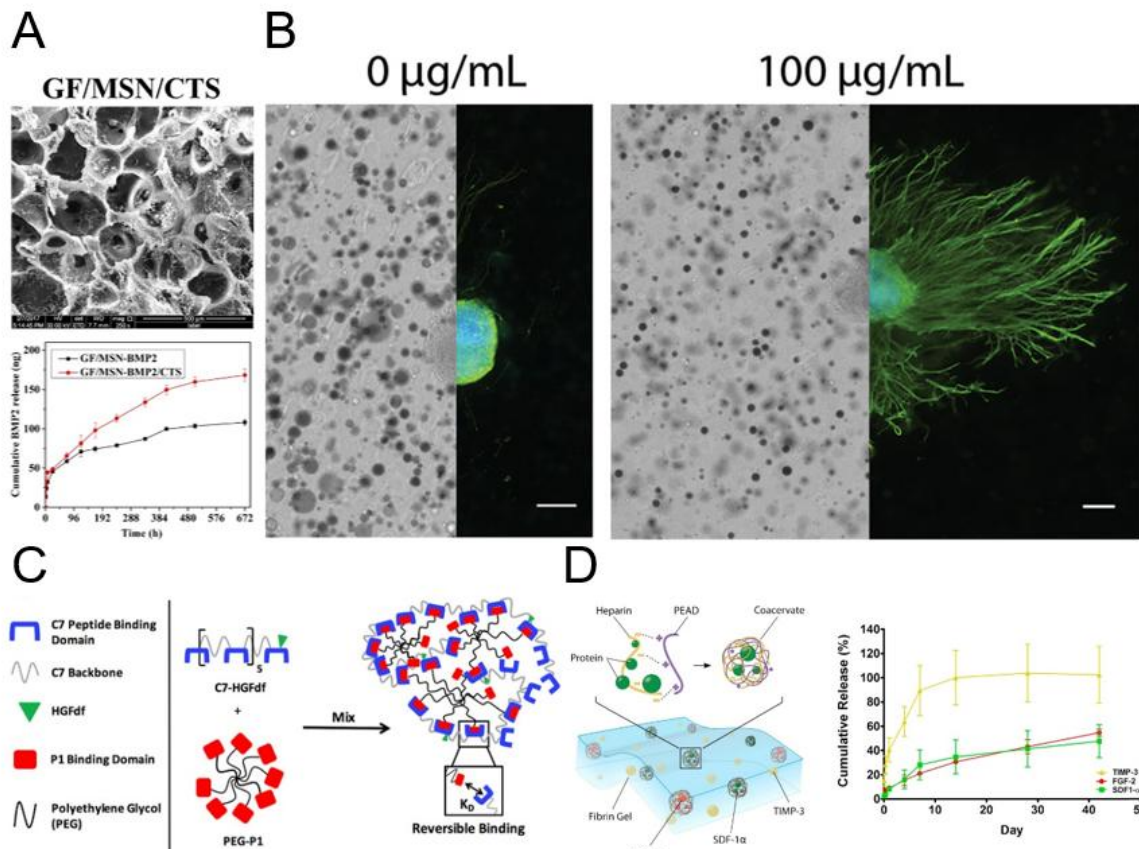
1494 Of course, other material formulations can be embedded in a scaffold especially
1495 for the co-delivery of growth factors. Kuttapan *et al.* notably reinforced a gelatin
1496 scaffold containing silica-coated nanoHAP with oriented poly(L-lactic acid) (PLLA)
1497 fibrous yarns [152]. This system was studied for the co-delivery of VEGF+BMP2 and
1498 FGF2+BMP2 due to the angiogenesis property of VEGF and the ability of FGF2 to
1499 stimulate stem cell migration.

1500

1501 As seen above, BMP2 is not the only protein studied for bone tissue engineering:
1502 VEGF notably induces interest. It has for example been loaded in alginate MPs
1503 further embedded in a COL-HAP scaffold, combining the angiogenesis ability of
1504 VEGF and the osteoinductive property of HAP [167]. In another study, it was loaded
1505 with L-ascorbic acid 2-phosphate, a derivative of ascorbic acid which is essential for
1506 COL biosynthesis, in avidin-modified PLGA NPs [100]. These NPs were then
1507 embedded in a polymer solution made of poly(vinyl acetate) (PVAc), CHI, PLLA and
1508 biotin-modified-PEI before freeze-drying. The good integration of the NPs in the
1509 polymer solution was due to the avidin-biotin conjugation.

1510 SDF-1 was also interesting due to its ability to promote cell migration and
1511 osteogenic differentiation. Then, Zhang *et al.* proposed an HAP scaffold coated with
1512 alginate [14]. This coating allowed the loading of SDF-1 and dexamethasone (DEX)-
1513 loaded hydroxypropyl- β -cyclodextrin microspheres. The *in vitro* experiment showed
1514 the migration of rat bone marrow MSCs inside the scaffold and their osteogenic
1515 differentiation.

1516 High-mobility group box 1 (HMGB1), an osteogenic cytokine, was also loaded in
1517 gelatin sponge, which was combined with MSCs sheets to increase fracture healing
1518 rate [193].



1519 **Figure 5:** A. SEM pictures of the scaffold and resulting release profile of BMP-2 (adapted from article [109]). B. In
 1520 vitro neurite outgrowth in presence of NGF unloaded and loaded microparticles (adapted from article [194]). C.
 1521 Schematic illustration of the HG (adapted from article [144]) D. Schematic illustration of the HG and the release
 1522 profile of the different proteins (reproduced from article [195])
 1523

1524

1525

V.1.2 Fibers

1526

1527 Fibers are very interesting scaffolds for tissue engineering as their structure
 1528 mimics the ECM and provide good support for cell adhesion, migration and
 1529 proliferation. A very used material to design fibers for bone tissue engineering is PLA,
 1530 alone or in combination. For example, Bhattarai *et al.* developed PLA/BMP2 core –
 1531 PLA/TUDCA sheath fibers to deliver two therapeutic agents: BMP2 and
 1532 tauroursodeoxycholic acid (TUDCA), an angiogenic factor. The *in vitro* studies
 1533 conducted on hMSCs and human umbilical vein endothelial cells (HUVECs)
 1534 confirmed the ability of the system to promote angiogenic and osteogenic
 1535 differentiation [196]. Regarding the combinations, it has notably been associated with
 1536 PVA. Da Silva *et al.* notably studied the delivery of BMP2 from PVA/BMP2 core-PLA
 1537 sheath fibers compared to monolithic PLA and PVA fibers [154] and Wang *et al.*
 1538 evaluated the impact of cold atmospheric plasma treatment on BSA/PVA core-PLLA
 1539 sheath fibers characteristics [80]. In these examples, the protein cargo was loaded
 1540 only in the core of the fiber, but other possibilities have been explored. For example,
 1541 Cheng *et al.* reported the synthesis of BMP2/PVA core- silk fibroin/PCL sheath fibers
 1542 coated by CHI and connective tissue growth factor (CTGF), another angiogenic
 1543 growth factor, via LBL [197].

1543

1544 At last, in another study reported by Aragón *et al.*, PCL/HAP nanorods core-PCL
 1545 or PVAc sheath fibers were decorated with BMP2-loaded PLGA NPs via
 simultaneous electrospinning during the coaxial electrospinning [81].

1546

1547

V.1.3 Hydrogels

1548

1549

1550

1551

1552

1553

1554

1555

HG systems have also been proposed for the delivery of BMP2 for bone tissue engineering. Alginate HG has notably been investigated in comparison with COL sponge [198] and as a delivery system for BMP-loaded heparin MPs [71]. In both studies, the bioactivity of the released BMP2 was retained as assessed by ALP activity of MC3T3 cells and C2C12 cells respectively. Olthof *et al.* proposed another material, oligo[(polyethylene glycol) fumarate] bis[2-(methacryloyloxy) ethyl] phosphate (OPF-BP), to obtain an HG. BMP2-loaded PLGA MPs were then loaded within the HG by adsorption [61].

1556

1557

1558

1559

1560

1561

Some studies also reported the use of glue. For example, Huber *et al.* investigated the possibility to use commercial demineralized bone matrix (DBM) putty as BMP2 delivery system to enhance the osteoinductive ability of the DBM [199]. In another study, Enezei *et al.* compared the BMP2 and VEGF expression in dental stem cells after treatment with VEGF-loaded fibrin glue or VEGF-loaded fibrin glue treated with porous biphasic calcium phosphate [200].

1562

1563

V.2 Cartilage tissue engineering

1564

V.2.1 Fibers

1565

1566

1567

1568

1569

1570

1571

1572

1573

1574

1575

1576

1577

1578

1579

TGF- β is a family of cytokines essential for fibrocartilage and cartilage formation, which make these cytokines proteins of choice for cartilage tissue engineering. Thus, several fibers have been designed for their delivery. Among the organic material, PCL is often used as building block due to its biocompatibility, good biodegradability and low interactions with cells (bio-inert material). For example, Qu *et al.* synthesized monolithic fibers composed of PCL, PLGA, BSA and TGF- β 3 for the delivery of TGF- β 3 and this system allowed the proliferation and fibrochondrogenic differentiation of synovium-derived stem cells (SDSC) [201]. PCL fibers were also used as the support for LBL coating of TGF- β 3-loaded CHI nanogels and polyanions. This study notably aimed at showing the possibility to fabricate this construct and to test several polyanions for it (alginate, chondroitin sulfate, HA) [202]. Core-sheath fibers were also proposed for this protein. For example, Wang *et al.* synthesized rhTGF- β 3/BSA/PBS core – P(LLA-CL)/COL sheath fibers and showed that the bioactivity of TGF- β 3 was retained after release by checking the production of COL type II and GAGs by chondrocytes [203].

1580

1581

1582

1583

1584

Inorganic nanofibers have also been studied for the delivery of TGF- β 1 and growth differentiation factor-5 (GDF-5) due to their ability to induce human adipose stromal cell differentiation into intervertebral disk nucleopulpocytes. More precisely, the system was rod-shape colloidal silica nanofibers and the study assessed the bioactivity of the released proteins [204].

1585

1586

V.2.2 Macroporous scaffolds

1587

1588

1589

1590

1591

A MacPS has been proposed for anterior cruciate ligament (ACL) regeneration. The scaffold consisted of silk mesh cross-linked to SDF-1-loaded COL sponge. The authors studied the effect of the SDF-1 release on ligament-derived stem/progenitor cells (LSPCs) and the results showed the SDF-1-induced recruitment of LSPCs inside the scaffold and formation of tendon tissue [104].

1592

1593

V.3 Nerve tissue engineering

1594

V.3.1 Fibers

1595 The use of fibers for nerve repair is very interesting as the structure of the fiber
1596 can direct the growth of neurons and enhance it. Whitehead *et al.* reported the
1597 synthesis of NGF-loaded PLGA MPs embedded in HA aligned fibers [194]. The
1598 system provided a mechanically good environment for dorsal root ganglia (DRG)
1599 growth. As illustrated in Erreur ! Source du renvoi introuvable. **B**, the aligned fibers
1600 enhanced the neurite outgrowth of DRG in presence of NGF-loaded MPs. A dual
1601 delivery scaffold has also been developed for such application [162]. The system
1602 consisted of PLLA fibers encapsulating β -NGF with VEGF adsorbed on its surface.
1603 This design allowed a fast release of VEGF as it was adsorbed on the surface and a
1604 slow continuous release of NGF, allowing the enhancement of neural differentiation
1605 of induced pluripotent stem cells-derived neural crest stem cells (iPSCs-NCSCs) *in*
1606 *vitro*.

1607

1608 V.3.2 Hydrogels

1609 HG is a good system for neural regeneration, as it is a good support in which cells
1610 can migrate and proliferate, which is also used to help the transplantation of cells. HG
1611 systems delivering proteins have been developed these last five years for these
1612 reasons [205]. One interesting system combining PLA nanofibers of different sizes
1613 and self-assembling peptide-Fmoc/DIKVAV HGs in order to well mimic the ECM has
1614 been proposed [206]. The system was studied for the release of GDNF or brain-
1615 derived neurotrophic factor (BDNF) individually, both known for their ability to
1616 increase neuron survival and metabolic activity. The study tried different loading: the
1617 GDNF was embedded in the fibers by blending while the BDNF was immobilized on
1618 the fibers surface through covalent bond. This led to different release profiles, which
1619 were a burst release for GDNF and a sustained release for BDNF.

1620

1621 V.3.3 Macroporous scaffolds

1622 Nguyen *et al.* proposed an hybrid scaffold delivering neurotrophin-3 (NT-3), which
1623 actions leads to neuronal survival, axonal sprouting and regeneration, and miR-222,
1624 a model microRNA which can promote severed axons regeneration by participating in
1625 the synthesis of proteins at distal axons [76]. The system consisted of poly (ϵ -
1626 caprolactone-co-ethyl ethylene phosphate) (PCLEEP) nanofibers embedded in a
1627 COL solution prior to freeze-drying to obtain the scaffold. NT-3 was loaded inside the
1628 COL solution while the miR-222 was loaded in micellar NPs made of PCL-PEG and
1629 PCL-PPEEA (poly(ϵ -caprolactone)-block-poly(2-aminoethyl ethylene phosphate)).
1630 The system notably showed positive results *in vivo*, as it will be described in section
1631 VII.

1632

1633 V.3.4 Films

1634 A multifunctional film has also been proposed for the guidance of neuron growth.
1635 The study reported the synthesis of a PLLA film presenting longitudinal micropattern.
1636 The film was loaded with β -NGF on the surface following a gradient and with β -NGF-
1637 polyanhydride MPs. The surface loading allowed a fast release of the growth factor
1638 while the MPs allowed a controlled release. Altogether, it could guide and direct
1639 neurite outgrowth of PC12 cells [92].

1640 To the best of our knowledge, this is the only example of auto-supported film
1641 delivering proteins developed these last years for implantation. However, films as
1642 protein delivery systems can be designed as coatings to be added on implants. For
1643 example, Sivak *et al.* compared the effect of silk-trehalose film loaded with

1644 chondroitinase ABC and/or GDNF inserted in a silk nerve conduit on the regeneration
1645 of rat sciatic nerve [207].

1646 **V.4 Cardiac tissue engineering**

1647 **V.4.1 Patches**

1648 The development of patches for cardiac tissue engineering is interesting due to
1649 several reasons. For example, O'Neill *et al.* developed an alginate MPs-loaded COL
1650 patch for the delivery of HGF and insulin-like growth factor-1 (IGF-1) from the MPs.
1651 These proteins induce the recruitment and proliferation of cardiac stem cells (CSCs).
1652 Then, the implantation of such system could promote the *in vivo* CSCs migration and
1653 proliferation at the infarct site and so avoid the implantation of *in vitro* cultured CSCs
1654 [208]. Fleischer *et al.*, on their site, developed a system that could mimic the structure
1655 of cardiac tissue [209]. Their system consisted of an LBL patch incorporating cells,
1656 particles and drug. More precisely, the layers were made with albumin electrospun
1657 fibers further carved with a laser. One layer presented microchannels to orient the
1658 seeded endothelial cells, one layer presented microtunnels with side cages and was
1659 loaded with endothelial cells as well and VEGF-loaded PLGA NPs, for the VEGF
1660 angiogenesis property, and the last layer was caged-like patterned and was loaded
1661 with DEX-loaded PLGA NPs, for the anti-inflammatory property of DEX.

1662 **V.4.2 Hydrogels**

1663 HGs have also been used to ensure a better delivery of growth factors after MI.
1664 Then, Steele *et al.* designed an HG for the delivery of HGFdf as it has anti-apoptotic,
1665 pro-angiogenic and cardio-protective properties [144]. More precisely, they designed
1666 a “Shear-thinning Hydrogels for Injectable Encapsulation and Long-term Delivery”
1667 named SHIELD, which is an HG able to support injection. Indeed, it turns to a
1668 solution state when submitted to shear force, and then turns back to HG state. The
1669 HG they developed is illustrated in Erreur ! Source du renvoi introuvable.**C.** The
1670 shear-thinning/self-healing ability of the HG was assured by the P1-C7 peptidic
1671 molecular recognition and reversible binding. Co-delivery of several growth factors
1672 have also been proposed by Awada *et al.* [195]. They loaded a fibrin gel with tissue
1673 inhibitor of metalloproteinases 3 (TIMP-3) and two types of coacervate made with the
1674 synthetic polycation poly(ethylene argininy laspartate diglyceride) (PEAD) and
1675 heparin/protein. The protein was either bFGF-2 or SDF-1 α . This system combines
1676 the cell recruitment ability of SDF-1 α , the angiogenesis property of bFGF2 and the
1677 ability of TIMP-3 to reduce ECM degradation. This system is illustrated in Erreur !
1678 Source du renvoi introuvable.**D.**

1680 **V.5 Other applications of implantable matrices**

1681 **V.5.1 Diabetes treatment**

1682 A possibility to treat diabetes type I is the use of islet transplantation, which then
1683 implies to find a good site of implantation without causing a high immune response.
1684 Thus, Liu *et al.* developed a system delivering the cytokine IL-33, which can have
1685 pro- or anti-inflammatory effect depending on its environment, to support cell
1686 transplantation in adipose tissue. The systems consisted of a disk-shape inner layer
1687 made of mannitol and IL-33-loaded PLGA MPs compressed between two outer
1688 layers of PLGA. The bioactivity of the released IL-33 was assessed by checking the
1689 production of IL-13 from naïve T cells [210].

1690 **V.5.2 Cancer treatment**

1693 An HG delivery system has been proposed for cancer treatment to provide local
 1694 drug delivery and overcome the possible difficulty of circulating systems to reach their
 1695 target. The system was an oligopeptide HG encapsulating hirudin for its anti-
 1696 angiogenic property and TRAIL for its apoptosis property. More precisely, the HG
 1697 was made of F-moc and FF-DOPA which the self-assembly was catalysed by the
 1698 protease WQ9-2. The anti-angiogenic activity of the system was assessed on
 1699 HUVECs and the apoptotic activity of TRAIL was assessed on human breast cancer
 1700 cells MDA-MB-231 [145].

1701
 1702

V.5.3 Internal wound healing

1703 Lokhande *et al.* proposed an injectable HG that could be used as hemostat to treat
 1704 internal haemorrhage. This HG was made with κ -carrageenan and was reinforced
 1705 with 2D nanosilicates. This addition of nanosilicate increased the hMSCs adhesion
 1706 and spreading on the HG. For example, with 2 % nanosilicate, the area on which
 1707 cells spread was increased by 400 %. The study also showed the ability of the
 1708 system to accelerate blood clotting and to deliver VEGF, which led to enhanced
 1709 wound healing in a scratch assay [72].

1710

1711 Some implantable matrices and their major *in vitro* results are summarized in

1712 **Table 4.**

1713 **Table 4:** Interesting *in vitro* results obtained with implantable matrices

System/ Application	Material	Protein / therapeutic moieity	Therapeutic ability	<i>In vitro</i> cell line model	Main result	Ref
MacPS Bone tissue eng.	PDA-coated PLA 3D printed wheel	BMP2	Osteogenesis	MG-63 hMSCs	Biocompatibility, osteogenesis	[111]
MacPS Bone tissue eng.	MesoCS NPs in PCL 3D-printed scaffold	BMP2	BMP2: osteogenesis MesoCS: bone-like apatite formation	WJMSCs	Osteogenic differentiation, calcium deposition	[112]
MacPS Bone tissue eng.	Commercial gelatin sponge	HMGB1	Osteogenesis	MSCs, MSCs sheets	STAT3-mediated osteogenic differentiation	[193]
Fiber Bone tissue eng.	PLGA-NPs on PCL/HAPn core- PCL or PVAc sheath	BMP2 and HAPn	PCL: osteoinduction and osteoconduction BMP2: osteogenesis HAPn: osteoconduction	Human osteoblasts	Enhanced bone markers expression (ALP, OCN, OPN)	[81]
HG Bone tissue eng.	Fibrin glue with or without porous BCP	VEGF	Angiogenesis	Dental stem cells	Higher osteogenesis and angiogenesis gene expression	[200]
Fiber Cartilage tissue eng.	PCL/PLGA/BSA fibers as a mesh	TGF- β 3	Fibrochondrogenic differentiation, increases COL synthesis	SDSCs	Fibrocilage-like matrix deposition	[201]
MacPS Cartilage tissue eng.	Knitted silk mesh cross-linked to COL sponge	SDF-1	Cell recruitment	LSPCs	Stem cell recruitment of the scaffold	[104]
Fiber Nerve tissue eng.	PLLA fibers used as nerve conduit	VEGF ¹⁶⁵ β -NGF	VEGF: angiogenesis β -NGF: neurogenesis	iPSCs- NCSCs	Enhanced proliferation and neural differentiation	[162]
HG Nerve tissue eng.	PLA nanofibers in Fmoc/DIKVAV HG	GDNF BDNF	Increase neuron survival and metabolic activity	Primary CNCs culture	Increased metabolic activity	[206]
Film Nerve tissue eng.	PLLA porous film and polyanhydride MPs	β -NGF	Promote neurite outgrowth	PC12 cells	Guided neurite outgrowth	[92]
Patch Cardiac tissue eng.	Alginate MPs in COL patch	HGF IGF-1	HGF: cell migration IGF-1: cell proliferation and anti-apoptotic effect	c-Kit ^{POS} Cardiac Stem Cells	Cell migration and enhanced proliferation	[208]
HG Cardiac tissue eng.	SHIELD (PEG-P1 and C7-HGFdf)	HGFdf	Anti-apoptotic, pro- angiogenic and cardioprotective	NCm, HUVECs	Cell viability against hypoxia, angiogenesis	[144]

Fiber Diabete	CHI/PEO	Insulin	Hypoglycemic effect	3T3-L1	Released insulin is bioactive	[211]
MacPS Diabete	PLGA	Cytokine IL-33	Ani-inflammatory effect	Naïve T cells	Released IL-33 is bioactive	[210]
HG Cancer	Oligopeptides Fmoc-F and FF-DOPA	Hirudin TRAIL	Hirudin: anti-angiogenesis TRAIL: proapoptotic agent	MDA-MB-231, MCF-10A HUVECs	Anti-tumor activity of the co-delivering system	[145]

1714 MacPS MacroPorous scaffold; eng. Engineering; PDA polydopamine; PLA poly(lactic acid); BMP2 bone morphogenetic protein
1715 2; MG-63 human osteoblast-like cell line; hMSCs human mesenchymal stem cells; MesoCS mesoporous calcium silicate; NPs
1716 Nanoparticles; PCL poly(caprolactone); WJMSCs Human Wharton's Jelly mesenchymal stem cells; HMGB1 high-mobility group
1717 box 1; PLGA poly(lactic-co-glycolic acid); HAPn hydroxyapatite nanorods; PVAc polyvinyl acetate; ALP alkaline phosphatase;
1718 OCN osteocalcin; OPN osteopontin; BCP biphasic calcium phosphate; VEGF vascular endothelial growth factor; BSA bovine
1719 serum albumin; TGF-β3 transforming growth factor-β3; SDSCs synovium-derived stem cells; SDF-1 stromal cell derived factor-
1720 1; LSPCs ligament-derives stem/progenitor cells; PLLA poly(L-lactic acid); β-NGF β-nerve growth factor; iPSCs-NCSCs induced
1721 pluripotent stem cells-derived neural crest stem cells; IGF-1 insulin-like growth factor-1; BDNF brain-derived neurotrophic factor;
1722 NSCs neural stem cells; Fmoc/DIKVAV fluorenylmethyloxycarbonyl capped aspartic acid-isoleucinelysine- valine-alanine-valine;
1723 GDNF glial cell-line derived neurotrophic factor; CNCs cortical neurons cell; MPs microparticles; PC12 cells Rat
1724 pheochromocytome; HGF hepatocyte growth factor; SHIELD Shear thinning Hydrogels for Injectable Encapsulation and Long-
1725 term Delivery; HGFdf hepatocyte growth factor dimeric fragment; NCm neonatal cardiomyocytes; HUVECs human umbilical vein
1726 endothelial cells; CHI chitosan; PEO poly(ethylene oxide); 3T3-L1 preadipocyte cells; TRAIL tumor necrosis factor-related
1727 apoptosis inducing ligand; MDA-MB-231 human breast cancer cells; MCF-10A human normal breast epithelial cells
1728
1729

1730

1731 VI Covering systems

1732 Covering systems refer to systems that are aimed at being deposited on a body
1733 surface. Such systems are mainly used to regenerate damaged skin tissue, but can
1734 also be used as transdermal delivery system to cross the skin barrier or even as
1735 transbuccal delivery systems.

1736 VI.1 Tissue healing

1737 VI.1.1 Fibers

1738 As fibers mimic the ECM architecture, they are a system of choice to deliver
1739 proteins to regenerate the skin. Neovascularization is an important phenomenon to
1740 reach tissue regeneration, which makes VEGF a very good growth factor to deliver
1741 as it promotes angiogenesis.

1742 Thus, Zigdon-Giladi *et al.* synthesized PEO/VEGF core-PCL/PEG sheath fibers to
1743 improve angiogenesis [212]. The authors notably studied the effect of PEG quantity
1744 on the pore size of the shell and release profile of VEGF. The results showed that the
1745 pore size and density increase with increased PEG quantity. The release profile
1746 presented typically a burst release followed by a sustained release. The authors
1747 showed the possibility to tune the sustained release time by playing on the PEG
1748 quantity: the continuous release increased from 4 to 18 h by decreasing the PEG
1749 amount from 3 % to 0.25 %.

1750 VEGF has also been co-delivered with TGF- β 3 [163]. In this study, PLGA
1751 nanofibers were coated with heparin/protein (VEGF or TGF)-PEAD coacervate. This
1752 coating strategy was operated to avoid the exposition of the growth factors to the
1753 electrospinning formulation conditions. The bioactivity of the released growth factors
1754 was assessed by checking the proliferation of human dermal fibroblast and tubule
1755 formation of HUVECs. The results showed the higher biological response of
1756 nanofibers loaded with the dual-drug coacervate, compared to the sample treated
1757 with VEGF-coacervate-loaded fibers and free TGF- β 3 (Coa-V-Free T) and to the
1758 sample treated with TGF- β 3-coacervate-loaded fibers and free VEGF (Coa-T-Free
1759 V). The capillary tubule total length was around 13 mm for the dual-drug coacervate-
1760 loaded fibers while it was around 9 mm for the Coa-V-Free T and around 7 mm for
1761 the Coa-T-Free V in the tubule formation experiment with HUVECs.

1762 As the migration and proliferation of fibroblasts are important phenomena for
1763 wound healing, the delivery of PDGF-BB for this application is a good strategy to
1764 investigate as it can promote these phenomena. Thus, Piran *et al.* embedded PDGF-
1765 BB-loaded CHI NPs in PCL nanofibers for wound healing and evaluated its effect on
1766 fibroblast migration and proliferation [213]. The results showed a chemotactic
1767 behaviour more pronounced toward PDGF-BB-containing scaffold and a three-fold
1768 higher expression of the Arp2 gene when cells were seeded on PDGF-BB-containing
1769 scaffold. This gene is involved in cell protrusion, a phenomenon occurring during cell
1770 migration. Altogether these results showed the ability of the PDGF-BB-containing
1771 scaffold to promote cell migration.

1772 VI.1.2 Films

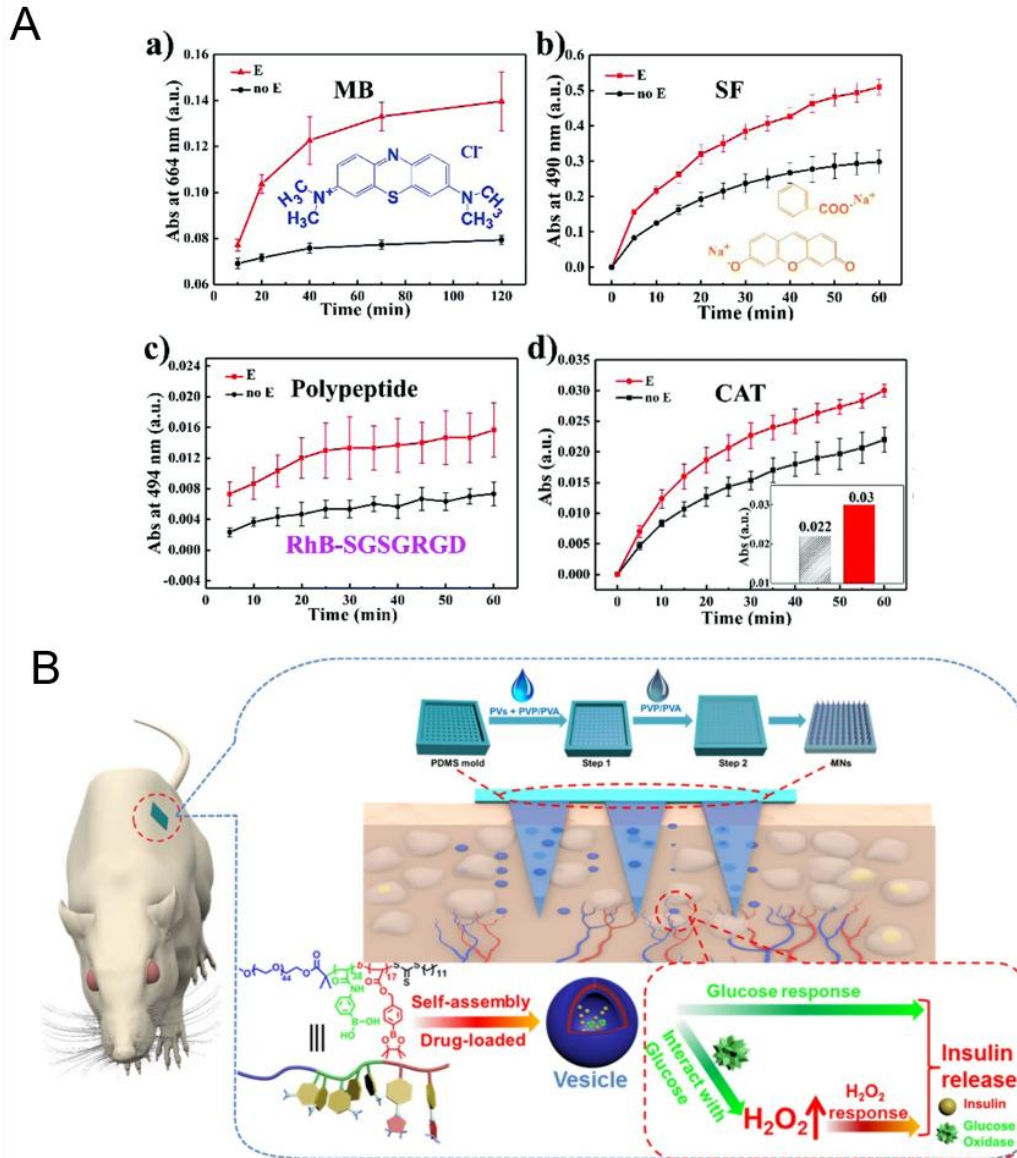
1773 A certain interest in the design of films for wound healing is growing, notably
1774 because it can cover the wound and then protect it from the environment.

1775 Thus, Qi *et al.* developed a zein-based film [97]. These authors notably modified
1776 zein with citric acid and acetic anhydride to modify its hydrophilicity. The fibrous film
1777 was then cross-linked with sodium hexametaphosphate, which gave it the ability to
1778
1779

1780 swell in pure water and phosphate buffer solution like an HG. The obtained films
1781 were completely characterized and their protein adsorption and release ability were
1782 tested with BSA and cytochrome C due to their opposite charge. The experiments
1783 showed better results with the positively-charged cytochrome C.

1784 On their side, Mandapalli *et al.* proposed an LBL film made of CHI and sodium
1785 alginate for the co-delivery of the growth promoting agent epidermal growth factor
1786 (EGF) and the TGF- β small interfering RNA (TGF- β siRNA) [214]. This siRNA is
1787 supposed to silent the TGF- β gene expression, which will stop the COL production.
1788 This will avoid scar formation during the healing as it is due to a surproduction of
1789 COL caused by a surpopulation of fibroblast and a decrease of collagenase within
1790 the wound site. The two therapeutics were added to the film as layers in the LBL
1791 process and the study compared their individual and co-delivery. The unloaded LBL
1792 film notably showed good cell adhesion of A431 epidermal keratinocytes without
1793 bacterial colony formation as tested with *Escherichia coli* (*E. coli*) and
1794 *Staphylococcus aureus* (*S. aureus*). The efficiency of the loaded LBL film was
1795 assessed *in vivo* and will be described in the next section.

1796 More recently, Zhang *et al.* reported the development of a complex LBL film which
1797 is mechanically sensitive [126]. The system consists of a first layer being a
1798 piezoelectric-dielectric film, the mechano-sensitive part of the system. More precisely,
1799 this layer is made with the piezoelectric polymer poly(vinylidene fluoride-co-
1800 hexafluoropropylene) (PVDF-HFP) filled with 4-azidotetrafluorobenzoic acid (TFB)-
1801 modified rGO (graphene oxide). Then, LBL adsorption was performed on this layer,
1802 first with PAH and MSNs and second with PAH and 4,4'-Diazostilbene-2,2-disulfonic
1803 acid disodium salt (DAS). This PAH/DAS part was further cross-linked under UV light
1804 and the system was then loaded with positively charged methylene blue (MB),
1805 negatively charged sodium fluorescein (SF), zwitterionic peptide RhB-SGSGRGD or
1806 the enzyme catalase (CAT). The results showed the ability of the film to accelerate
1807 the drug release under mechanical stimuli, whatever the cargo as it can be seen in
1808 **Figure 6A**. More importantly, the CAT activity, which is the disruption of H₂O₂ into
1809 H₂O and O₂, was retained. Indeed, the viability of human lung fibroblast cells
1810 (HLFCs) exposed to H₂O₂ was increased by 10-30 % after treatment with the CAT-
1811 loaded film.



1812

1813 **Figure 6:** A. Release of several proteins by a piezoelectric-dielectric film with and without finger-pressing
 1814 (adapted from article [126]). B. Schematic illustration of the fabrication of the patch and the release pathways
 1815 (reproduced from article [95]).

1816

1817 VI.1.3 Hydrogels

1818 A study reported the development of liposome/gelatin methacrylate composite HG
 1819 for the delivery of SDF-1 α to induce cells migration to the wound site [171]. The use
 1820 of type B gelatin assured the biocompatibility of the system, as it is a denatured form
 1821 of COL, and its protease-induced degradability. As for the use of liposome to
 1822 encapsulate SDF-1 α , it was operated to better control the release of the protein drug.
 1823 *In vitro* experiment showed that the system retained SDF-1 α activity as it enhanced
 1824 hMSCs migration and induced mTOR signalling activity. This was interesting as the
 1825 mTOR pathway is involved in the stimulation of cells metabolism, migration and pro-
 1826 healing protein production.

1827

1828
1829
1830
1831
1832
1833
1834
1835
1836
1837
1838
1839
1840
1841
1842
1843
1844
1845
1846
1847
1848
1849
1850
1851
1852
1853
1854
1855
1856
1857
1858
1859
1860
1861
1862
1863
1864
1865
1866
1867
1868
1869
1870
1871
1872
1873
1874
1875
1876

VI.1.4 Macroporous scaffolds

A MacPS scaffold has been designed for wound healing, combining the ability of silk fibroin particles to protect sensitive molecules, the ability of silk fibroin scaffold to promote wound healing by supporting cell growth and several functionalities of insulin [105]. Indeed, insulin can stimulate the migration and proliferation of keratinocytes as well as tube formation of endothelial cells, a typical angiogenesis phenomenon improving wound healing. The system was made by LBL of silk fibroin solution and insulin core-silk fibroin shell MPs and showed improved wound closure in scratch assay operated with HaCaT cells and EA. Hy926 cells, which are human keratinocyte cell line and human endothelial cell line respectively.

VI.2 Transdermal drug delivery

MNs patches are widely developed for transdermal delivery, and notably for the treatment of diabetes as it allows the delivery of drugs without damaging the tissue, bleeding and pain. The protein drug can then be directly loaded in the system, as proposed by Seong *et al.* who designed an MNs patch with bullet-shaped MNs made of two layers [93]. The external layer was made of swellable PS-PAA while the internal layer was made of non-swellable PS. *In vitro* experiment showed that 60 % of the loaded insulin was released and that 70 % of the released insulin retained its structure integrity.

In another study, the release of loaded proteins was ensured by a charge-invertible polymer micelle [88]. The MNs patch was made with PLLA and was then coated with the charge-invertible polymeric micelles made of poly(2-(diisopropylamino) ethyl methacrylate – block – methacrylic acid) (P(DPAEMA-b-MAA)). Then, LBL was operated with proteins (lysozyme, OVA or Cy5-OVA) and polymer (polyamine or PAA). This system was able to deliver the LBL film within one minute to the epidermis due to the charge-inversion of the micelle which disrupts the cohesion between the MNs patch and the LBL film.

The therapeutic protein can also be loaded into particles embedded in the MNs patch. For example, Liu *et al.* simply loaded insulin in CaCO₃ MPs that they embedded in a PVP MNs patch [94]. But more complex system has also been reported: Chen *et al.* proposed an alginate MNs patch integrating mineralized particles loaded with either GOx or Ex4, a glucagon-like peptide-1 receptor agonist able to induce insulin production by β -cells [119]. More precisely, GOx was immobilized in copper phosphate mineralized particles, while Ex4 was loaded in calcium phosphate mineralized particles. These different integrations of the protein drugs allowed the release of Ex4 while keeping the glucose-responsive GOx inside the MNs patch. Another example is illustrated in Erreur! Source du renvoi introuvable.**B**. In this example, insulin and GOx were loaded in glucose- and H₂O₂-responsive particles made of PEG, poly(phenylboronic acid) (glucose-sensitive block), and poly(phenylboronic acid pinacol ester) (H₂O₂-sensitive block). These particles were then embedded in the MNs of a PVP/PVA MNs patch [95].

At last, a light responsive system has also been reported for transdermal protein delivery. Indeed, Haine *et al.* added PSS/PAH-coated gold nanorods to a transparent HG film made of gellan gum, chondroitin sulfate and HA. The objective was to use the photothermal property of gold nanorods to enhance the protein delivery to the skin under NIR irradiation [123].

VI.3 Transbuccal drug delivery

1877 The buccal mucosa is a great route for drug administration as it is easy to reach,
 1878 allows the use of non-invasive systems and is estimated to be 4,000 more permeable
 1879 than skin. Delivering drug through buccal mucosa also avoid losing drug because of
 1880 the enzymatic activity and different pH conditions met through the gastrointestinal
 1881 tract. These properties have been exploited by Lancina *et al.* to design a transbuccal
 1882 delivery system for insulin as a solution to avoid subcutaneous injection or infusion
 1883 pump in the treatment of diabetes [211]. The delivery system consisted of
 1884 CHI/PEO/insulin electrospun fibers and the authors notably studied the impact of
 1885 PEO quantity on fibers characteristics. The increase of PEO content induced a
 1886 decrease of the diameter of the fibers and an increase of the release kinetics. The
 1887 activity of released insulin was assessed by checking the AKT phosphorylation of
 1888 3T3-L1 preadipocyte cells, which was significantly increased.

1889 Delivery through the buccal mucosa has also been exploited for the delivery of
 1890 anti-hypertensive peptide (AhP) by the group of M. Pintado. In a first study, they
 1891 loaded AhP in PLGA NPs further embedded in a guar-gum film (GfNP) [155]. The
 1892 permeability of the system was assessed in an *in vitro* model of the epithelium of
 1893 buccal mucosa using TR146 buccal cells. The results showed that the free AhP had
 1894 a faster permeation than AhP-loaded GfNP but that the final amount of AhP found
 1895 within the cell monolayer was higher for the GfNP system. In another study, they
 1896 loaded the AhP in CHI MPs further embedded in CHI film [91]. Experimental designs
 1897 were used to obtain optimal CHI MPs and CHI film and TR146 cells were also used
 1898 as human buccal epithelium model. The optimal MPs had a diameter of 2.5 μm and a
 1899 loading efficiency of 76 % and the optimal film was composed of 0.79 % of CHI, 6.74
 1900 % of sorbitol and 0.82 % of citric acid (w/v). The viability assay on TR146 cells
 1901 showed no cytotoxicity of the system.

1902 The systems and their major *in vitro* results are summarized in **Table 5**.

1903 **Table 5:** Interesting *in vitro* results obtained with covering systems
 1904

System/ Application	Material	Protein / therapeutic moieity	Therapeutic ability	<i>In vitro</i> cell line model	Main result	Ref
Fiber Tissue healing	Coacervate- coated PLGA fibers	VEGF TGF- β 3	VEGF: angiogenesis, reduction of necrosis TGF- β 3: angiogenesis	CCL-64, hDFBs, HUVECs	Bioactivity of growth factors retained	[163]
Fiber Tissue healing	CHI NPs in PCL fibers	PDGF-BB	PDGF-BB: cell proliferation, fibroblast migration CHI: anti-inflammatory	Fibroblast cells	Improved cell mass growth and cell movement	[213]
Film Tissue healing	CHI and Sodium alginate organized in layers	EGF and/or TGF- β siRNA	EGF: growth promoting TGF- β siRNA: reduction of COL production	A431 cells, <i>E. coli</i> , <i>S. aureus</i>	Cytocompatible, prevents bacterial colony formation	[214]
HG Tissue healing	Nanosilicate in κ -carrageenan	VEGF	Angiogenesis	hMSCs, HUVECs	Enhanced wound healing in a scratch assay	[72]
MacPS Tissue healing	Silk fibroin MPs in silk fibroin sponge	Insulin	Angiogenesis, migration and proliferation of keratinocytes	HaCaT cells, EA. hy926 cells	Stimulation of cell migration	[105]
Patch Transdermal drug delivery	Polymeric vesicles in PVP/PVA patch	Insulin and GOx	Insulin: hypoglycemic effect	MCF-7 cells	Cytocompatibility of the loaded polymeric vesicles	[95]
Film Transbuccal drug delivery	PLGA NPs in guar-gum film	AhP	Anti-hypertensive	TR146 cell line	Improved permeation through cell multilayer	[155]

1905 PLGA poly(lactic-co-glycolic acid); VEGF vascular endothelial growth factor; TGF- β 3 transforming growth factor- β 3; CCL-64
 1906 Mink lung epithelial cell line; hDFBs human dermal fibroblasts; HUVECs human umbilical vein endothelial cells; CHI chitosan;
 1907 NPs nanoparticles; PCL polycaprolactone; PDGF-BB platelet-derived growth factor-BB; EGF epidermal growth factor; TGF- β

1908 siRNA transforming growth factor- β small interfering ribonucleic acid; A431 human epidermoid carcinoma cells; *E. coli*
1909 *Escherichia coli*; *S. aureus Staphylococcus aureus*; hMSCs human mesenchymal stem cells; MPs microparticles; HaCaT
1910 immortal human keratinocyte line; EA. hy926 human endothelial cell line; PVP poly(vinylpyrrolidone); PVA poly(vinylalcohol);
1911 GOx glucose oxidase; MCF-7 cells human breast adenocarcinoma cells; AhP anti-hypertensive peptide TR146 human buccal
1912 carcinoma cell line
1913

1914

1915
1916
1917
1918
1919
1920
1921
1922
1923
1924
1925
1926
1927
1928
1929
1930
1931
1932
1933
1934
1935
1936
1937
1938

VII *In vivo* studies

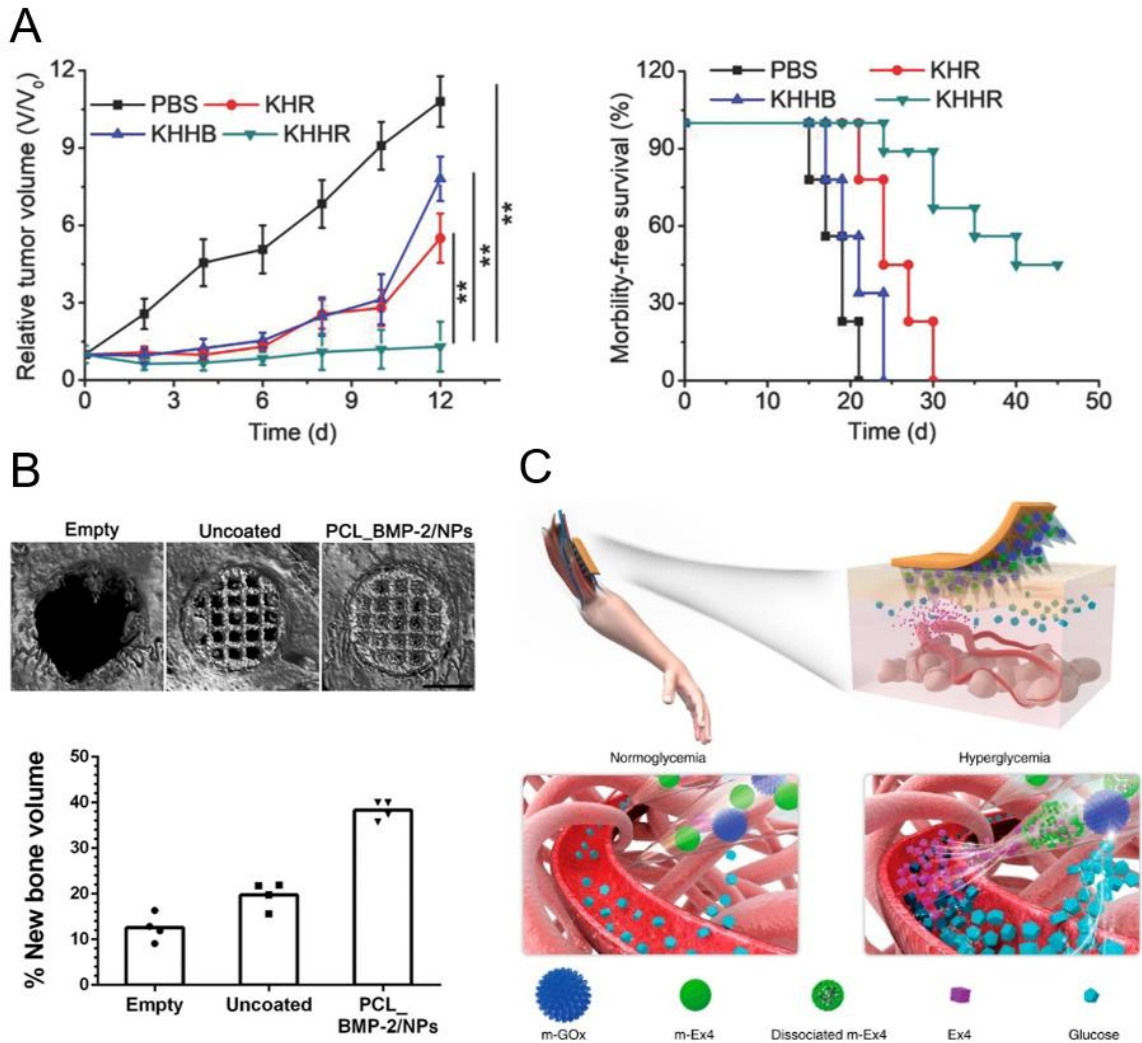
VII.1 Circulating systems

VII.1.1 Cancer treatment

The use of cancerous-cells xenograft tumour-bearing mice is the dominant model to evaluate the efficiency of particle systems on tumours. Then, several cell lines can be used. For example, 4T1 xenograft tumour-bearing BALB/c mice were used as a model to test the efficiency of RNBC-loaded KPEI nanocomplex coated with HA-hematoporphyrin (KHHR) [122]. As illustrated in Erreur! Source du renvoi introuvable.A, the KHHR system stopped the tumour growth, compared to KHHB where RNBC is replaced by BSA, KHR where there is no hematoporphyrin, and PBS. This model has also been used to test the efficiency of PH20-ExSM together with PC3 xenograft tumour-bearing BALBc nu/nu mice. The results showed 83 % inhibition of the PC3 tumour growth and a reduction of the 4T1 tumour volume [56].

HeLa xenograft has also been used and showed the enhanced anti-cancer efficiency of diselenide bridge-containing MSNs when there were coated with cancer cell membrane [35]. Unzueta *et al.* chose the subcutaneous CXCR4+ colorectal cancer xenograft model applied in female Swiss nu/nu mice to confirm the specific accumulation of their T22-GFP-H6 BIB *in vivo* (study presented in perspective due to its originality) [158].

HT29 xenograft tumour-bearing male BALB/c nu/nu mice and CT26.CL25 xenograft tumour-bearing BALB/c mice were also used by Cho *et al.* to evaluate the anti-cancer activity of their SIRP α -ExSM, showing a delayed tumour growth in the HT29 xenograft model and the inhibition of the CT26.CL25 xenograft tumour growth [57].



1939

1940 **Figure 7:** A. Tumor volume and survival rate of mice treated with different particle systems (adapted from article
 1941 [122]). B. Micro-CT images of calvarial defect 8 weeks post-implantation and volume of new bone (adapted from
 1942 article [138]). C. Schematic representation of the glucose-responsive MNs patch (reproduced from Article [119])

1943

1944 **VII.1.2 Diabetes treatment**

1945 In the case of diabetes, the disease is usually induced by injection of a chemical.
 1946 For example, Meneguín *et al.* used alloxan to induce diabetes in Wistar rats to test
 1947 the efficiency of their insulin-loaded gellan gum MPs coated with retrograded starch
 1948 and pectin. The results showed a reduction of glucose up to 7 h post-injection with a
 1949 maximum reduction up to 51.02 % [22]. Another example is the study of Fan *et al.*,
 1950 who induced diabetes in Sprague-Dawley (SD) rats with streptozotocin to confirm the
 1951 absorption mechanism of their insulin-loaded deoxycholic acid-modified CHI NPs.
 1952 The mechanism was confirmed and the study showed a slower but longer reduction
 1953 of blood glucose level notably compared to free insulin [182].

1954

1955 **VII.1.3 Tissue engineering**

1956 A medial meniscal transection (MTT) injury has been reported in SD rats to test
 1957 the ability of TSG-6-loaded heparin MPs to reduce cartilage damage for osteoarthritis
 1958 treatment. TSG-6 is the tumour necrosis factor-alpha stimulated gene 6, it has anti-
 1959 inflammatory property as well as the capacity to inhibits the plasmin responsible for

1960 ECM degradation in osteoarthritis joints. The evaluation of cartilage thickness,
1961 volume and attenuation showed the higher efficiency of TSG-6 when released by the
1962 heparin MPs compared to free TSG-6 [215].

1963 In the domain of nerve tissue engineering, Santhosh *et al.* applied severe clip-
1964 compression SCI at mid-thoracic level in SD rats to test their rhNrg-1 β 1-loaded PLGA
1965 MPs. The results showed that the system reduced scar formation and
1966 neuroinflammation and promoted oligodendrocytes and axons preservation [185].

1967 For cardiac tissue engineering application, the ligation of the left anterior
1968 descending (LAD) coronary artery is quite common for *in vivo* experiment. This model
1969 has been applied in SD rats to check the efficiency of liraglutide-loaded PLGA-PEG
1970 NPs [157]. The injection of these NPs led to the improvement of cardiac functions,
1971 the attenuation of infarct size, the preservation of wall thickness, the promotion of
1972 angiogenesis and the prevention of cardiomyocyte apoptosis. Of course, it is not the
1973 only model used. For example, Díaz-Herráez *et al.* used a chronic MI model applied
1974 in SD rats to study their system, which was Nrg-1-loaded PLGA/COL/PDL MPs with
1975 adipose-derived stem cells adhered on their surface [159]. The study showed the
1976 synergistic effect of the stem cells and the Nrg-1, leading to better
1977 neovascularization. The presence of Nrg-1 also stimulated cardiomyocyte
1978 proliferation and altogether, these effects led to better heart regeneration.

1979 1980 VII.1.4 Inflammatory bowel disease

1981 Ling *et al.* tested their alginate/CHI MPs in two *in vivo* models [116]. They first
1982 used C57BL/6 mice to check the small intestine uptake of eGFP NPs-loaded MPs
1983 and this showed that the system could reach the total gastrointestinal tract. Then,
1984 they checked the efficiency of the AvrA-NPs-loaded MPs in a dextran sulfate sodium
1985 (DSS) colitis mouse model. This study showed the efficiency of the system by
1986 showing the reduction of weight loss and of Disease Activity Index.

1987 1988 VII.2 Implantable matrices

1989 VII.2.1 Bone tissue engineering

1990 VII.2.1.1 Macroporous scaffolds

1991 Bone defect is the most common model used to evaluate the ability of MacPSs to
1992 induce bone regeneration, and among the possible ones, calvarial defect seems to
1993 be the most chosen. It has for example been used in SD rats to check the co-delivery
1994 of rhBMP2 and alendronate by COL sponge. The results showed a greater
1995 regeneration with the co-delivery system, with the new bone presenting a dense
1996 structure with less fatty marrow tissue compared to the rhBMP2 only-loaded COL
1997 sponge [102]. This model has also been applied in Wistar rats by Quinlan *et al.* [167]
1998 and by Kuttappan *et al.* [152]. Indeed, Quinlan *et al.* chose this model to study the
1999 effect of their COL/HAP system containing VEGF-loaded alginate MPs. The
2000 implantation of the system led to the enhancement of angiogenesis and thus to better
2001 osteogenesis [167]. As for Kuttappan *et al.* they chose it to study their gelatin scaffold
2002 containing silica-coated nanoHAP and oriented PLLA yarns. As said previously, the
2003 authors studied the delivery of VEGF+BMP2 and FGF2+BMP2. The *in vivo* studies
2004 showed that both co-delivery induced angiogenesis and bone formation without
2005 differences between the two groups [152].

2006 Finally, the calvarial bone defect model has been applied in New Zealand (NZ)
2007 white rabbit by Kim *et al.* to check their system: a 3D-printed HAP scaffold coated
2008 with a PCL solution containing rhBMP2-loaded PLGA NPs. The study showed

2009 improved bone regeneration as it can be seen in Erreur! Source du renvoi
2010 introuvable. **B** [138]. NZ white rabbits have been used in other studies with a radius
2011 critical bone defect. Bone regeneration with this model has been observed after
2012 implantation of true bone ceramic containing P28-loaded enlarged pores MSNs [156]
2013 and after implantation of BMP2/IL-8-loaded mesoporous bioactive glass. This system
2014 was also implanted in tight muscle pouches of mice as an ectopic bone formation
2015 model [191]. This study showed the ability of the system to recruit stem cells and to
2016 have the formation of cartilage due to IL-8 and the formation of bone due to BMP2.

2017 Other bones can support osteotomy. Thus, Hettiaratchi *et al.* used a femoral
2018 defect in SASCO SD rats to study the effect of their COL sponge surrounded by PCL
2019 nanofiber mesh containing BMP2-loaded heparin MPs. The result showed no
2020 difference in heterotopic ossification, probably due to interactions between heparin
2021 and BMP2 and heparin and proteins present in the serum [192]. As for Xue *et al.*,
2022 they created a radial defect in SD rats to study their HMGB1-loaded gelatin sponge
2023 combined with MSCs sheets. The implantation of the system showed an enhanced
2024 fracture healing promoted by HMGB1 via the STAT3 pathway [193].

2025 MacPSs implantation can also be realized in other tissues. For example,
2026 implantation in muscle has already been mentioned above. The abdominal muscle
2027 pouch model has been used in SD rats to check the osteoconductivity and
2028 osteoinductivity of rhBMP2/zoledronic acid-loaded gelatin/HAP/calcium sulphate
2029 cryogel. The results showed that zoledronic acid allowed the reduction of the rhBMP2
2030 dose and that their co-delivery led to bone formation [151]. It has also been used to
2031 check the osteoinductive property of SDF-1/Dex@CDMs-loaded HAP scaffold [14].
2032 This scaffold was notably implanted in dorsal muscle of beagles and the results
2033 showed the cell recruitment and vascularization into the scaffold and the cell
2034 differentiation leading to the formation of mineralized tissue. Subcutaneous
2035 implantation has also been used in Wistar rats and athymic nude mice. In the first
2036 case, a PLLA nanofibrous scaffold, coated with HAP and grafted with BMP2-loaded
2037 liposomes, was implanted and induced bone formation [75]. In the second case, a
2038 CHI/agarose/gelatin scaffold containing CHI/heparin NPs was implanted after loading
2039 with SDF-1 to check its ability to recruit MSCs [106].

2040 Finally, the ACL reconstruction model has been used in NZ white rabbit to check
2041 the ability of osteoprotegerin/BMP2-loaded COL sponge to promote tendon-bone
2042 healing [189]. This tendon-bone healing was improved with the reduction of bone
2043 tunnel enlargement and an enhanced formation of fibrocartilage and COL fibers at
2044 the tendon-bone interface.

2045

2046

VII.2.1.2 Fibers

2047 The ability of some fibrous systems to promote bone formation has been tested *in*
2048 *vivo* with subcutaneous implantation or implantation in a calvarial bone defect. Both
2049 models were used by Cheng *et al.* to test CTGF/CHI-coated BMP2/PVA core-silk
2050 fibroin/PCL sheath fibers [197]. The first experiment was subcutaneous implantation
2051 in the abdominal midline of nude mice and showed the ability of the system to
2052 promote angiogenesis and osteogenesis. Then, the system was implanted in
2053 calvarial bone defect created in C57BL/6 mice and showed its ability to promote
2054 osteogenesis with ~ 70 % of newly formed bone compared to other groups who
2055 presented maximum ~ 50 %. The calvarial bone defect model has also been used by
2056 Bhattarai *et al.* in NZ white rabbits to check their BMP2/PLA core-TDCU/PLA sheath
2057 fibers. The results showed higher blood vessel and bone formation after the
2058 implantation of the loaded fibers [196].

2059
2060
2061
2062
2063
2064
2065
2066
2067
2068
2069
2070
2071
2072
2073
2074
2075
2076
2077
2078
2079
2080
2081
2082
2083
2084
2085
2086
2087
2088
2089
2090
2091
2092
2093
2094
2095
2096
2097
2098
2099
2100
2101
2102
2103
2104
2105
2106

VII.2.1.3 Hydrogels

HGs were also tested *in vivo*. A femoral bone defect created in SD rats has notably been used by Krishnan *et al.* and by Hettiaratchi *et al.* In the first case, the authors have assessed their alginate HG in comparison with commercial COL sponge to deliver rhBMP2 [198]. Their goal was to evaluate if the alginate HG could prevent heterotopic bone formation when a high dose of rhBMP2 is delivered. The results showed that the implantation of the alginate HG, compared to COL sponge, led to the formation of a higher volume of bone but with the same volume of heterotopic bone. The authors suggested that the high dose of rhBMP2 may be sufficient to induce the heterotopic bone formation. In the second case, the system studied was an alginate HG loaded with BMP2-loaded heparin MPs and contained in a PCL nanofiber mesh tube [71]. The study notably compared this system with BMP2-loaded alginate HG. The results showed that the loading in the heparin MPs allowed higher retention of BMP2 in the bone defect but led to a lower volume of newly formed bone. It is interesting to notice that this system was primarily tested *in vivo* by subcutaneous implantation in SD rats to evaluate some properties of the scaffold, such as the retention of BMP2 in the system *in vivo* and the ability of the system to form mineral tissue.

Subcutaneous implantation was also the model chosen by Olthof *et al.* to check their OPF-BP HG containing BMP2-loaded PLGA MPs [61]. More precisely, they did a comparison between this system, BMP2-loaded PLGA MPs and BMP2-loaded OPF-BP HG. The systems showed different release profiles and the HG alone, with its burst release, showed better bone formation. Last model presented here, the sheep drill hole defect model applied in Merino-mix sheep by Huber *et al.* to test their BMP2-loaded demineralized bone matrix putty. The results confirmed the ability of the system to induce bone healing [199].

VII.2.2 Cartilage tissue engineering

The ACL reconstruction model has been applied in NZ white rabbit to check the ability of SDF-1-loaded COL sponge surrounded by silk mesh to regenerate bone-tendon in combination with intra-articular injection of LSPCs. The experiment showed tendon regeneration and bone tunnel healing with reduction of osteoarthritis [104].

VII.2.3 Nerve tissue engineering

A common way to test if a system is efficient for nerve tissue regeneration is to induce nerve defect. For example, B. Xia and Y. Lv created critical sized defect in SD rats' sciatic nerve to test their VEGF/ β -NGF-loaded PLLA fibrous nerve conduit [162]. The results showed a synergistic effect of both protein drugs leading to neovascularization and nerve healing. Another example is the hemi-incision model at cervical level 5 in SD rats' spinal cord created by Nguyen *et al.* [76]. Their system was an NT-3-loaded COL scaffold containing aligned PCLEEP nanofibers in which miR-222-loaded micelles were embedded. The results showed direct axon regeneration and remyelination without inflammation or scar tissue formation.

VII.2.4 Cardiac tissue engineering

The previously described LBL patch containing endothelial cells, VEGF-loaded PLGA NPs and DEX-loaded PLGA NPs was tested *in vivo*. More precisely, it was

2107 implanted subcutaneously in SD rats' back. The results confirmed the angiogenesis
2108 of the system by showing infiltration of new blood vessels inside the patch [209].

2109 Two HGs were also tested in an *in vivo* MI model induced by ligation of the LAD
2110 coronary artery in rats. The first system, tested in SD rats, consisted of fibrin HG
2111 loaded with TIMP-3 and two types of coacervate, containing either FGF2 or SDF-1 α
2112 [195]. The results showed good tissue repair thanks to revascularization, stem cell
2113 homing and preservation of cardiomyocytes. The implantation of the system also led
2114 to the reduction of inflammation, fibrosis, ECM degradation and ventricular dilation.
2115 The second system, tested in Wistar rats, was the HGFdf-loaded SHIELD HG. The
2116 results showed that the implantation of the system could improve angiogenesis and
2117 reduce fibrosis, limiting adverse remodelling [144].

2118

2119 VII.2.5 Other applications: cancer and diabetes treatment

2120 Like for particles systems, the efficiency of implantable matrices against cancer
2121 can be evaluated in xenograft tumour-bearing mice. Thus, Jiang *et al.* tested their
2122 hirudin/TRAIL-loaded oligopeptide HG in such tumour model, induced by injection of
2123 MDA-MB-231 cells in nude mice. [145]. The synergistic anti-tumour effect of the co-
2124 delivery system was assessed, with a tumour inhibition ratio of ~ 64 % compared to
2125 saline treatment.

2126 In the fate of diabetes treatment, IL-33-loaded PLGA scaffolds were implanted in
2127 C57BL/6 mice after induction of diabetes by injection of streptozotocin [210]. The
2128 results showed that the transplantation of allogeneic islet led to the increase of graft
2129 protective T cell population, the decrease of destructive T cell population but delayed
2130 the islet engraftment.

2131

2132 VII.3 Covering systems

2133 VII.3.1 Tissue healing

2134 VII.3.1.1 Fibers

2135 A first nanofiber system was tested *in vivo* by applying the skin flap model in mice
2136 [163]. This system consisted of coacervate-coated PLGA nanofibers, with the
2137 coacervate containing PEAD, heparin and VEGF and/or TGF- β 3. The experiment
2138 showed a synergistic effect with the co-delivery leading to better skin flap survival
2139 with reduction of necrosis and improvement of blood perfusion. Another system
2140 consisting of VEGF/PEO core-PCL/PEG sheath fibers was tested *in vivo* by
2141 subcutaneous implantation in severe combined immunodeficiency (SCID) mice. This
2142 experiment confirmed the ability of the system to promote cell migration and improve
2143 angiogenesis [212].

2144

2145 VII.3.1.2 Film

2146 A CHI/sodium alginate film was tested in an excisional wound healing model in
2147 C57BL/6 mice to check the effect of TGF- β siRNA and EGF alone or together [214].
2148 The single delivery of the siRNA could reduce the TGF- β protein expression and thus
2149 reduce COL production while the single delivery of EGF improved wound contraction.
2150 The co-delivery of these proteins accelerated wound healing and decreased scar
2151 formation due to the reduction of COL production.

2152

2153 VII.3.1.3 Macroporous scaffold

2154 A MacPS made by LBL of silk fibroin sponge and insulin-loaded silk fibroin MPs
2155 was tested in diabetic SD rats [105]. The diabetes was induced by injection of

2156 streptozotocin and full-thickness wounds were created on rats' back for the treatment
 2157 with the scaffold. The experiment showed that the system significantly accelerated
 2158 the wound closure healing by accelerating wound closure, COL deposition and
 2159 vascularization.

2160

2161 VII.3.2 Transdermal drug delivery

2162 As said before, transdermal delivery is widely looked for the treatment of diabetes.
 2163 Thus, streptozotocin-induced diabetic SD rats were used to test several systems. The
 2164 first one was the PVP/PVA MNs patch containing insulin/GOx-loaded glucose-and
 2165 H₂O₂-responsive vehicles [95]. This experiment showed that the system could reduce
 2166 the blood glucose level with a slower rate but could maintain it in the normoglycemic
 2167 level for 4 h, against 1 h for injection of insulin. In addition, the return to the initial
 2168 blood glucose level was also slower than for injection of insulin (more than 12 h post-
 2169 treatment against 7 h post-injection). This model was also used to test PVP MNs
 2170 patch containing insulin-loaded CaCO₃ MPs. [94]. Here again, the blood regulation
 2171 was slower but longer with the system. The insulin relative bioavailability, which is the
 2172 percentage of insulin absorbed intact by the circulatory system when delivered by the
 2173 DDS compared to subcutaneous injection, was evaluated at 96.6 %. Another
 2174 possibility to study the efficiency of a delivery system to treat diabetes is to use
 2175 C57BL/6 db/db mice, as it is an *in vivo* model for diabetes type II. This model has
 2176 been chosen by Chen *et al.* to test their system illustrated in Erreur ! Source du
 2177 renvoi introuvable. **C**: an alginate MNs patch containing GOx and Ex4 loaded in
 2178 mineralized particles. This study confirmed the ability of the system to regulate blood
 2179 glucose level [119].

2180 Healthy animals were also used to test MNs patches. For example, Seong *et al.*
 2181 used both SD rats and C57BL/6 J mice to evaluate the ability of their double-layered
 2182 MNs patch to deliver insulin [93]. The results confirmed the possibility to use the
 2183 patch as painless transdermal delivery system as it showed a prolonged release of
 2184 insulin and the decrease of blood glucose level. Another system was tested by
 2185 application on the ear of healthy C57BL/6 mice [88]. The system was PLLA MNs
 2186 patch coated with a charge-invertible polymer and an LBL film of OVA and polymer.
 2187 The results showed that the film was delivered to the epidermis in only 1 min and that
 2188 OVA was delivered in a sustained manner over 3 days, leading to an increased
 2189 immune response. Male ddY mice were also used without any induced disease to
 2190 confirm the improved transdermal delivery of FITC-OVA, used as a model protein,
 2191 due to the photothermal property of PSS/PAH-coated gold nanorods embedded in
 2192 gellan gum/chondroitin sulfate/HA film [123].

2193

2194 Some systems and their major results obtained by *in vivo* experiments are
 2195 summarized in **Table 6**.

2196 **Table 6:** Interesting *in vivo* results

System/ Application	Material	Protein / therapeutic moeity	Therapeutic ability	<i>In vivo</i> model	Main result	Ref
CIRCULATING SYSTEMS						
NPs Cancer	RNBC in KPEI nanocomplex coated PS-HA	RNase A Hematopor- phyrin	RNase A: cleaves RNA Hematoporphyrin: ROS production	4T1 tumour in mice	Tumour growth stopped	[122]
ExSM	Exosome from	SIRP α	CD47 antagonist	HT29 or	Tumour growth	[57]

Cancer	HEKT293T cells			CT26.CL25 tumor in mice	delayed (HT29) or inhibited (CT26.CL25)	
MPs Diabetes	Retrograded start/ pectin-coated Gellan gum MPs	Insulin	Hypoglycemic effect	Alloxan diabetes in rats	Maximum glucose reduction up to 51 %	[22]
MPs Bone tissue eng.	Desulfated heparin	TSG-6	Anti-plasmin and anti-inflammatory properties	MMT injury in rats	Reduction of cartilage damage	[215]
MPs Nerve tissue eng.	PLGA	rhNrh-1β1	Differentiation of NPCs into myelin-forming oligodendrocytes	Severe clip-compression SCI in rats	Reduction of scar formation, axons preservation	[185]
MPs Cardiac tissue eng.	Adipose-derived SCs on PLGA/ COL/PDL MPs	Nrg-1	Angiogenesis, cardiomyocyte proliferation, cell survival	Chronic MI model in rats	Synergistic effect inducing better heart regeneration	[159]
IMPLANTABLE MATRICES						
MacPS Bone tissue eng.	Alginate MPs in COL/HAP scaffold	rhVEGF ₁₆₅	rhVEGF ₁₆₅ : angiogenesis HAP: osteoinductive	Calvarial BD in rats	Enhanced angiogenesis and osteogenesis	[167]
MacPS Bone tissue eng.	CDMs-loaded HAP scaffold	DEX SDF-1	DEX: osteogenesis SDF-1: osteogenesis and cell migration	Implantation in dorsal muscle of beagles	Synergic effect: acceleration of bone formation	[14]
Fiber Bone tissue eng.	PVA core – silk fibroin/PCL sheath	BMP2 CTGF	BMP2: osteogenesis CTGF: angiogenesis	Calvarial BD model in mice	Improvement of bone regeneration by 43 %	[197]
HG Bone tissue eng.	Demineralized Bone Matrix putty	BMP2	Osteoinduction	Sheep drill hole defect model in Merino-mix sheep	Complete bone healing	[199]
MacPS Cartilage tissue eng.	Knitted silk mesh cross-linked to COL sponge	SDF-1 LSPCs	SDF-1: cell recruitment LSPCs: tendon-forming cells	ACL model in rabbits	Bone and tendon healing, osteo-arthritis reduction	[104]
Fiber Nerve tissue eng.	PLLA fibers used as nerve conduit	VEGF ₁₆₅ β-NGF	VEGF: angiogenesis β-NGF: neurogenesis	Defect in rat sciatic nerve model	Enhanced neovascularization and nerve healing	[162]
HG Cardiac tissue eng.	Coacervate in fibrin gel	TIMP-3, FGF-2, SDF-1α	TIMP-3: reduction of ECM degradation FGF-2: angiogenesis SDF-1α: recruitment of progenitor cells	MI model in rats by LADCA ligation	Heart tissue regeneration	[195]
COVERING SYSTEMS						
Fiber Tissue healing	PEO core – PCL/PEG sheath	rhVEGF ₁₆₅	Angiogenesis	Subcutaneous mouse model in SCID mice	Cell migration and significant improvement of angiogenesis	[212]
Film Tissue healing	CHI and Sodium alginate organized in layers	EGF and/or TGF-β siRNA	EGF: growth promoting TGF-β siRNA: reduction of COL production	Excisional wound healing in mice	Synergistic effect: reduction of COL deposition and faster wound healing	[214]
MacPS Tissue healing	Silk fibroin MPs in silk fibroin sponge	Insulin	Angiogenesis, migration and proliferation of keratinocytes	Wound in rats Streptozotocin-induced diabetes	Accelerated wound healing	[105]
Patch Transdermal drug delivery	CaCO ₃ MPs in PVP microneedles	Insulin	Hypoglycemic effect	Streptozocin diabete in rats	Slower and longer blood glucose regulation	[94]
Film Transdermal drug delivery	PSS/PAH-coated gold nanorods in gellan gum/chondroitin sulfate/HA film	FITC-ovalbumin	Model protein	ddY mice	Improved protein transdermal delivery thanks to skin heating	[123]

2197 NPs nanoparticles; RNBC 4-nitrophenyl 4-(4,4,5,5-tetramethyl-1,3,2-dioxaborolan-2-yl)benzylcarbonate-modified RNase; KPEI ketal cross-linked polyethylenimine; PS-HA photosensitizer-hyaluronic acid; RNase A ribonuclease A; RNA ribonucleic acid; 2198 ROS Reactive Oxygen Species; 4T1 mouse mammary carcinoma cells; ExSM exosome; SIRPα signal regulatory protein α; 2199 HT29 human colon adenocarcinoma HT29 cells; MPs microparticles; TSG-6 tumor necrosis factor-alpha stimulated gene 6; 2200 MMT medial meniscal transection; PLGA poly(lactic-co-glycolic acid); rhNrh-1β1 recombinant human neuregulin-1β1 peptide; 2201 MMT medial meniscal transection; PLGA poly(lactic-co-glycolic acid); rhNrh-1β1 recombinant human neuregulin-1β1 peptide; 2202 NPCs neural progenitor cells; SCI spinal cord injury; SCs stem cells; COL collagen; PDL poly(-D-lysine); Nrg neuregulin; MI

2203 myocardial infarction; MacPS MacroPorous Scaffold; eng. Engineering; HAP hydroxyapatite; rhVEGF recombinant human
2204 vascular endothelial growth factor; BD bone defect; CDMs hydroxypropyl- β -cyclodextrin microspheres; DEX dexamethasone;
2205 SDF stromal cell-derived factor 1; PVA poly(vinylalcohol); PCL polycaprolactone; BMP2 bone morphogenetic protein 2; CTGF
2206 connective tissue growth factor; LSPCs ligament-derived stem/progenitor cells; ACL anterior cruciate ligament; PLLA poly(L-
2207 lactic acid); β -NGF β -nerve growth factor; TIMP-3 tissue inhibitor of metalloproteinases-3; FGF-2 basic fibroblast growth factor;
2208 SDF-1 α stromal cell-derived factor 1- α ; LADCA left anterior descending coronary artery; PEO poly(ethylene oxide); PEG
2209 poly(ethylene glycol); SCID severe combined immunodeficiency; CHI chitosan; EGF epidermal growth factor; TGF- β siRNA
2210 transforming growth factor- β small interfering ribonucleic acid; PVP poly(vinylpyrrolidone); PSS poly(sodium 4-styrenesulfonate);
2211 PAH poly(allylamine hydrochloride); FITC fluorescein isothiocyanate
2212

2213
2214
2215
2216
2217
2218
2219
2220
2221
2222
2223
2224
2225
2226
2227
2228
2229
2230
2231
2232
2233
2234
2235
2236
2237
2238
2239
2240
2241
2242
2243
2244
2245
2246
2247
2248
2249
2250
2251
2252
2253
2254
2255
2256
2257
2258
2259
2260
2261

VIII Perspectives

New strategies have emerged in the last years in the protein delivery system domain. A first one is to use protein-rich materials in order to deliver a pool of proteins instead of only one or two isolated proteins. Such a strategy should lead to the activation of all the required phenomena to treat a disease such as tissue regeneration for example. On other one is to deliver plasmid DNA to induce the production of proteins by cells or RNA to modulate the expression of a specific gene. Finally, some authors studied the possibility to develop systems able to sequester proteins, to deliver them and recharge for the next delivery. These three strategies will be presented in this section, with the last part presenting other applications for which protein delivery systems can be designed.

VIII.1 Protein-rich materials

The use of protein-rich materials allows the delivery of a cocktail of proteins to the disease site, which can lead to the activation of several phenomena necessary to obtain proper healing. They can be used as a building block for the formulation of the material or only as the cargo.

VIII.2.1 Implantable systems for tissue regeneration

Platelet-rich plasma (PRP) has already been studied to treat several types of injury, and has recently been investigated for the regeneration of bone tissue as it contains several useful growth factors. Among these, it is possible to find platelet-derived growth factor (PDGF) which is a chemotactic signal for MSCs, VEGF that promotes angiogenesis, TGF- β 1 that promotes MSCs osteogenic differentiation and COL expression and IGF-1, able to promote cell proliferation, and notably osteoblast proliferation. In a first study, PRP was integrated into a calcium deficient HAP/COL scaffold obtained by 3D-printing [113]. The release of TGF- β 1 and PDGF were notably monitored during 35 days and showed a sustained release of both growth factors. *In vitro* studies were also conducted by seeding preosteoblasts MC3T3-E1 on the PRP-loaded scaffold and this showed a better cell growth and differentiation compared to seeding on the empty scaffold. In another study, PRP was integrated into coaxial fibers [216]. More precisely, the fibers were composed of PRP and PVA in the core and silk fibroin and PCL in the sheath. The release profiles of VEGF, IGF, PDGF-BB and TGF- β were evaluated for 30 days and showed the delivery of a higher dose of PDGF-BB in a sustained manner after a burst release of one day. The system was tested *in vitro* on bone MSCs and showed the highest migration, proliferation and differentiation of cells. Indeed, the number of mineralized nodules was the highest in the sample treated with the PRP-loaded fibers. The system was also implanted in a calvarial bone defect created in C57BL/6 mice, confirming the ability of the fibers to enhance bone regeneration.

A platelet rich in growth factor (PRGF-Endoret) was used as building block to prepare an injectable HG for tissue regeneration to avoid the potential undesirable fibrin retraction [217]. PRGF-Endoret was chosen as the material for the HG due to its biocompatibility and biodegradability but also because it is a growth factor reservoir able to release them. The release profiles of EGF, IGF-1, PDGF-AB and TGF- β 1 were notably studied and primary human dermal fibroblasts were used to test its cytotoxicity and ability to promote cell proliferation. This study showed the ability of the system to promote cell differentiation when seeded inside the HG as well as its ability to promote matrix production such as HA and COL type I.

2262 Another possibility is to use secretome which is a pool of bioactive molecules
2263 released by cells. Thus, Waters *et al.* loaded secretome secreted by human adipose-
2264 derived stem cells in a gelatin HG containing Laponite® for the treatment of MI [218].
2265 This system was tested *in vitro* and in an *in vivo* MI model in Fischer rats. The results
2266 showed the increase of angiogenesis, the reduction of scar formation and
2267 cardioprotection, enhancing cardiac functions.

2268

2269

VIII.2.2 Wound healing

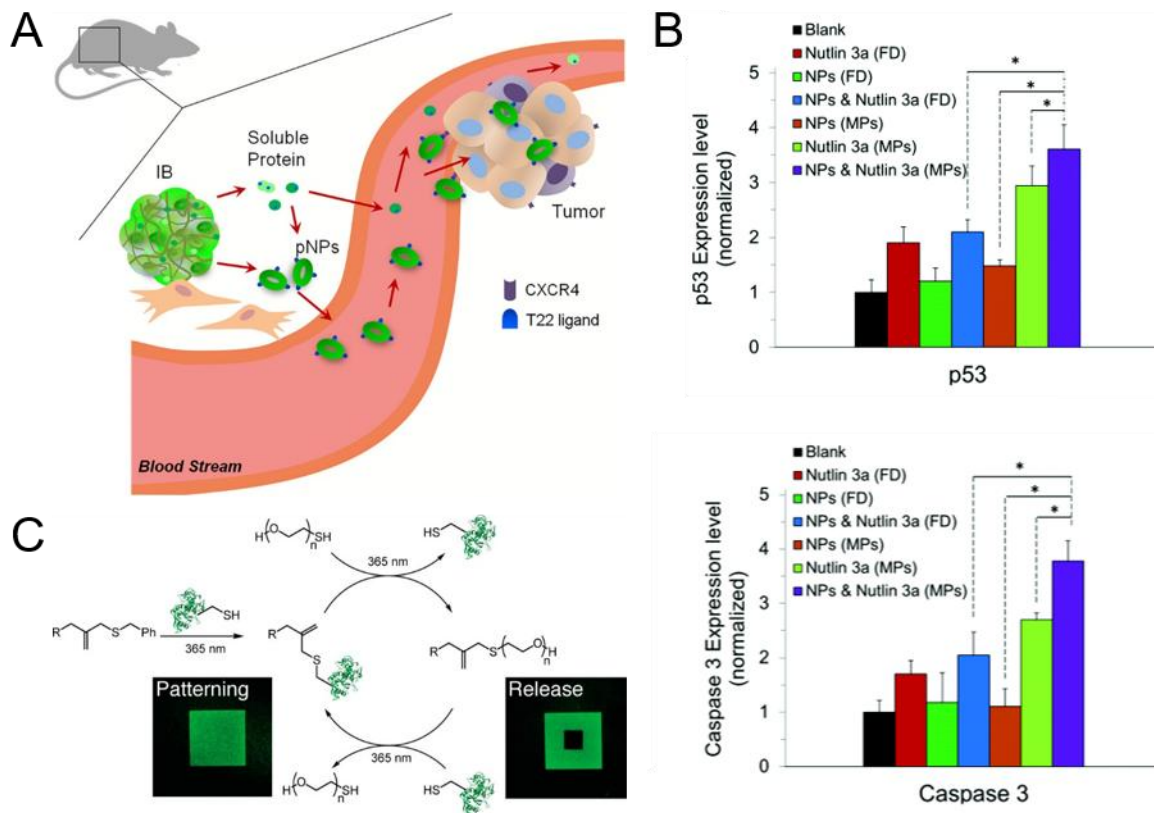
2270 Soy protein hydrolysate (SPH) has been used as building block with cellulose
2271 acetate to produce fibers for skin regeneration due to several reasons. First, soy
2272 protein contains several ECM-mimetic peptides that support tissue regeneration.
2273 Second, both materials are plant-based, not animal-derived or synthetic. And finally,
2274 they are able to mimic the ECM structure. The ability of the system to promote cell
2275 proliferation, migration and infiltration was tested with dermal fibroblast and its ability
2276 to enhance wound healing was assessed in an excisional wound splinting model
2277 applied in C57BL/6NCrl mice [82]. Human platelet lysate (hPL) is another material
2278 containing a pool of growth factors and cytokines able to induce regeneration. Thus,
2279 Pignatelli *et al.* integrated hPL in a silk fibroin solution to obtain a fibrous patch by
2280 electrospinning [219]. The study showed the possibility to control hPL release by
2281 controlling fibroin crystallinity and the bioactivity of the release hPL was showed by
2282 the increased cell viability and proliferation of primary human dermal fibroblasts. Last
2283 example, Tansathien *et al.* used a Deer Antler Velvet (DAV) extract to treat skin
2284 [220]. More precisely, the DAV extract was integrated into a cream containing sponge
2285 microspicules. The ability of the system to promote cell proliferation was assessed *in*
2286 *vitro* with human normal foreskin fibroblasts and positive effect were observed by
2287 application on the skin of healthy human volunteers.

2288

2289

VIII.2.3 Cancer treatment

2290 A specific protein can also be used to synthesize a DDS, as proposed by Unzueta
2291 *et al.* with their “death star-like approach” [158]. More precisely, they reported the
2292 synthesis of bacterial inclusion body (BIB) made of protein-based NPs (pNPs) to
2293 deliver the protein inside cancer cells as presented in **Figure 8A**. The pNPs were
2294 formed by the self-assembling proteins T22-GFP-H6 or R9-GFP-H6, as T22 and R9
2295 parts target CXCR4 receptor, which is overexpressed in colorectal cancer. The
2296 segments encoding for these proteins were transfected in *E. coli*, the bacteria then
2297 produced these proteins, which self-assembled in pNPs and then in BIB. The specific
2298 CXCR4-mediated cellular uptake was assessed in HeLa cells treated with CXCR4
2299 inhibitor AMD3100. A clear inhibition of the cellular uptake was observed, as the
2300 median fluorescence intensity decreased from ~ 200 F.U to ~ 0 F.U in presence of
2301 AMD3100 for the T22-GFP-H6 system. This system was tested only with GFP as a
2302 proof of concept but this part of it the self-assembling proteins could be adapted with
2303 other therapeutic proteins to have specific effect.



2304

2305 **Figure 8** : A. Schematic presentation of the BIB and the protein delivery to cancer cell (reproduced from [158]). B.
 2306 p53 and Caps-3 cell expression depending the delivery system (adapted from [221]). C. Schematic representation
 2307 of the release and self-loading of hydrogel (reproduced from [222])

2308

2309 VIII.2 Bioinduction of protein release through gene therapy (DNA, plasmid 2310 DNA, siRNA)

2311 An emerging strategy is the transfection of cells with DNA, plasmid DNA (pDNA)
 2312 or RNA. It is important to note that in this case, it is not a direct release of protein, but
 2313 a way to make the organism produce the desired protein or to prevent it from
 2314 producing some when the corresponding gene is silenced.

2315

2316 VIII.1.1 Gene delivery (proofs of concept)

2317 Several materials can be used to deliver such molecules. For example, pEGFP-
 2318 LUC, a plasmid encoding for firefly luciferase and GFP, was loaded in CHI NPs,
 2319 themselves loaded in zein MPs [153]. Lipids are also designed to obtain gene
 2320 delivery systems. For example, Colombani *et al.* studied the influence of the linker
 2321 function in the two lipids used to obtain lipoplexes when mixed with this type of
 2322 molecule [173]. More precisely, they used paromomycin-based cationic lipid and
 2323 imidazole-based helper lipid, both presenting a dioleoyl backbone as the hydrophobic
 2324 tail. The linker was an amide function or a phosphoramidate function and they studied
 2325 the effect of the linker nature on the lipoplexe (same or hybrid). They studied the
 2326 formation of lipoplexes using pGWIZ-Luc (encoding for luciferase), pGWIZ-eGFP,
 2327 mRNA (encoding for luciferase and GFP) and human anti-laminA/C siRNA. As for
 2328 Patel *et al.*, they tested 11 cationic and ionisable lipids to obtain lipid NPs able to
 2329 deliver mRNA to the retina [169].

2330 Fibers were also designed for gene delivery or gene silencing. For example,
2331 Zhang *et al.* designed a gene vector made of a lipophilic tail, tetraphenylethene and a
2332 peptide containing four arginines named TR4 to self-assemble with pDNA, leading to
2333 the obtention of nanofibers [223]. As for Pinese *et al.*, they chose the load siRNA in
2334 MSNs-PEI and to coat PCL fibers with these NPs [224].

2335 If these systems were tested for general gene delivery or gene silencing
2336 application, some systems have been designed for specific applications.

2337

2338

VIII.1.2 Bone tissue engineering

2339 As BMP2 is very used for bone regeneration, delivering pDNA encoding for this
2340 protein completely makes sense when exploring gene delivery for this application.
2341 Thus, different scaffolds were developed to do so. For example, Tenkumo *et al.*
2342 proposed a nanoHAP/COL scaffold containing pBMP2-functionalized calcium
2343 phosphate NPs to enhance bone regeneration [225]. The system was
2344 subcutaneously implanted in Wistar rats' back and the results showed that it induced
2345 the release of a higher quantity of BMP2 and for a longer time compared to the
2346 system containing naked pBMP2 and BMP2 in solution. Raftery *et al.*, on their side,
2347 evaluated if modified pBMP2 could be more efficient in enhancing bone formation
2348 [226]. Thus, they first evaluated the release of the plasmid from CHI NPs and its
2349 activity and then embedded these loaded CHI NPs in a COL/HAP scaffold for
2350 implantation in a calvarial bone defect created in Wistar rats. The results showed that
2351 the modification of the plasmid led to a higher production of BMP2 from cells and
2352 thus to a higher bone formation.

2353 Particles were also designed for such application: McMillan *et al.* integrated
2354 nanocomplexes composed of mineral-coated HAP MPs and lipofectamine/pDNA into
2355 MSC aggregates [227]. This work was based on the fact that MSC aggregates can
2356 form bone-like tissues when guided by addition of certain proteins in the culture
2357 media. The pDNAs were pBMP2 and pTGF- β 1, delivered alone or in combination,
2358 and three porcine donors were used to form the bone-marrow-derived MSC
2359 aggregates due to possible variation of properties among donors. Globally speaking,
2360 the results showed the ability of the nanocomplexes to promote osteogenesis in the
2361 different MSC aggregates.

2362

2363

VIII.1.3 Cancer treatment

2364 Specific pDNA can be used for cancer treatment. For example, Davoodi *et al.*
2365 designed core-shell particles to deliver p53 pDNA together with nutlin-3a [221]. The
2366 p53 gene is the most inactivated or mutated gene in tumour tissues, which is
2367 problematic as the p53 protein activity leads to the apoptosis of tumour cells.
2368 Intracellularly, the p53 protein activity is regulated by the murine double minute 2
2369 (MDM2) protein which forms a complex with it to stop the apoptotic activity. However,
2370 MDM2 can be upregulated in cancer cells. Thus, the strategy adopted by Davoodi *et al.*
2371 was to use nutlin-3a to disrupt the MDM2-p53 protein complex and to deliver p53
2372 pDNA to promote p53 protein production. To deliver these therapeutics, they
2373 designed PLGA core-PDLLA (poly(D,L-lactic acid)) shell MPs. Prior to fabrication,
2374 nutlin-3a and p53 pDNA-loaded β -cyclodextrin-graft-CHI NPs were mixed in the
2375 PLGA solution. The *in vitro* experiment showed a synergistic anti-tumour effect of
2376 nutlin-3a and p53 pDNA by a high production of p53 protein and Casp3 as presented
2377 in **Figure 8B** and a high intracellular ROS level.

2378 Another circulating system was proposed for anti-cancer application: poly(styrene-
2379 alt-maleic anhydride) was grafted with PEG and two amino acids via disulphide bond

2380 to obtain a molecule able to self-assemble into micelles [165]. The disulphide bond
2381 was bringing reduction-responsiveness and the two amino acids were histidine to
2382 bring pH-responsiveness and arginine to bind to nucleic acids. The micelle was
2383 loaded with doxorubicin and coated with polo like kinase 1 siRNA (PLK-1 siRNA).
2384 The dual responsiveness and anti-cancer effect were then tested *in vitro* and *in vivo*.

2385 An MNs patch has also been designed for cancer treatment [160]. The MNs patch
2386 was made with polycarbonate and was first immersed in dopamine solution to obtain
2387 a polydopamine coating. LBL was then operated with the adjuvant
2388 polyriboinosinic:polyribocytidylic (poly(I:C)), a TLR3 agonist able to activate natural
2389 cancer cell killer, and oligo sulfamethazine conjugated poly(β -amino ester urethane)
2390 (OSM-(PEG-PAEU)). The last layer was a coating of polyplex made with pOVA as
2391 vaccine DNA and bPEI-deoxycholic acid (DA3) conjugate. The system was also
2392 tested *in vitro* and *in vivo* and the experiment showed its ability to induce OVA
2393 expression and to inhibit tumour growth in a metastatic cancer model.

2394

2395

VIII.3 Sequestration of proteins

2396 Some systems are designed to sequester proteins secreted by cells to better
2397 control the cellular environment. Such a strategy has been adopted by Rinker *et al.* to
2398 modulate chondrocytic differentiation [228]. They synthesized heparin MPs and PEG
2399 MPs and incubated them in ATDC5 cells transwell culture (2D) and in ATDC5
2400 spheroid culture (3D). A delay in differentiation was observed in presence of heparin
2401 MPS, and the analysis of the proteins contained in the MPs revealed that they
2402 sequestered insulin-like growth factor binding proteins (IGFBP)-3 and 5. An additional
2403 experiment consisting of incubating the cells with an inhibitor of IGFBPs confirmed
2404 that the delayed differentiation in presence of heparin MPs was due to protein
2405 sequestration.

2406 An HG was also designed for protein sequestration [222]. The goal was to obtain
2407 an HG able to deliver protein and to recharge itself with fresh protein. To do so, they
2408 added an allyl sulfide moiety to an HG, which allowed the immobilization and release
2409 of protein via a thiol-ene reaction as showed by **Figure 8C**. More precisely, the HG
2410 was made with an eight-armed PEG-dibenzylcyclooctyne functionalized with a cell
2411 adhesive azido-RGDS peptide and the azido allyl sulphide. The ability of the HG to
2412 release protein and to recharge itself has been assessed, notably with TGF- β 1 which
2413 bioactivity was retained.

2414

2415

VIII.4 Other possible applications

2416 Delivery to the retina has already been mentioned once, with a system delivering
2417 mRNA. Delplace *et al.*, on their side, designed an HA/methylcellulose HG to deliver
2418 the ciliary neurotrophic factor (CNTF), known for its neuroprotective effect on retina
2419 [229]. More precisely, they modified CNTF with Src homology 3 (SH3) and
2420 methylcellulose with SH3 binding peptide to assure the immobilization of CNTF in the
2421 HG. *In vitro* experiment performed with TF1- α cells assessed the bioactivity of the
2422 released CNTF and experiment performed on C57BL/6 J mice confirmed the release
2423 of bioactive CNTF *in vivo* with the quantification of numerous markers.

2424 Dai *et al.* proposed a system for inner ear therapy [230]. The systems consisted of
2425 interferon α -2b (IFN α -2b)-loaded PLGA NPs embedded in a CHI/ β -
2426 glycerophosphate thermosensitive HG. IFN α -2b was chosen as interferons showed
2427 anti-viral and immunomodulatory effect in the treatment of sudden deafness. *In vivo*
2428 experiment was conducted by injecting the HG in the inner ear of albino guinea pigs

2429 and the results showed that the system increased the IFN α -2b residence time in the
2430 inner ear by 3-fold compared to IFN α -2b-loaded HG.

2431 A protein delivery system has also been proposed for the treatment of short
2432 stature children, and more precisely for the delivery of rhGH [24]. Indeed, this
2433 disease can be caused by a deficiency in growth hormone and this one is known to
2434 promote longitudinal bone growth. Thus, Gao *et al.* synthesized poly(ester urea)
2435 nanofibers to deliver it and used sugar-glass NPs to stabilize it. The results showed
2436 that the nanofibers could release rhGH in a sustained manner for up to six weeks
2437 without production of acid degradation products. The bioactivity of the released rhGH
2438 was also assessed by checking the proliferation of rat node lymphoma cells (Nb2
2439 cells).

2440 The last example presented here has been developed to treat MI. If the application
2441 has already been seen before, the authors developed a quite original system. They
2442 used MSC as the initial material and performed LBL on it with alginate and VEGF-
2443 loaded gelatin [161]. The objective was to exploit the tropism of MSCs to myocardial
2444 infarct zone to be sure that the system would go to the heart and deliver the cells and
2445 the encapsulated VEGF, thus enhancing angiogenesis and cardiac function. The *in*
2446 *vitro* experiment showed that the system was able to deliver VEGF in a sustained
2447 manner and had a tropism to SDF-1. An MI model was created in SD rats by
2448 punctually blocking the left coronary artery to check the system *in vivo*. The results
2449 showed that the system migrated to the myocardial infarct site, promoting
2450 angiogenesis and enhancing cardiac function, confirming that it is a promising
2451 material to treat MI.

2452

2453

2454 **IX Conclusions**

2455 As seen through this review, a large range of delivery systems have been
2456 developed these last years for the specific delivery of proteins: MPs, NPs, HGs,
2457 fibers, films, patches and MacPSs, in a monolithic or composite formulation. All these
2458 systems can be formulated using very well-established techniques, such as emulsion
2459 for NPs, layer-by-layer for films and patches or freeze-drying for MacPSs.
2460 Noteworthy, other techniques are emerging, such as the rotary jet spinning for the
2461 formulation of fibers, which is interesting as it does not necessitate the application of
2462 an electrical field to the polymer solution and thus, eliminates a stress applied to the
2463 protein cargo.

2464 These protein cargos can be loaded via three different techniques, which are
2465 diffusion, immersion and immobilization, and can then be released via three major
2466 mechanisms: diffusion, natural erosion via local stimuli (pH, ROS, redox, glucose,
2467 protease) and triggered degradation via external stimuli (visible and NIR light,
2468 magnetic field, mechanical stress). A wide range of characterization techniques is
2469 available to measure the amount of loaded and released proteins. In simple samples,
2470 techniques such as light absorption or fluorimetry can be sufficient. The ELISA test is
2471 also widely used for sensitive proteins due to its high specificity and high sensitivity.
2472 However, in case of more complex samples, such as biologic ones, composed of
2473 several proteins, a first separation step can be necessary, which notably led to the
2474 development of the Western blot technique. The release mechanism can then be
2475 modelled more finely thanks to mathematical methods.

2476 In this review, the DDSs have been categorized into three main types: circulating
2477 systems, implantable systems and covering systems. Circulating systems - which are
2478 MPs, NPs, capsules and exosomes - have mainly been developed for the treatment
2479 of cancer, and more precisely for the delivery of RNase A to cancer cells. However,
2480 some systems have been developed for the treatment of diabetes and tissue
2481 engineering. Regarding implantable systems, they are mostly developed for tissue
2482 engineering (bone, cartilage, nerve, heart) even if some systems were designed for
2483 the treatment of diabetes, cancer or internal wound healing. The formulations types
2484 found in this category are MacPSs, fibers, HGs, films and patches. As for covering
2485 systems - which often consist of films and patches, but can also be fibers and HGs -
2486 they are mainly used for skin regeneration but are also used for transdermal and
2487 transbuccal delivery.

2488 At last, many of these systems have been tested *in vivo*, and the most common
2489 models have been presented here, such as xenograft tumour-bearing mice for cancer
2490 or bone critical defect for bone tissue engineering, as well as the major results
2491 associated to the experiment.

2492 Finally, emerging routes for the design of new protein delivery systems have been
2493 presented in this review such as the use of protein-rich materials, to deliver a pool of
2494 proteins rather than a single protein, and the delivery of plasmid DNA or RNA to
2495 induce the production of proteins by cells directly at the injury site. Some interesting
2496 unusual applications of such delivery systems have also been shown in this last part.

2497 As seen here, the main systems for therapeutic protein delivery were developed to
2498 respond by natural leaking or upon local biochemical stimuli. We expect that an
2499 emerging domain for future development in this field will be the remote release of

2500 proteins (or other fragile biomacromolecules) that may be induced remotely by
2501 external fields applied (magnetic field, near infra-red light or ultra sounds). In such
2502 approaches, a common mechanism is to convert the magnetic/phonic/acoustic wave
2503 energy into a local heat. To achieve this, important developments should be achieved
2504 considered in the design of thermo-responsive interface suitable specifically for
2505 proteins immobilization/and release.

2506

2507

2508 **Author contributions**

2509 **Joëlle Bizeau:** Conceptualization, Methodology, Writing - Original Draft, **Damien**
2510 **Mertz:** Conceptualization, Methodology, Writing - Review & Editing, Supervision,
2511 Funding acquisition.

2512

2513 **Acknowledgements**

2514 D.M. acknowledges the Materials Institute Carnot Alsace (project ProtRemote) and
2515 the Agence Nationale de la Recherche (grant ANR-19-CE09-0004 – CoreImag) for
2516 financial supports.

2517

Bibliography

- 2519 [1] Vermonden T, Censi R, Hennink WE. Hydrogels for Protein Delivery. *Chem*
2520 *Rev* 2012;112:2853–88. <https://doi.org/10.1021/cr200157d>.
- 2521 [2] Yu M, Wu J, Shi J, Farokhzad OC. Nanotechnology for protein delivery:
2522 Overview and perspectives. *Journal of Controlled Release* 2016;240:24–37.
2523 <https://doi.org/10.1016/j.jconrel.2015.10.012>.
- 2524 [3] Lu Y, Sun W, Gu Z. Stimuli-responsive nanomaterials for therapeutic protein
2525 delivery. *Journal of Controlled Release* 2014;194:1–19.
2526 <https://doi.org/10.1016/j.jconrel.2014.08.015>.
- 2527 [4] Sinha VR, Trehan A. Biodegradable microspheres for protein delivery. *Journal*
2528 *of Controlled Release* 2003;90:261–80. [https://doi.org/10.1016/S0168-](https://doi.org/10.1016/S0168-3659(03)00194-9)
2529 [3659\(03\)00194-9](https://doi.org/10.1016/S0168-3659(03)00194-9).
- 2530 [5] Medlicott NJ, Tucker IG. Pulsatile release from subcutaneous implants.
2531 *Advanced Drug Delivery Reviews* 1999;38:139–49.
2532 [https://doi.org/10.1016/S0169-409X\(99\)00013-7](https://doi.org/10.1016/S0169-409X(99)00013-7).
- 2533 [6] Kikuchi A, Okano T. Pulsatile drug release control using hydrogels. *Advanced*
2534 *Drug Delivery Reviews* 2002;54:53–77. [https://doi.org/10.1016/S0169-](https://doi.org/10.1016/S0169-409X(01)00243-5)
2535 [409X\(01\)00243-5](https://doi.org/10.1016/S0169-409X(01)00243-5).
- 2536 [7] Chen L, Mei L, Feng D, Huang D, Tong X, Pan X, et al. Anhydrous reverse
2537 micelle lecithin nanoparticles/PLGA composite microspheres for long-term
2538 protein delivery with reduced initial burst. *Colloids and Surfaces B:*
2539 *Biointerfaces* 2018;163:146–54. <https://doi.org/10.1016/j.colsurfb.2017.12.040>.
- 2540 [8] Sedyakina NE, Zakharov AN, Krivoshchepov AF, Pribytkova AP, Bogdanova
2541 YA, Feldman NB, et al. Effect of carbon chain length of dicarboxylic acids as
2542 cross-linking agents on morphology, encapsulation, and release features of
2543 protein-loaded chitosan microparticles. *Colloid Polym Sci* 2017;295:1915–24.
2544 <https://doi.org/10.1007/s00396-017-4171-0>.
- 2545 [9] Rinker TE, Philbrick BD, Temenoff JS. Core-shell microparticles for protein
2546 sequestration and controlled release of a protein-laden core. *Acta Biomaterialia*
2547 2017;56:91–101. <https://doi.org/10.1016/j.actbio.2016.12.042>.
- 2548 [10] Kumar A, Montemagno C, Choi H-J. Smart Microparticles with a pH-responsive
2549 Macropore for Targeted Oral Drug Delivery. *Scientific Reports* 2017;7:1–15.
2550 <https://doi.org/10.1038/s41598-017-03259-x>.
- 2551 [11] Galliani M, Tremolanti C, Signore G. Nanocarriers for Protein Delivery to the
2552 Cytosol: Assessing the Endosomal Escape of Poly(Lactide-co-Glycolide)-
2553 Poly(Ethylene Imine) Nanoparticles. *Nanomaterials* 2019;9:652.
2554 <https://doi.org/10.3390/nano9040652>.
- 2555 [12] Hsiao L-W, Lai Y-D, Lai J-T, Hsu C-C, Wang N-Y, Wang S SS, et al. Cross-
2556 linked polypeptide-based gel particles by emulsion for efficient protein
2557 encapsulation. *Polymer* 2017;115:261–72.
2558 <https://doi.org/10.1016/j.polymer.2017.03.055>.
- 2559 [13] Rahmani V, Elshereef R, Sheardown H. Optimizing electrostatic interactions for
2560 controlling the release of proteins from anionic and cationically modified
2561 alginate. *European Journal of Pharmaceutics and Biopharmaceutics*
2562 2017;117:232–43. <https://doi.org/10.1016/j.ejpb.2017.04.025>.
- 2563 [14] Zhang B, Li H, He L, Han Z, Zhou T, Zhi W, et al. Surface-decorated
2564 hydroxyapatite scaffold with on-demand delivery of dexamethasone and
2565 stromal cell derived factor-1 for enhanced osteogenesis. *Materials Science and*
2566 *Engineering: C* 2018;89:355–70. <https://doi.org/10.1016/j.msec.2018.04.008>.

- 2567 [15] Fröhlich K, Hartzke D, Schmidt F, Eucker J, Gurlo A, Sittinger M, et al. Delayed
2568 release of chemokine CCL25 with bioresorbable microparticles for mobilization
2569 of human mesenchymal stem cells. *Acta Biomaterialia* 2018;69:290–300.
2570 <https://doi.org/10.1016/j.actbio.2018.01.036>.
- 2571 [16] Wu C, Baldursdottir S, Yang M, Mu H. Lipid and PLGA hybrid microparticles as
2572 carriers for protein delivery. *Journal of Drug Delivery Science and Technology*
2573 2018;43:65–72. <https://doi.org/10.1016/j.jddst.2017.09.006>.
- 2574 [17] Saengruengrit C, Ritprajak P, Wanichwecharungruang S, Sharma A, Salvan G,
2575 Zahn DRT, et al. The combined magnetic field and iron oxide-PLGA composite
2576 particles: Effective protein antigen delivery and immune stimulation in dendritic
2577 cells. *Journal of Colloid and Interface Science* 2018;520:101–11.
2578 <https://doi.org/10.1016/j.jcis.2018.03.008>.
- 2579 [18] Lv J, He B, Yu J, Wang Y, Wang C, Zhang S, et al. Fluoropolymers for
2580 intracellular and in vivo protein delivery. *Biomaterials* 2018;182:167–75.
2581 <https://doi.org/10.1016/j.biomaterials.2018.08.023>.
- 2582 [19] Yang X, Tang Q, Jiang Y, Zhang M, Wang M, Mao L. Nanoscale ATP-
2583 Responsive Zeolitic Imidazole Framework-90 as a General Platform for
2584 Cytosolic Protein Delivery and Genome Editing. *J Am Chem Soc*
2585 2019;141:3782–6. <https://doi.org/10.1021/jacs.8b11996>.
- 2586 [20] Ardeshiryajimi A, Ghaderian SM-H, Omrani MD, Moradi SL. Biomimetic
2587 scaffold containing PVDF nanofibers with sustained TGF- β release in
2588 combination with AT-MSCs for bladder tissue engineering. *Gene*
2589 2018;676:195–201. <https://doi.org/10.1016/j.gene.2018.07.046>.
- 2590 [21] Song M, Li L, Zhang Y, Chen K, Wang H, Gong R. Carboxymethyl- β -
2591 cyclodextrin grafted chitosan nanoparticles as oral delivery carrier of protein
2592 drugs. *Reactive and Functional Polymers* 2017;117:10–5.
2593 <https://doi.org/10.1016/j.reactfunctpolym.2017.05.008>.
- 2594 [22] Meneguín AB, Beyssac E, Garrait G, Hsein H, Cury BSF. Retrograded
2595 starch/pectin coated gellan gum-microparticles for oral administration of insulin:
2596 A technological platform for protection against enzymatic degradation and
2597 improvement of intestinal permeability. *European Journal of Pharmaceutics and*
2598 *Biopharmaceutics* 2018;123:84–94. <https://doi.org/10.1016/j.ejpb.2017.11.012>.
- 2599 [23] Meng X, Liu J, Yu X, Li J, Lu X, Shen T. Pluronic F127 and D- α -Tocopheryl
2600 Polyethylene Glycol Succinate (TPGS) Mixed Micelles for Targeting Drug
2601 Delivery across The Blood Brain Barrier. *Scientific Reports* 2017;7:1–12.
2602 <https://doi.org/10.1038/s41598-017-03123-y>.
- 2603 [24] Gao Y, Xu Y, Land A, Harris J, Policastro GM, Childers EP, et al. Sustained
2604 Release of Recombinant Human Growth Hormone from Bioresorbable
2605 Poly(ester urea) Nanofibers. *ACS Macro Lett* 2017;6:875–80.
2606 <https://doi.org/10.1021/acsmacrolett.7b00334>.
- 2607 [25] Yuan D, Jacquier JC, O’Riordan ED. Entrapment of proteins and peptides in
2608 chitosan-polyphosphoric acid hydrogel beads: A new approach to achieve both
2609 high entrapment efficiency and controlled in vitro release. *Food Chemistry*
2610 2018;239:1200–9. <https://doi.org/10.1016/j.foodchem.2017.07.021>.
- 2611 [26] Wu C, van de Weert M, Baldursdottir SG, Yang M, Mu H. Effect of excipients
2612 on encapsulation and release of insulin from spray-dried solid lipid
2613 microparticles. *International Journal of Pharmaceutics* 2018;550:439–46.
2614 <https://doi.org/10.1016/j.ijpharm.2018.09.007>.
- 2615 [27] Tavares M, Cabral RP, Costa C, Martins P, Fernandes AR, Casimiro T, et al.
2616 Development of PLGA dry powder microparticles by supercritical CO₂-assisted

- 2617 spray-drying for potential vaccine delivery to the lungs. *The Journal of*
 2618 *Supercritical Fluids* 2017;128:235–43.
 2619 <https://doi.org/10.1016/j.supflu.2017.06.004>.
- [28] 2620 Chen N, Johnson MM, Collier MA, Gallovic MD, Bachelder EM, Ainslie KM.
 2621 Tunable degradation of acetalated dextran microparticles enables controlled
 2622 vaccine adjuvant and antigen delivery to modulate adaptive immune
 2623 responses. *Journal of Controlled Release* 2018;273:147–59.
 2624 <https://doi.org/10.1016/j.jconrel.2018.01.027>.
- [29] 2625 Hao N, Nie Y, Xu Z, Closson AB, Usherwood T, Zhang JXJ. Microfluidic
 2626 continuous flow synthesis of functional hollow spherical silica with hierarchical
 2627 sponge-like large porous shell. *Chemical Engineering Journal* 2019;366:433–8.
 2628 <https://doi.org/10.1016/j.cej.2019.02.095>.
- [30] 2629 Foster GA, Headen DM, González-García C, Salmerón-Sánchez M, Shirwan H,
 2630 García AJ. Protease-degradable microgels for protein delivery for
 2631 vascularization. *Biomaterials* 2017;113:170–5.
 2632 <https://doi.org/10.1016/j.biomaterials.2016.10.044>.
- [31] 2633 Yu L, Sun Q, Hui Y, Seth A, Petrovsky N, Zhao C-X. Microfluidic formation of
 2634 core-shell alginate microparticles for protein encapsulation and controlled
 2635 release. *Journal of Colloid and Interface Science* 2019;539:497–503.
 2636 <https://doi.org/10.1016/j.jcis.2018.12.075>.
- [32] 2637 Stöber W, Fink A, Bohn E. Controlled growth of monodisperse silica spheres in
 2638 the micron size range. *Journal of Colloid and Interface Science* 1968;26:62–9.
 2639 [https://doi.org/10.1016/0021-9797\(68\)90272-5](https://doi.org/10.1016/0021-9797(68)90272-5).
- [33] 2640 Omar H, Croissant JG, Alamoudi K, Alsaïari S, Alradwan I, Majrashi MA, et al.
 2641 Biodegradable Magnetic Silica@Iron Oxide Nanovectors with Ultra-Large
 2642 Mesopores for High Protein Loading, Magnetothermal Release, and Delivery.
 2643 *Journal of Controlled Release* 2017;259:187–94.
 2644 <https://doi.org/10.1016/j.jconrel.2016.11.032>.
- [34] 2645 Deng C, Zhang Q, Fu C, Zhou F, Yang W, Yi D, et al. Template-Free Synthesis
 2646 of Chemically Asymmetric Silica Nanotubes for Selective Cargo Loading and
 2647 Sustained Drug Release. *Chem Mater* 2019;31:4291–8.
 2648 <https://doi.org/10.1021/acs.chemmater.9b01530>.
- [35] 2649 Shao D, Li M, Wang Z, Zheng X, Lao Y-H, Chang Z, et al. Bioinspired
 2650 Diselenide-Bridged Mesoporous Silica Nanoparticles for Dual-Responsive
 2651 Protein Delivery. *Advanced Materials* 2018;30:1801198.
 2652 <https://doi.org/10.1002/adma.201801198>.
- [36] 2653 Tian Z, Xu Y, Zhu Y. Aldehyde-functionalized dendritic mesoporous silica
 2654 nanoparticles as potential nanocarriers for pH-responsive protein drug delivery.
 2655 *Materials Science and Engineering: C* 2017;71:452–9.
 2656 <https://doi.org/10.1016/j.msec.2016.10.039>.
- [37] 2657 Mertz D, Tan P, Wang Y, Goh TK, Blencowe A, Caruso F. Bromoisobutyramide
 2658 as an Intermolecular Surface Binder for the Preparation of Free-standing
 2659 Biopolymer Assemblies. *Advanced Materials* 2011;23:5668–73.
 2660 <https://doi.org/10.1002/adma.201102890>.
- [38] 2661 Mertz D, Cui J, Yan Y, Devlin G, Chaubaroux C, Dochter A, et al. Protein
 2662 Capsules Assembled via Isobutyramide Grafts: Sequential Growth,
 2663 Biofunctionalization, and Cellular Uptake. *ACS Nano* 2012;6:7584–94.
 2664 <https://doi.org/10.1021/nn302024t>.
- [39] 2665 Li B, Harlepp S, Gensbittel V, Wells CJR, Bringel O, Goetz JG, et al. Near infra-
 2666 red light responsive carbon nanotubes@mesoporous silica for photothermia

- 2667 and drug delivery to cancer cells. *Materials Today Chemistry* 2020;17:100308.
2668 <https://doi.org/10.1016/j.mtchem.2020.100308>.
- 2669 [40] Perton F, Tasso M, Muñoz Medina GA, Ménard M, Blanco-Andujar C,
2670 Portiansky E, et al. Fluorescent and magnetic stellate mesoporous silica for
2671 bimodal imaging and magnetic hyperthermia. *Applied Materials Today*
2672 2019;16:301–14. <https://doi.org/10.1016/j.apmt.2019.06.006>.
- 2673 [41] Perton F, Harlepp S, Follain G, Parkhomenko K, Goetz JG, Bégin-Colin S, et
2674 al. Wrapped stellate silica nanocomposites as biocompatible luminescent
2675 nanoplatforms assessed in vivo. *Journal of Colloid and Interface Science*
2676 2019;542:469–82. <https://doi.org/10.1016/j.jcis.2019.01.098>.
- 2677 [42] Wang Y, Wise AK, Tan J, Maina JW, Shepherd RK, Caruso F. Mesoporous
2678 Silica Supraparticles for Sustained Inner-Ear Drug Delivery. *Small*
2679 2014;10:4244–8. <https://doi.org/10.1002/sml.201401767>.
- 2680 [43] Yang Y, Zhu H, Wang J, Fang Q, Peng Z. Enzymatically Disulfide-Crosslinked
2681 Chitosan/Hyaluronic Acid Layer-by-Layer Self-Assembled Microcapsules for
2682 Redox-Responsive Controlled Release of Protein. *ACS Appl Mater Interfaces*
2683 2018;10:33493–506. <https://doi.org/10.1021/acsami.8b07120>.
- 2684 [44] Ramalapa B, Crasson O, Vandevenne M, Gibaud A, Garcion E, Cordonnier T,
2685 et al. Protein–polysaccharide complexes for enhanced protein delivery in
2686 hyaluronic acid templated calcium carbonate microparticles. *J Mater Chem B*
2687 2017;5:7360–8. <https://doi.org/10.1039/C7TB01538K>.
- 2688 [45] Wang J, Kumeria T, Bezem MT, Wang J, Sailor MJ. Self-Reporting
2689 Photoluminescent Porous Silicon Microparticles for Drug Delivery. *ACS Appl*
2690 *Mater Interfaces* 2018;10:3200–9. <https://doi.org/10.1021/acsami.7b09071>.
- 2691 [46] Zuidema JM, Kumeria T, Kim D, Kang J, Wang J, Hollett G, et al. Oriented
2692 Nanofibrous Polymer Scaffolds Containing Protein-Loaded Porous Silicon
2693 Generated by Spray Nebulization. *Advanced Materials* 2018;30:1706785.
2694 <https://doi.org/10.1002/adma.201706785>.
- 2695 [47] Bae S-E, Lyu SK, Kim K-J, Shin HJ, Kwon H, Huh S. Intracellular delivery of a
2696 native functional protein using cell-penetrating peptide functionalized cubic
2697 MSNs with ultra-large mesopores. *J Mater Chem B* 2018;6:3456–65.
2698 <https://doi.org/10.1039/C8TB00330K>.
- 2699 [48] Mout R, Ray M, Tay T, Sasaki K, Yesilbag Tonga G, Rotello VM. General
2700 Strategy for Direct Cytosolic Protein Delivery via Protein–Nanoparticle Co-
2701 engineering. *ACS Nano* 2017;11:6416–21.
2702 <https://doi.org/10.1021/acs.nano.7b02884>.
- 2703 [49] Volodkin DV, Larionova NI, Sukhorukov GB. Protein Encapsulation via Porous
2704 CaCO₃ Microparticles Templating. *Biomacromolecules* 2004;5:1962–72.
2705 <https://doi.org/10.1021/bm049669e>.
- 2706 [50] Volodkin DV, von Klitzing R, Möhwald H. Pure Protein Microspheres by
2707 Calcium Carbonate Templating. *Angewandte Chemie* 2010;122:9444–7.
2708 <https://doi.org/10.1002/ange.201005089>.
- 2709 [51] Tan J, Wang Y, Yip X, Glynn F, Shepherd RK, Caruso F. Nanoporous Peptide
2710 Particles for Encapsulating and Releasing Neurotrophic Factors in an Animal
2711 Model of Neurodegeneration. *Advanced Materials* 2012;24:3362–6.
2712 <https://doi.org/10.1002/adma.201200634>.
- 2713 [52] Ménard M, Meyer F, Parkhomenko K, Leuvrey C, Francius G, Bégin-Colin S, et
2714 al. Mesoporous silica templated-albumin nanoparticles with high doxorubicin
2715 payload for drug delivery assessed with a 3-D tumor cell model. *Biochimica et*

- 2716 Biophysica Acta (BBA) - General Subjects 2019;1863:332–41.
 2717 <https://doi.org/10.1016/j.bbagen.2018.10.020>.
- 2718 [53] Mertz D, Wu H, Wong JS, Cui J, Tan P, Alles R, et al. Ultrathin, bioresponsive
 2719 and drug-functionalized protein capsules. *J Mater Chem* 2012;22:21434–42.
 2720 <https://doi.org/10.1039/C2JM33737A>.
- 2721 [54] Mertz D, Affolter-Zbaraszczuk C, Barthès J, Cui J, Caruso F, Baumert TF, et al.
 2722 Templated assembly of albumin-based nanoparticles for simultaneous gene
 2723 silencing and magnetic resonance imaging. *Nanoscale* 2014;6:11676–80.
 2724 <https://doi.org/10.1039/C4NR02623C>.
- 2725 [55] Dutta K, Hu D, Zhao B, Ribbe AE, Zhuang J, Thayumanavan S. Templated
 2726 Self-Assembly of a Covalent Polymer Network for Intracellular Protein Delivery
 2727 and Traceless Release. *J Am Chem Soc* 2017;139:5676–9.
 2728 <https://doi.org/10.1021/jacs.7b01214>.
- 2729 [56] Hong Y, Nam G-H, Koh E, Jeon S, Kim GB, Jeong C, et al. Exosome as a
 2730 Vehicle for Delivery of Membrane Protein Therapeutics, PH20, for Enhanced
 2731 Tumor Penetration and Antitumor Efficacy. *Advanced Functional Materials*
 2732 2018;28:1703074. <https://doi.org/10.1002/adfm.201703074>.
- 2733 [57] Cho E, Nam G-H, Hong Y, Kim YK, Kim D-H, Yang Y, et al. Comparison of
 2734 exosomes and ferritin protein nanocages for the delivery of membrane protein
 2735 therapeutics. *Journal of Controlled Release* 2018;279:326–35.
 2736 <https://doi.org/10.1016/j.jconrel.2018.04.037>.
- 2737 [58] Lima DS, Tenório-Neto ET, Lima-Tenório MK, Guilherme MR, Scariot DB,
 2738 Nakamura CV, et al. pH-responsive alginate-based hydrogels for protein
 2739 delivery. *Journal of Molecular Liquids* 2018;262:29–36.
 2740 <https://doi.org/10.1016/j.molliq.2018.04.002>.
- 2741 [59] Wei W, Li J, Qi X, Zhong Y, Zuo G, Pan X, et al. Synthesis and characterization
 2742 of a multi-sensitive polysaccharide hydrogel for drug delivery. *Carbohydrate*
 2743 *Polymers* 2017;177:275–83. <https://doi.org/10.1016/j.carbpol.2017.08.133>.
- 2744 [60] Qi X, Wei W, Li J, Zuo G, Pan X, Su T, et al. Salecan-Based pH-Sensitive
 2745 Hydrogels for Insulin Delivery. *Mol Pharmaceutics* 2017;14:431–40.
 2746 <https://doi.org/10.1021/acs.molpharmaceut.6b00875>.
- 2747 [61] Olthof MGL, Kempen DHR, Liu X, Dadsetan M, Tryfonidou MA, Yaszemski MJ,
 2748 et al. Bone morphogenetic protein-2 release profile modulates bone formation
 2749 in phosphorylated hydrogel. *Journal of Tissue Engineering and Regenerative*
 2750 *Medicine* 2018;12:1339–51. <https://doi.org/10.1002/term.2664>.
- 2751 [62] McAvan BS, Khuphe M, Thornton PD. Polymer hydrogels for glutathione-
 2752 mediated protein release. *European Polymer Journal* 2017;87:468–77.
 2753 <https://doi.org/10.1016/j.eurpolymj.2016.09.032>.
- 2754 [63] Ma X, Xu T, Chen W, Qin H, Chi B, Ye Z. Injectable hydrogels based on the
 2755 hyaluronic acid and poly (γ -glutamic acid) for controlled protein delivery.
 2756 *Carbohydrate Polymers* 2018;179:100–9.
 2757 <https://doi.org/10.1016/j.carbpol.2017.09.071>.
- 2758 [64] Koshy ST, Zhang DKY, Grolman JM, Stafford AG, Mooney DJ. Injectable
 2759 nanocomposite cryogels for versatile protein drug delivery. *Acta Biomaterialia*
 2760 2018;65:36–43. <https://doi.org/10.1016/j.actbio.2017.11.024>.
- 2761 [65] Dai L, Cheng T, Wang Y, Lu H, Nie S, He H, et al. Injectable all-polysaccharide
 2762 self-assembling hydrogel: a promising scaffold for localized therapeutic
 2763 proteins. *Cellulose* 2019;26:6891–901. <https://doi.org/10.1007/s10570-019-02579-7>.
- 2764

- 2765 [66] Shigemitsu H, Fujisaku T, Tanaka W, Kubota R, Minami S, Urayama K, et al.
 2766 An adaptive supramolecular hydrogel comprising self-sorting double nanofibre
 2767 networks. *Nature Nanotechnology* 2018;13:165–72.
 2768 <https://doi.org/10.1038/s41565-017-0026-6>.
- 2769 [67] Phan VH, Thambi T, Gil MS, Lee DS. Temperature and pH-sensitive
 2770 injectable hydrogels based on poly(sulfamethazine carbonate urethane) for
 2771 sustained delivery of cationic proteins. *Polymer* 2017;109:38–48.
 2772 <https://doi.org/10.1016/j.polymer.2016.12.039>.
- 2773 [68] Ozel B, Cikrikci S, Aydin O, Oztop MH. Polysaccharide blended whey protein
 2774 isolate-(WPI) hydrogels: A physicochemical and controlled release study. *Food*
 2775 *Hydrocolloids* 2017;71:35–46. <https://doi.org/10.1016/j.foodhyd.2017.04.031>.
- 2776 [69] Khang MK, Zhou J, Huang Y, Hakamivala A, Tang L. Preparation of a novel
 2777 injectable in situ-gelling nanoparticle with applications in controlled protein
 2778 release and cancer cell entrapment. *RSC Adv* 2018;8:34625–33.
 2779 <https://doi.org/10.1039/C8RA06589F>.
- 2780 [70] Wang R, Yang Z, Luo J, Hsing I-M, Sun F. B12-dependent photoresponsive
 2781 protein hydrogels for controlled stem cell/protein release. *PNAS*
 2782 2017;114:5912–7. <https://doi.org/10.1073/pnas.1621350114>.
- 2783 [71] Hettiaratchi MH, Rouse T, Chou C, Krishnan L, Stevens HY, Li M-TA, et al.
 2784 Enhanced in vivo retention of low dose BMP-2 via heparin microparticle
 2785 delivery does not accelerate bone healing in a critically sized femoral defect.
 2786 *Acta Biomaterialia* 2017;59:21–32. <https://doi.org/10.1016/j.actbio.2017.06.028>.
- 2787 [72] Lokhande G, Carrow JK, Thakur T, Xavier JR, Parani M, Bayless KJ, et al.
 2788 Nanoengineered injectable hydrogels for wound healing application. *Acta*
 2789 *Biomaterialia* 2018;70:35–47. <https://doi.org/10.1016/j.actbio.2018.01.045>.
- 2790 [73] Wongkanya R, Chuysinuan P, Pengsuk C, Techasakul S, Lirdprapamongkol K,
 2791 Svasti J, et al. Electrospinning of alginate/soy protein isolated nanofibers and
 2792 their release characteristics for biomedical applications. *Journal of Science:*
 2793 *Advanced Materials and Devices* 2017;2:309–16.
 2794 <https://doi.org/10.1016/j.jsamd.2017.05.010>.
- 2795 [74] Machado-Paula MM, Corat MAF, Lancellotti M, Mi G, Marciano FR, Vega ML,
 2796 et al. A comparison between electrospinning and rotary-jet spinning to produce
 2797 PCL fibers with low bacteria colonization. *Materials Science and Engineering: C*
 2798 2020;111:110706. <https://doi.org/10.1016/j.msec.2020.110706>.
- 2799 [75] Mohammadi M, Alibolandi M, Abnous K, Salmasi Z, Jaafari MR, Ramezani M.
 2800 Fabrication of hybrid scaffold based on hydroxyapatite-biodegradable
 2801 nanofibers incorporated with liposomal formulation of BMP-2 peptide for bone
 2802 tissue engineering. *Nanomedicine: Nanotechnology, Biology and Medicine*
 2803 2018;14:1987–97. <https://doi.org/10.1016/j.nano.2018.06.001>.
- 2804 [76] Nguyen LH, Gao M, Lin J, Wu W, Wang J, Chew SY. Three-dimensional
 2805 aligned nanofibers-hydrogel scaffold for controlled non-viral drug/gene delivery
 2806 to direct axon regeneration in spinal cord injury treatment. *Scientific Reports*
 2807 2017;7:1–12. <https://doi.org/10.1038/srep42212>.
- 2808 [77] Jha BS, Colello RJ, Bowman JR, Sell SA, Lee KD, Bigbee JW, et al. Two pole
 2809 air gap electrospinning: Fabrication of highly aligned, three-dimensional
 2810 scaffolds for nerve reconstruction. *Acta Biomaterialia* 2011;7:203–15.
 2811 <https://doi.org/10.1016/j.actbio.2010.08.004>.
- 2812 [78] Wang J, Windbergs M. Controlled dual drug release by coaxial electrospun
 2813 fibers – Impact of the core fluid on drug encapsulation and release.

- 2814 International Journal of Pharmaceutics 2019;556:363–71.
2815 <https://doi.org/10.1016/j.ijpharm.2018.12.026>.
- 2816 [79] Wen P, Wen Y, Huang X, Zong M-H, Wu H. Preparation and Characterization
2817 of Protein-Loaded Electrospun Fiber Mat and Its Release Kinetics. *J Agric Food*
2818 *Chem* 2017;65:4786–96. <https://doi.org/10.1021/acs.jafc.7b01830>.
- 2819 [80] Wang M, Zhou Y, Shi D, Chang R, Zhang J, Keidar M, et al. Cold atmospheric
2820 plasma (CAP)-modified and bioactive protein-loaded core–shell nanofibers for
2821 bone tissue engineering applications. *Biomater Sci* 2019;7:2430–9.
2822 <https://doi.org/10.1039/C8BM01284A>.
- 2823 [81] Aragón J, Salerno S, De Bartolo L, Irusta S, Mendoza G. Polymeric electrospun
2824 scaffolds for bone morphogenetic protein 2 delivery in bone tissue engineering.
2825 *Journal of Colloid and Interface Science* 2018;531:126–37.
2826 <https://doi.org/10.1016/j.jcis.2018.07.029>.
- 2827 [82] Ahn S, Chantre CO, Gannon AR, Lind JU, Campbell PH, Grevesse T, et al.
2828 Soy Protein/Cellulose Nanofiber Scaffolds Mimicking Skin Extracellular Matrix
2829 for Enhanced Wound Healing. *Advanced Healthcare Materials*
2830 2018;7:1701175. <https://doi.org/10.1002/adhm.201701175>.
- 2831 [83] Straeten A vander, Bratek-Skicki A, Germain L, D’Haese C, Eloy P, Fustin C-A,
2832 et al. Protein–polyelectrolyte complexes to improve the biological activity of
2833 proteins in layer-by-layer assemblies. *Nanoscale* 2017;9:17186–92.
2834 <https://doi.org/10.1039/C7NR04345G>.
- 2835 [84] vander Straeten A, Dupont-Gillain C. Self-Reorganizing Multilayer to Release
2836 Free Proteins from Self-Assemblies. *Langmuir* 2020;36:972–8.
2837 <https://doi.org/10.1021/acs.langmuir.9b03547>.
- 2838 [85] Cho Y, Hong J. Sustained release of therapeutic proteins from multilayers
2839 adsorbed on the sidewalls of porous membranes. *Colloids and Surfaces A:*
2840 *Physicochemical and Engineering Aspects* 2019;562:296–303.
2841 <https://doi.org/10.1016/j.colsurfa.2018.11.010>.
- 2842 [86] Park S, Choi D, Jeong H, Heo J, Hong J. Drug Loading and Release Behavior
2843 Depending on the Induced Porosity of Chitosan/Cellulose Multilayer Nanofilms.
2844 *Mol Pharmaceutics* 2017;14:3322–30.
2845 <https://doi.org/10.1021/acs.molpharmaceut.7b00371>.
- 2846 [87] Zhao Y-N, Xu X, Wen N, Song R, Meng Q, Guan Y, et al. A Drug Carrier for
2847 Sustained Zero-Order Release of Peptide Therapeutics. *Scientific Reports*
2848 2017;7:1–9. <https://doi.org/10.1038/s41598-017-05898-6>.
- 2849 [88] He Y, Hong C, Li J, Howard MT, Li Y, Turvey ME, et al. Synthetic Charge-
2850 Invertible Polymer for Rapid and Complete Implantation of Layer-by-Layer
2851 Microneedle Drug Films for Enhanced Transdermal Vaccination. *ACS Nano*
2852 2018;12:10272–80. <https://doi.org/10.1021/acs.nano.8b05373>.
- 2853 [89] Choi M, Choi D, Han U, Hong J. Inkjet-based multilayered growth factor-
2854 releasing nanofilms for enhancing proliferation of mesenchymal stem cells in
2855 vitro. *Journal of Industrial and Engineering Chemistry* 2017;50:36–40.
2856 <https://doi.org/10.1016/j.jiec.2017.02.014>.
- 2857 [90] Ageitos JM, Pulgar A, Csaba N, Garcia-Fuentes M. Study of nanostructured
2858 fibroin/dextran matrixes for controlled protein release. *European Polymer*
2859 *Journal* 2019;114:197–205. <https://doi.org/10.1016/j.eurpolymj.2019.02.028>.
- 2860 [91] Batista P, Castro P, Madureira AR, Sarmiento B, Pintado M. Development and
2861 Characterization of Chitosan Microparticles-in-Films for Buccal Delivery of
2862 Bioactive Peptides. *Pharmaceutics* 2019;12:32.
2863 <https://doi.org/10.3390/ph12010032>.

- 2864 [92] Uz M, Sharma AD, Adhikari P, Sakaguchi DS, Mallapragada SK. Development
2865 of multifunctional films for peripheral nerve regeneration. *Acta Biomaterialia*
2866 2017;56:141–52. <https://doi.org/10.1016/j.actbio.2016.09.039>.
- 2867 [93] Seong K-Y, Seo M-S, Hwang DY, O’Cearbhaill ED, Sreenan S, Karp JM, et al.
2868 A self-adherent, bullet-shaped microneedle patch for controlled transdermal
2869 delivery of insulin. *Journal of Controlled Release* 2017;265:48–56.
2870 <https://doi.org/10.1016/j.jconrel.2017.03.041>.
- 2871 [94] Liu D, Yu B, Jiang G, Yu W, Zhang Y, Xu B. Fabrication of composite
2872 microneedles integrated with insulin-loaded CaCO₃ microparticles and PVP for
2873 transdermal delivery in diabetic rats. *Materials Science and Engineering: C*
2874 2018;90:180–8. <https://doi.org/10.1016/j.msec.2018.04.055>.
- 2875 [95] Tong Z, Zhou J, Zhong J, Tang Q, Lei Z, Luo H, et al. Glucose- and H₂O₂-
2876 Responsive Polymeric Vesicles Integrated with Microneedle Patches for
2877 Glucose-Sensitive Transcutaneous Delivery of Insulin in Diabetic Rats. *ACS*
2878 *Appl Mater Interfaces* 2018;10:20014–24.
2879 <https://doi.org/10.1021/acsami.8b04484>.
- 2880 [96] Zhang Z, Liu C, Yang C, Wu Y, Yu F, Chen Y, et al. Aptamer-Patterned
2881 Hydrogel Films for Spatiotemporally Programmable Capture and Release of
2882 Multiple Proteins. *ACS Appl Mater Interfaces* 2018;10:8546–54.
2883 <https://doi.org/10.1021/acsami.8b00191>.
- 2884 [97] Qi H, Cao J, Xin Y, Mao X, Xie D, Luo J, et al. Dual responsive zein hydrogel
2885 membrane with selective protein adsorption and sustained release property.
2886 *Materials Science and Engineering: C* 2017;70:347–56.
2887 <https://doi.org/10.1016/j.msec.2016.09.010>.
- 2888 [98] Cacicedo ML, Islan GA, Drachemberg MF, Alvarez VA, Bartel LC, Bolzán AD,
2889 et al. Hybrid bacterial cellulose–pectin films for delivery of bioactive molecules.
2890 *New J Chem* 2018;42:7457–67. <https://doi.org/10.1039/C7NJ03973E>.
- 2891 [99] Economidou SN, Pere CPP, Reid A, Uddin MJ, Windmill JFC, Lamprou DA, et
2892 al. 3D printed microneedle patches using stereolithography (SLA) for
2893 intradermal insulin delivery. *Materials Science and Engineering: C*
2894 2019;102:743–55. <https://doi.org/10.1016/j.msec.2019.04.063>.
- 2895 [100] M. Czekanska E, Geng J, Glinka M, White K, Kanczler J, D Evans N, et al.
2896 Combinatorial delivery of bioactive molecules by a nanoparticle-decorated and
2897 functionalized biodegradable scaffold. *Journal of Materials Chemistry B*
2898 2018;6:4437–45. <https://doi.org/10.1039/C8TB00474A>.
- 2899 [101] Marciello M, Rossi S, Caramella C, Remuñán-López C. Freeze-dried cylinders
2900 carrying chitosan nanoparticles for vaginal peptide delivery. *Carbohydrate*
2901 *Polymers* 2017;170:43–51. <https://doi.org/10.1016/j.carbpol.2017.04.051>.
- 2902 [102] Cho TH, Kim IS, Lee B, Park S-N, Ko J-H, Hwang SJ. Early and Marked
2903 Enhancement of New Bone Quality by Alendronate-Loaded Collagen Sponge
2904 Combined with Bone Morphogenetic Protein-2 at High Dose: A Long-Term
2905 Study in Calvarial Defects in a Rat Model. *Tissue Engineering Part A*
2906 2017;23:1343–60. <https://doi.org/10.1089/ten.tea.2016.0557>.
- 2907 [103] Cai Y, Tong S, Zhang R, Zhu T, Wang X. In vitro evaluation of a bone
2908 morphogenetic protein- 2 nanometer hydroxyapatite collagen scaffold for bone
2909 regeneration. *Molecular Medicine Reports* 2018;17:5830–6.
2910 <https://doi.org/10.3892/mmr.2018.8579>.
- 2911 [104] Hu Y, Ran J, Zheng Z, Jin Z, Chen X, Yin Z, et al. Exogenous stromal derived
2912 factor-1 releasing silk scaffold combined with intra-articular injection of

- 2913 progenitor cells promotes bone-ligament-bone regeneration. *Acta Biomaterialia*
 2914 2018;71:168–83. <https://doi.org/10.1016/j.actbio.2018.02.019>.
- 2915 [105] Li X, Liu Y, Zhang J, You R, Qu J, Li M. Functionalized silk fibroin dressing with
 2916 topical bioactive insulin release for accelerated chronic wound healing.
 2917 *Materials Science and Engineering: C* 2017;72:394–404.
 2918 <https://doi.org/10.1016/j.msec.2016.11.085>.
- 2919 [106] Wang B, Guo Y, Chen X, Zeng C, Hu Q, Yin W, et al. Nanoparticle-modified
 2920 chitosan-agarose-gelatin scaffold for sustained release of SDF-1 and BMP-2.
 2921 *Int J Nanomedicine* 2018;13:7395–408. <https://doi.org/10.2147/IJN.S180859>.
- 2922 [107] Azizian S, Hadjizadeh A, Niknejad H. Chitosan-gelatin porous scaffold
 2923 incorporated with Chitosan nanoparticles for growth factor delivery in tissue
 2924 engineering. *Carbohydrate Polymers* 2018;202:315–22.
 2925 <https://doi.org/10.1016/j.carbpol.2018.07.023>.
- 2926 [108] Wang B, Lv X, Chen S, Li Z, Yao J, Peng X, et al. Use of heparinized bacterial
 2927 cellulose based scaffold for improving angiogenesis in tissue regeneration.
 2928 *Carbohydrate Polymers* 2018;181:948–56.
 2929 <https://doi.org/10.1016/j.carbpol.2017.11.055>.
- 2930 [109] Yao Q, Liu Y, Selvaratnam B, Koodali RT, Sun H. Mesoporous silicate
 2931 nanoparticles/3D nanofibrous scaffold-mediated dual-drug delivery for bone
 2932 tissue engineering. *Journal of Controlled Release* 2018;279:69–78.
 2933 <https://doi.org/10.1016/j.jconrel.2018.04.011>.
- 2934 [110] Bastami F, Paknejad Z, Jafari M, Salehi M, Rezai Rad M, Khojasteh A.
 2935 Fabrication of a three-dimensional β -tricalcium-phosphate/gelatin containing
 2936 chitosan-based nanoparticles for sustained release of bone morphogenetic
 2937 protein-2: Implication for bone tissue engineering. *Materials Science and*
 2938 *Engineering: C* 2017;72:481–91. <https://doi.org/10.1016/j.msec.2016.10.084>.
- 2939 [111] Cheng C-H, Chen Y-W, Kai-Xing Lee A, Yao C-H, Shie M-Y. Development of
 2940 mussel-inspired 3D-printed poly (lactic acid) scaffold grafted with bone
 2941 morphogenetic protein-2 for stimulating osteogenesis. *J Mater Sci: Mater Med*
 2942 2019;30:78. <https://doi.org/10.1007/s10856-019-6279-x>.
- 2943 [112] Huang K-H, Lin Y-H, Shie M-Y, Lin C-P. Effects of bone morphogenic protein-2
 2944 loaded on the 3D-printed MesoCS scaffolds. *Journal of the Formosan Medical*
 2945 *Association* 2018;117:879–87. <https://doi.org/10.1016/j.jfma.2018.07.010>.
- 2946 [113] Lee J, Kim G. Calcium-Deficient Hydroxyapatite/Collagen/Platelet-Rich Plasma
 2947 Scaffold with Controlled Release Function for Hard Tissue Regeneration. *ACS*
 2948 *Biomater Sci Eng* 2018;4:278–89.
 2949 <https://doi.org/10.1021/acsbiomaterials.7b00640>.
- 2950 [114] Unagolla JM, Jayasuriya AC. Drug transport mechanisms and in vitro release
 2951 kinetics of vancomycin encapsulated chitosan-alginate polyelectrolyte
 2952 microparticles as a controlled drug delivery system. *European Journal of*
 2953 *Pharmaceutical Sciences* 2018;114:199–209.
 2954 <https://doi.org/10.1016/j.ejps.2017.12.012>.
- 2955 [115] Maciel VBV, Yoshida CMP, Pereira SMSS, Goycoolea FM, Franco TT.
 2956 Electrostatic Self-Assembled Chitosan-Pectin Nano- and Microparticles for
 2957 Insulin Delivery. *Molecules* 2017;22:1707.
 2958 <https://doi.org/10.3390/molecules22101707>.
- 2959 [116] Ling K, Wu H, Neish AS, Champion JA. Alginate/chitosan microparticles for
 2960 gastric passage and intestinal release of therapeutic protein nanoparticles.
 2961 *Journal of Controlled Release* 2019;295:174–86.
 2962 <https://doi.org/10.1016/j.jconrel.2018.12.017>.

- 2963 [117] Wu D-Y, Ma Y, Hou X-S, Zhang W-J, Wang P, Chen H, et al. Co-delivery of
 2964 antineoplastic and protein drugs by chitosan nanocapsules for a collaborative
 2965 tumor treatment. *Carbohydrate Polymers* 2017;157:1470–8.
 2966 <https://doi.org/10.1016/j.carbpol.2016.11.027>.
- 2967 [118] Zhang Y, Chi C, Huang X, Zou Q, Li X, Chen L. Starch-based nanocapsules
 2968 fabricated through layer-by-layer assembly for oral delivery of protein to lower
 2969 gastrointestinal tract. *Carbohydrate Polymers* 2017;171:242–51.
 2970 <https://doi.org/10.1016/j.carbpol.2017.04.090>.
- 2971 [119] Chen W, Tian R, Xu C, Yung BC, Wang G, Liu Y, et al. Microneedle-array
 2972 patches loaded with dual mineralized protein/peptide particles for type 2
 2973 diabetes therapy. *Nature Communications* 2017;8:1–11.
 2974 <https://doi.org/10.1038/s41467-017-01764-1>.
- 2975 [120] Mumcuoglu D, de Miguel L, Jekhmane S, Siverino C, Nickel J, Mueller TD, et
 2976 al. Collagen I derived recombinant protein microspheres as novel delivery
 2977 vehicles for bone morphogenetic protein-2. *Materials Science and Engineering:
 2978 C* 2018;84:271–80. <https://doi.org/10.1016/j.msec.2017.11.031>.
- 2979 [121] Ménard M, Meyer F, Affolter-Zbaraszczuk C, Rabineau M, Adam A, Ramirez
 2980 PD, et al. Design of hybrid protein-coated magnetic core-mesoporous silica
 2981 shell nanocomposites for MRI and drug release assessed in a 3D tumor cell
 2982 model. *Nanotechnology* 2019;30:174001. <https://doi.org/10.1088/1361-6528/aafe1c>.
- 2984 [122] He H, Chen Y, Li Y, Song Z, Zhong Y, Zhu R, et al. Effective and Selective
 2985 Anti-Cancer Protein Delivery via All-Functions-in-One Nanocarriers Coupled
 2986 with Visible Light-Responsive, Reversible Protein Engineering. *Advanced
 2987 Functional Materials* 2018;28:1706710.
 2988 <https://doi.org/10.1002/adfm.201706710>.
- 2989 [123] Haine AT, Koga Y, Hashimoto Y, Higashi T, Motoyama K, Arima H, et al.
 2990 Enhancement of transdermal protein delivery by photothermal effect of gold
 2991 nanorods coated on polysaccharide-based hydrogel. *European Journal of
 2992 Pharmaceutics and Biopharmaceutics* 2017;119:91–5.
 2993 <https://doi.org/10.1016/j.ejpb.2017.06.005>.
- 2994 [124] Tuncaboylu DC, Friess F, Wischke C, Lendlein A. A multifunctional
 2995 multimaterial system for on-demand protein release. *Journal of Controlled
 2996 Release* 2018;284:240–7. <https://doi.org/10.1016/j.jconrel.2018.06.022>.
- 2997 [125] Mertz D, Sandre O, Bégin-Colin S. Drug releasing nanoplatforms activated by
 2998 alternating magnetic fields. *Biochimica et Biophysica Acta (BBA) - General
 2999 Subjects* 2017;1861:1617–41. <https://doi.org/10.1016/j.bbagen.2017.02.025>.
- 3000 [126] Zhang Y, Tong C, Ma Z, Lu L, Fu H, Pan S, et al. A self-powered delivery
 3001 substrate boosts active enzyme delivery in response to human movements.
 3002 *Nanoscale* 2019;11:14372–82. <https://doi.org/10.1039/C9NR04673A>.
- 3003 [127] Xu C, Wei Z, Gao H, Bai Y, Liu H, Yang H, et al. Bioinspired Mechano-
 3004 Sensitive Macroporous Ceramic Sponge for Logical Drug and Cell Delivery.
 3005 *Advanced Science* 2017;4:1600410. <https://doi.org/10.1002/advs.201600410>.
- 3006 [128] Mertz D, Vogt C, Hemmerlé J, Debry C, Voegel J-C, Schaaf P, et al. Tailored
 3007 design of mechanically sensitive biocatalytic assemblies based on
 3008 polyelectrolyte multilayers. *J Mater Chem* 2011;21:8324–31.
 3009 <https://doi.org/10.1039/C0JM03496G>.
- 3010 [129] Mertz D, Vogt C, Hemmerlé J, Mutterer J, Ball V, Voegel J-C, et al.
 3011 Mechanotransductive surfaces for reversible biocatalysis activation. *Nature
 3012 Materials* 2009;8:731–5. <https://doi.org/10.1038/nmat2504>.

- 3013 [130] Aitken A, Learmonth MP. Protein Determination by UV Absorption. The Protein
3014 Protocols Handbook, Humana Press, Totowa, NJ; 2009, p. 3–6.
3015 https://doi.org/10.1007/978-1-59745-198-7_1.
- 3016 [131] Bradford MM. A rapid and sensitive method for the quantitation of microgram
3017 quantities of protein utilizing the principle of protein-dye binding. *Analytical*
3018 *Biochemistry* 1976;72:248–54. [https://doi.org/10.1016/0003-2697\(76\)90527-3](https://doi.org/10.1016/0003-2697(76)90527-3).
- 3019 [132] Kruger NJ. The Bradford Method For Protein Quantitation. In: Walker JM,
3020 editor. The Protein Protocols Handbook, Totowa, NJ: Humana Press; 2009, p.
3021 17–24. https://doi.org/10.1007/978-1-59745-198-7_4.
- 3022 [133] Brady PN, Macnaughtan MA. Evaluation of Colorimetric Assays for Analyzing
3023 Reductively Methylated Proteins: Biases and Mechanistic Insights. *Anal*
3024 *Biochem* 2015;491:43–51. <https://doi.org/10.1016/j.ab.2015.08.027>.
- 3025 [134] Smith PK, Krohn RI, Hermanson GT, Mallia AK, Gartner FH, Provenzano MD,
3026 et al. Measurement of protein using bicinchoninic acid. *Analytical Biochemistry*
3027 1985;150:76–85. [https://doi.org/10.1016/0003-2697\(85\)90442-7](https://doi.org/10.1016/0003-2697(85)90442-7).
- 3028 [135] Walker JM. The Bicinchoninic Acid (BCA) Assay for Protein Quantitation. In:
3029 Walker JM, editor. The Protein Protocols Handbook, Totowa, NJ: Humana
3030 Press; 2009, p. 11–5. https://doi.org/10.1007/978-1-59745-198-7_3.
- 3031 [136] Wang X, Li Y, Li Q, Neufeld CI, Pouli D, Sun S, et al. Hyaluronic acid
3032 modification of RNase A and its intracellular delivery using lipid-like
3033 nanoparticles. *Journal of Controlled Release* 2017;263:39–45.
3034 <https://doi.org/10.1016/j.jconrel.2017.01.037>.
- 3035 [137] Cao Q, He Z, Sun WQ, Fan G, Zhao J, Bao N, et al. Improvement of calcium
3036 phosphate scaffold osteogenesis in vitro via combination of glutamate-modified
3037 BMP-2 peptides. *Materials Science and Engineering: C* 2019;96:412–8.
3038 <https://doi.org/10.1016/j.msec.2018.11.048>.
- 3039 [138] Kim B-S, Yang S-S, Kim CS. Incorporation of BMP-2 nanoparticles on the
3040 surface of a 3D-printed hydroxyapatite scaffold using an ϵ -polycaprolactone
3041 polymer emulsion coating method for bone tissue engineering. *Colloids and*
3042 *Surfaces B: Biointerfaces* 2018;170:421–9.
3043 <https://doi.org/10.1016/j.colsurfb.2018.06.043>.
- 3044 [139] Gobeaux F, Bizeau J, Samson F, Marichal L, Grillo I, Wien F, et al. Albumin-
3045 driven disassembly of lipidic nanoparticles: the specific case of the squalene-
3046 adenosine nanodrug. *Nanoscale* 2020;12:2793–809.
3047 <https://doi.org/10.1039/C9NR06485K>.
- 3048 [140] Bhakuni V, Gupta CM. Interactions of tuftsin with bovine serum albumin. *FEBS*
3049 *Letters* 1986;205:347–50. [https://doi.org/10.1016/0014-5793\(86\)80926-7](https://doi.org/10.1016/0014-5793(86)80926-7).
- 3050 [141] Tian J, Liu J, Hu Z, Chen X. Interaction of wogonin with bovine serum albumin.
3051 *Bioorganic & Medicinal Chemistry* 2005;13:4124–9.
3052 <https://doi.org/10.1016/j.bmc.2005.02.065>.
- 3053 [142] Jahanban-Esfahlan A, Panahi-Azar V. Interaction of glutathione with bovine
3054 serum albumin: Spectroscopy and molecular docking. *Food Chemistry*
3055 2016;202:426–31. <https://doi.org/10.1016/j.foodchem.2016.02.026>.
- 3056 [143] Qu Y, Wei T, Zhan W, Hu C, Cao L, Yu Q, et al. A reusable supramolecular
3057 platform for the specific capture and release of proteins and bacteria. *J Mater*
3058 *Chem B* 2017;5:444–53. <https://doi.org/10.1039/C6TB02821G>.
- 3059 [144] Steele AN, Cai L, Truong VN, Edwards BB, Goldstone AB, Eskandari A, et al. A
3060 novel protein-engineered hepatocyte growth factor analog released via a shear-
3061 thinning injectable hydrogel enhances post-infarction ventricular function.

3062 Biotechnology and Bioengineering 2017;114:2379–89.
3063 <https://doi.org/10.1002/bit.26345>.

3064 [145] Jiang T, Shen S, Wang T, Li M, He B, Mo R. A Substrate-Selective Enzyme-
3065 Catalysis Assembly Strategy for Oligopeptide Hydrogel-Assisted Combinatorial
3066 Protein Delivery. *Nano Lett* 2017;17:7447–54.
3067 <https://doi.org/10.1021/acs.nanolett.7b03371>.

3068 [146] Udenfriend S, Stein S, Böhlen P, Dairman W, Leimgruber W, Weigele M.
3069 Fluorescamine: A Reagent for Assay of Amino Acids, Peptides, Proteins, and
3070 Primary Amines in the Picomole Range. *Science* 1972;178:871–2.
3071 <https://doi.org/10.1126/science.178.4063.871>.

3072 [147] fluorescamine , Chemical Structures , Manuals & Protocols | Thermo Fisher
3073 Scientific n.d.
3074 <https://www.thermofisher.com/search/results?query=fluorescamine&persona=D>
3075 [ocSupport&navId=4294959583%2B4294959596&refinementAction=true&focus](https://www.thermofisher.com/search/results?query=fluorescamine&persona=D)
3076 [area=Rechercher](https://www.thermofisher.com/search/results?query=fluorescamine&persona=D) (accessed June 8, 2020).

3077 [148] Engvall E, Perlmann P. Enzyme-linked immunosorbent assay (ELISA)
3078 quantitative assay of immunoglobulin G. *Immunochemistry* 1971;8:871–4.
3079 [https://doi.org/10.1016/0019-2791\(71\)90454-X](https://doi.org/10.1016/0019-2791(71)90454-X).

3080 [149] Systems in ELISA. *Methods Mol Biol* 2009;516:9–42.
3081 https://doi.org/10.1007/978-1-60327-254-4_2.

3082 [150] Overview of ELISA - FR n.d. [https://www.thermofisher.com/fr/fr/home/life-](https://www.thermofisher.com/fr/fr/home/life-science/protein-biology/protein-biology-learning-center/protein-biology-resource-library/pierce-protein-methods/overview-elisa.html)
3083 [science/protein-biology/protein-biology-learning-center/protein-biology-](https://www.thermofisher.com/fr/fr/home/life-science/protein-biology/protein-biology-learning-center/protein-biology-resource-library/pierce-protein-methods/overview-elisa.html)
3084 [resource-library/pierce-protein-methods/overview-elisa.html](https://www.thermofisher.com/fr/fr/home/life-science/protein-biology/protein-biology-learning-center/protein-biology-resource-library/pierce-protein-methods/overview-elisa.html) (accessed June 9,
3085 2020).

3086 [151] Raina DB, Larsson D, Mrkonjic F, Isaksson H, Kumar A, Lidgren L, et al.
3087 Gelatin- hydroxyapatite- calcium sulphate based biomaterial for long term
3088 sustained delivery of bone morphogenic protein-2 and zoledronic acid for
3089 increased bone formation: In-vitro and in-vivo carrier properties. *Journal of*
3090 *Controlled Release* 2018;272:83–96.
3091 <https://doi.org/10.1016/j.jconrel.2018.01.006>.

3092 [152] Kuttappan S, Mathew D, Jo J, Tanaka R, Menon D, Ishimoto T, et al. Dual
3093 release of growth factor from nanocomposite fibrous scaffold promotes
3094 vascularisation and bone regeneration in rat critical sized calvarial defect. *Acta*
3095 *Biomaterialia* 2018;78:36–47. <https://doi.org/10.1016/j.actbio.2018.07.050>.

3096 [153] Farris E, Brown DM, Ramer-Tait AE, Pannier AK. Chitosan-zein nano-in-
3097 microparticles capable of mediating in vivo transgene expression following oral
3098 delivery. *Journal of Controlled Release* 2017;249:150–61.
3099 <https://doi.org/10.1016/j.jconrel.2017.01.035>.

3100 [154] da Silva TN, Gonçalves RP, Rocha CL, Archanjo BS, Barboza CAG, Pierre
3101 MBR, et al. Controlling burst effect with PLA/PVA coaxial electrospun scaffolds
3102 loaded with BMP-2 for bone guided regeneration. *Materials Science and*
3103 *Engineering: C* 2019;97:602–12. <https://doi.org/10.1016/j.msec.2018.12.020>.

3104 [155] Castro PM, Baptista P, Madureira AR, Sarmiento B, Pintado ME. Combination
3105 of PLGA nanoparticles with mucoadhesive guar-gum films for buccal delivery of
3106 antihypertensive peptide. *International Journal of Pharmaceutics*
3107 2018;547:593–601. <https://doi.org/10.1016/j.ijpharm.2018.05.051>.

3108 [156] Cui W, Liu Q, Yang L, Wang K, Sun T, Ji Y, et al. Sustained Delivery of BMP-2-
3109 Related Peptide from the True Bone Ceramics/Hollow Mesoporous Silica
3110 Nanoparticles Scaffold for Bone Tissue Regeneration. *ACS Biomater Sci Eng*
3111 2018;4:211–21. <https://doi.org/10.1021/acsbiomaterials.7b00506>.

- 3112 [157] Qi Q, Lu L, Li H, Yuan Z, Chen G, Lin M, et al. Spatiotemporal delivery of
3113 nanoformulated liraglutide for cardiac regeneration after myocardial infarction.
3114 *Int J Nanomedicine* 2017;12:4835–48. <https://doi.org/10.2147/IJN.S132064>.
- 3115 [158] Unzueta U, Cespedes MV, Sala R, Alamo P, Sánchez-Chardi A, Pesarrodonna
3116 M, et al. Release of targeted protein nanoparticles from functional bacterial
3117 amyloids: A death star-like approach. *Journal of Controlled Release*
3118 2018;279:29–39. <https://doi.org/10.1016/j.jconrel.2018.04.004>.
- 3119 [159] Díaz-Herráez P, Saludas L, Pascual-Gil S, Simón-Yarza T, Abizanda G,
3120 Prósper F, et al. Transplantation of adipose-derived stem cells combined with
3121 neuregulin-microparticles promotes efficient cardiac repair in a rat myocardial
3122 infarction model. *Journal of Controlled Release* 2017;249:23–31.
3123 <https://doi.org/10.1016/j.jconrel.2017.01.026>.
- 3124 [160] Duong HTT, Yin Y, Thambi T, Nguyen TL, Giang Phan VH, Lee MS, et al.
3125 Smart vaccine delivery based on microneedle arrays decorated with ultra-pH-
3126 responsive copolymers for cancer immunotherapy. *Biomaterials* 2018;185:13–
3127 24. <https://doi.org/10.1016/j.biomaterials.2018.09.008>.
- 3128 [161] Liu G, Li L, Huo D, Li Y, Wu Y, Zeng L, et al. A VEGF delivery system targeting
3129 MI improves angiogenesis and cardiac function based on the tropism of MSCs
3130 and layer-by-layer self-assembly. *Biomaterials* 2017;127:117–31.
3131 <https://doi.org/10.1016/j.biomaterials.2017.03.001>.
- 3132 [162] Xia B, Lv Y. Dual-delivery of VEGF and NGF by emulsion electrospun
3133 nanofibrous scaffold for peripheral nerve regeneration. *Materials Science and*
3134 *Engineering: C* 2018;82:253–64. <https://doi.org/10.1016/j.msec.2017.08.030>.
- 3135 [163] Lee MS, Ahmad T, Lee J, Awada HK, Wang Y, Kim K, et al. Dual delivery of
3136 growth factors with coacervate-coated poly(lactic-co-glycolic acid) nanofiber
3137 improves neovascularization in a mouse skin flap model. *Biomaterials*
3138 2017;124:65–77. <https://doi.org/10.1016/j.biomaterials.2017.01.036>.
- 3139 [164] Marvin M. Microscopy apparatus. US3013467A, 1961.
- 3140 [165] Aji Alex MR, Nehate C, Veerananarayanan S, Kumar DS, Kulshreshtha R, Koul V.
3141 Self assembled dual responsive micelles stabilized with protein for co-delivery
3142 of drug and siRNA in cancer therapy. *Biomaterials* 2017;133:94–106.
3143 <https://doi.org/10.1016/j.biomaterials.2017.04.022>.
- 3144 [166] Dutta D, Fauer C, Hickey K, Salifu M, Stabenfeldt SE. Tunable delayed
3145 controlled release profile from layered polymeric microparticles. *J Mater Chem*
3146 *B* 2017;5:4487–98. <https://doi.org/10.1039/C7TB00138J>.
- 3147 [167] Quinlan E, López-Noriega A, Thompson EM, Hibbitts A, Cryan SA, O'Brien FJ.
3148 Controlled release of vascular endothelial growth factor from spray-dried
3149 alginate microparticles in collagen–hydroxyapatite scaffolds for promoting
3150 vascularization and bone repair. *Journal of Tissue Engineering and*
3151 *Regenerative Medicine* 2017;11:1097–109. <https://doi.org/10.1002/term.2013>.
- 3152 [168] Kelly SM, Jess TJ, Price NC. How to study proteins by circular dichroism.
3153 *Biochimica et Biophysica Acta (BBA) - Proteins and Proteomics*
3154 2005;1751:119–39. <https://doi.org/10.1016/j.bbapap.2005.06.005>.
- 3155 [169] Patel S, Ryals RC, Weller KK, Pennesi ME, Sahay G. Lipid nanoparticles for
3156 delivery of messenger RNA to the back of the eye. *Journal of Controlled*
3157 *Release* 2019;303:91–100. <https://doi.org/10.1016/j.jconrel.2019.04.015>.
- 3158 [170] Wang A, Yang T, Fan W, Yang Y, Zhu Q, Guo S, et al. Protein Corona
3159 Liposomes Achieve Efficient Oral Insulin Delivery by Overcoming Mucus and
3160 Epithelial Barriers. *Advanced Healthcare Materials* 2019;8:1801123.
3161 <https://doi.org/10.1002/adhm.201801123>.

- 3162 [171] Yu JR, Janssen M, Liang BJ, Huang H-C, Fisher JP. A liposome/gelatin
3163 methacrylate nanocomposite hydrogel system for delivery of stromal cell-
3164 derived factor-1 α and stimulation of cell migration. *Acta Biomaterialia*
3165 2020;108:67–76. <https://doi.org/10.1016/j.actbio.2020.03.015>.
- 3166 [172] Chatzikleanthous D, Schmidt ST, Buffi G, Paciello I, Cunliffe R, Carboni F, et
3167 al. Design of a novel vaccine nanotechnology-based delivery system
3168 comprising CpGODN-protein conjugate anchored to liposomes. *Journal of*
3169 *Controlled Release* 2020;323:125–37.
3170 <https://doi.org/10.1016/j.jconrel.2020.04.001>.
- 3171 [173] Colombani T, Peuziat P, Dallet L, Haudebourg T, Mével M, Berchel M, et al.
3172 Self-assembling complexes between binary mixtures of lipids with different
3173 linkers and nucleic acids promote universal mRNA, DNA and siRNA delivery.
3174 *Journal of Controlled Release* 2017;249:131–42.
3175 <https://doi.org/10.1016/j.jconrel.2017.01.041>.
- 3176 [174] Costa P, Sousa Lobo JM. Modeling and comparison of dissolution profiles.
3177 *European Journal of Pharmaceutical Sciences* 2001;13:123–33.
3178 [https://doi.org/10.1016/S0928-0987\(01\)00095-1](https://doi.org/10.1016/S0928-0987(01)00095-1).
- 3179 [175] Korsmeyer RW, Gurny R, Doelker E, Buri P, Peppas NA. Mechanisms of solute
3180 release from porous hydrophilic polymers. *International Journal of*
3181 *Pharmaceutics* 1983;15:25–35. [https://doi.org/10.1016/0378-5173\(83\)90064-9](https://doi.org/10.1016/0378-5173(83)90064-9).
- 3182 [176] Alfrey T, Gurnee EF, Lloyd WG. Diffusion in glassy polymers. *Journal of*
3183 *Polymer Science Part C: Polymer Symposia* 1966;12:249–61.
3184 <https://doi.org/10.1002/polc.5070120119>.
- 3185 [177] Kosmidis K, Rinaki E, Argyrakis P, Macheras P. Analysis of Case II drug
3186 transport with radial and axial release from cylinders. *International Journal of*
3187 *Pharmaceutics* 2003;254:183–8. [https://doi.org/10.1016/S0378-](https://doi.org/10.1016/S0378-5173(03)00030-9)
3188 [5173\(03\)00030-9](https://doi.org/10.1016/S0378-5173(03)00030-9).
- 3189 [178] Ritger PL, Peppas NA. A simple equation for description of solute release I.
3190 Fickian and non-fickian release from non-swellable devices in the form of slabs,
3191 spheres, cylinders or discs. *Journal of Controlled Release* 1987;5:23–36.
3192 [https://doi.org/10.1016/0168-3659\(87\)90034-4](https://doi.org/10.1016/0168-3659(87)90034-4).
- 3193 [179] Ritger PL, Peppas NA. A simple equation for description of solute release II.
3194 Fickian and anomalous release from swellable devices. *Journal of Controlled*
3195 *Release* 1987;5:37–42. [https://doi.org/10.1016/0168-3659\(87\)90035-6](https://doi.org/10.1016/0168-3659(87)90035-6).
- 3196 [180] Peppas NA, Sahlin JJ. A simple equation for the description of solute release.
3197 III. Coupling of diffusion and relaxation. *International Journal of Pharmaceutics*
3198 1989;57:169–72. [https://doi.org/10.1016/0378-5173\(89\)90306-2](https://doi.org/10.1016/0378-5173(89)90306-2).
- 3199 [181] Matoušek J. Ribonucleases and their antitumor activity. *Comparative*
3200 *Biochemistry and Physiology Part C: Toxicology & Pharmacology*
3201 2001;129:175–91. [https://doi.org/10.1016/S1532-0456\(01\)90202-9](https://doi.org/10.1016/S1532-0456(01)90202-9).
- 3202 [182] Fan W, Xia D, Zhu Q, Li X, He S, Zhu C, et al. Functional nanoparticles exploit
3203 the bile acid pathway to overcome multiple barriers of the intestinal epithelium
3204 for oral insulin delivery. *Biomaterials* 2018;151:13–23.
3205 <https://doi.org/10.1016/j.biomaterials.2017.10.022>.
- 3206 [183] Cross LM, Carrow JK, Ding X, Singh KA, Gaharwar AK. Sustained and
3207 Prolonged Delivery of Protein Therapeutics from Two-Dimensional
3208 Nanosilicates. *ACS Appl Mater Interfaces* 2019;11:6741–50.
3209 <https://doi.org/10.1021/acsami.8b17733>.
- 3210 [184] Porter AG, Jänicke RU. Emerging roles of caspase-3 in apoptosis. *Cell Death*
3211 *Differ* 1999;6:99–104. <https://doi.org/10.1038/sj.cdd.4400476>.

- 3212 [185] Santhosh KT, Alizadeh A, Karimi-Abdolrezaee S. Design and optimization of
3213 PLGA microparticles for controlled and local delivery of Neuregulin-1 in
3214 traumatic spinal cord injury. *Journal of Controlled Release* 2017;261:147–62.
3215 <https://doi.org/10.1016/j.jconrel.2017.06.030>.
- 3216 [186] Fakhoury M. Microglia and Astrocytes in Alzheimer’s Disease: Implications for
3217 Therapy. *Curr Neuropharmacol* 2018;16:508–18.
3218 <https://doi.org/10.2174/1570159X15666170720095240>.
- 3219 [187] Zeng W, Liu Z, Li Y, Zhu S, Ma J, Li W, et al. Development and
3220 characterization of cores–shell poly(lactide-co-glycolide)-chitosan
3221 microparticles for sustained release of GDNF. *Colloids and Surfaces B:
3222 Biointerfaces* 2017;159:791–9. <https://doi.org/10.1016/j.colsurfb.2017.08.052>.
- 3223 [188] Rosini R, Rinaudo CD, Soriani M, Lauer P, Mora M, Maione D, et al.
3224 Identification of novel genomic islands coding for antigenic pilus-like structures
3225 in *Streptococcus agalactiae*. *Molecular Microbiology* 2006;61:126–41.
3226 <https://doi.org/10.1111/j.1365-2958.2006.05225.x>.
- 3227 [189] Wei B, Wang C, Yan C, Tang B, Yu X, Zhang H, et al. Osteoprotegerin/bone
3228 morphogenetic protein 2 combining with collagen sponges on tendon-bone
3229 healing in rabbits. *J Bone Miner Metab* 2020. <https://doi.org/10.1007/s00774-019-01078-w>.
- 3230
3231 [190] Fujioka-Kobayashi M, Schaller B, Saulacic N, Pippenger BE, Zhang Y, Miron
3232 RJ. Absorbable collagen sponges loaded with recombinant bone
3233 morphogenetic protein 9 induces greater osteoblast differentiation when
3234 compared to bone morphogenetic protein 2. *Clinical and Experimental Dental
3235 Research* 2017;3:32–40. <https://doi.org/10.1002/cre2.55>.
- 3236 [191] Lin D, Chai Y, Ma Y, Duan B, Yuan Y, Liu C. Rapid initiation of guided bone
3237 regeneration driven by spatiotemporal delivery of IL-8 and BMP-2 from
3238 hierarchical MBG-based scaffold. *Biomaterials* 2019;196:122–37.
3239 <https://doi.org/10.1016/j.biomaterials.2017.11.011>.
- 3240 [192] Hettiaratchi MH, Chou C, Servies N, Smeekens JM, Cheng A, Esancy C, et al.
3241 Competitive Protein Binding Influences Heparin-Based Modulation of Spatial
3242 Growth Factor Delivery for Bone Regeneration. *Tissue Engineering Part A*
3243 2017;23:683–95. <https://doi.org/10.1089/ten.tea.2016.0507>.
- 3244 [193] Xue D, Zhang W, Chen E, Gao X, Liu L, Ye C, et al. Local delivery of HMGB1
3245 in gelatin sponge scaffolds combined with mesenchymal stem cell sheets to
3246 accelerate fracture healing. *Oncotarget* 2017;8:42098–115.
3247 <https://doi.org/10.18632/oncotarget.16887>.
- 3248 [194] Whitehead TJ, Avila COC, Sundararaghavan HG. Combining growth factor
3249 releasing microspheres within aligned nanofibers enhances neurite outgrowth.
3250 *Journal of Biomedical Materials Research Part A* 2018;106:17–25.
3251 <https://doi.org/10.1002/jbm.a.36204>.
- 3252 [195] Awada HK, Long DW, Wang Z, Hwang MP, Kim K, Wang Y. A single injection
3253 of protein-loaded coacervate-gel significantly improves cardiac function post
3254 infarction. *Biomaterials* 2017;125:65–80.
3255 <https://doi.org/10.1016/j.biomaterials.2017.02.020>.
- 3256 [196] Bhattarai DP, Kim MH, Park H, Park WH, Kim BS, Kim CS. Coaxially fabricated
3257 polylactic acid electrospun nanofibrous scaffold for sequential release of
3258 tauroursodeoxycholic acid and bone morphogenetic protein2 to stimulate
3259 angiogenesis and bone regeneration. *Chemical Engineering Journal*
3260 2020;389:123470. <https://doi.org/10.1016/j.cej.2019.123470>.

- 3261 [197] Cheng G, Yin C, Tu H, Jiang S, Wang Q, Zhou X, et al. Controlled Co-delivery
3262 of Growth Factors through Layer-by-Layer Assembly of Core–Shell Nanofibers
3263 for Improving Bone Regeneration. *ACS Nano* 2019;13:6372–82.
3264 <https://doi.org/10.1021/acsnano.8b06032>.
- 3265 [198] Krishnan L, Priddy LB, Esancy C, Klosterhoff BS, Stevens HY, Tran L, et al.
3266 Delivery vehicle effects on bone regeneration and heterotopic ossification
3267 induced by high dose BMP-2. *Acta Biomaterialia* 2017;49:101–12.
3268 <https://doi.org/10.1016/j.actbio.2016.12.012>.
- 3269 [199] Huber E, Pobloth A-M, Bormann N, Kolarczik N, Schmidt-Bleek K, Schell H, et
3270 al. Demineralized Bone Matrix as a Carrier for Bone Morphogenetic Protein-2:
3271 Burst Release Combined with Long-Term Binding and Osteoinductive Activity
3272 Evaluated In Vitro and In Vivo. *Tissue Engineering Part A* 2017;23:1321–30.
3273 <https://doi.org/10.1089/ten.tea.2017.0005>.
- 3274 [200] Enezei HH, Ahmad A, Takeuchi K, Suzuki J, Khamis MF, Razak NHA, et al.
3275 Osteoinductive Activity of Bone Scaffold Bioceramic Companied with Control
3276 Release of VEGF Protein Treated Dental stem cells as A New Concept for
3277 Bone Regeneration: Part II. *Journal of Hard Tissue Biology* 2018;27:69–78.
3278 <https://doi.org/10.2485/jhtb.27.69>.
- 3279 [201] Qu D, Zhu JP, Childs HR, Lu HH. Nanofiber-based transforming growth factor-
3280 β 3 release induces fibrochondrogenic differentiation of stem cells. *Acta*
3281 *Biomaterialia* 2019;93:111–22. <https://doi.org/10.1016/j.actbio.2019.03.019>.
- 3282 [202] Sydow S, Cassan D de, Hänsch R, R. Gengenbach T, D. Easton C, Thissen H,
3283 et al. Layer-by-layer deposition of chitosan nanoparticles as drug-release
3284 coatings for PCL nanofibers. *Biomaterials Science* 2019;7:233–46.
3285 <https://doi.org/10.1039/C8BM00657A>.
- 3286 [203] Wang J, Sun B, Tian L, He X, Gao Q, Wu T, et al. Evaluation of the potential of
3287 rhTGF- β 3 encapsulated P(LLA-CL)/collagen nanofibers for tracheal cartilage
3288 regeneration using mesenchymal stems cells derived from Wharton’s jelly of
3289 human umbilical cord. *Materials Science and Engineering: C* 2017;70:637–45.
3290 <https://doi.org/10.1016/j.msec.2016.09.044>.
- 3291 [204] Henry N, Clouet J, Visage CL, Weiss P, Gautron E, Renard D, et al. Silica
3292 nanofibers as a new drug delivery system: a study of the protein–silica
3293 interactions. *J Mater Chem B* 2017;5:2908–20.
3294 <https://doi.org/10.1039/C7TB00332C>.
- 3295 [205] Tapeinos C, Larrañaga A, Tomatis F, Bizeau J, Marino A, Battaglini M, et al.
3296 Advanced Functional Materials and Cell-Based Therapies for the Treatment of
3297 Ischemic Stroke and Postischemic Stroke Effects. *Advanced Functional*
3298 *Materials* 2020;30:1906283. <https://doi.org/10.1002/adfm.201906283>.
- 3299 [206] Bruggeman KF, Wang Y, Maclean FL, Parish CL, Williams RJ, Nisbet DR.
3300 Temporally controlled growth factor delivery from a self-assembling peptide
3301 hydrogel and electrospun nanofibre composite scaffold. *Nanoscale*
3302 2017;9:13661–9. <https://doi.org/10.1039/C7NR05004F>.
- 3303 [207] Sivak WN, White JD, Bliley JM, Tien LW, Liao HT, Kaplan DL, et al. Delivery of
3304 chondroitinase ABC and glial cell line-derived neurotrophic factor from silk
3305 fibroin conduits enhances peripheral nerve regeneration. *Journal of Tissue*
3306 *Engineering and Regenerative Medicine* 2017;11:733–42.
3307 <https://doi.org/10.1002/term.1970>.
- 3308 [208] O’Neill HS, O’Sullivan J, Porteous N, Ruiz-Hernandez E, Kelly HM, O’Brien FJ,
3309 et al. A collagen cardiac patch incorporating alginate microparticles permits the
3310 controlled release of hepatocyte growth factor and insulin-like growth factor-1 to

- 3311 enhance cardiac stem cell migration and proliferation. *Journal of Tissue*
 3312 *Engineering and Regenerative Medicine* 2018;12:e384–94.
 3313 <https://doi.org/10.1002/term.2392>.
- 3314 [209] Fleischer S, Shapira A, Feiner R, Dvir T. Modular assembly of thick
 3315 multifunctional cardiac patches. *PNAS* 2017;114:1898–903.
 3316 <https://doi.org/10.1073/pnas.1615728114>.
- 3317 [210] Liu JMH, Zhang X, Joe S, Luo X, Shea LD. Evaluation of biomaterial scaffold
 3318 delivery of IL-33 as a localized immunomodulatory agent to support cell
 3319 transplantation in adipose tissue. *Journal of Immunology and Regenerative*
 3320 *Medicine* 2018;1:1–12. <https://doi.org/10.1016/j.regen.2018.01.003>.
- 3321 [211] Lancina MG, Shankar RK, Yang H. Chitosan nanofibers for transbuccal insulin
 3322 delivery. *Journal of Biomedical Materials Research Part A* 2017;105:1252–9.
 3323 <https://doi.org/10.1002/jbm.a.35984>.
- 3324 [212] Zigdon-Giladi H, Khutaba A, Elimelech R, Machtei EE, Srouji S. VEGF release
 3325 from a polymeric nanofiber scaffold for improved angiogenesis. *Journal of*
 3326 *Biomedical Materials Research Part A* 2017;105:2712–21.
 3327 <https://doi.org/10.1002/jbm.a.36127>.
- 3328 [213] Piran M, Vakilian S, Piran M, Mohammadi-Sangcheshmeh A, Hosseinzadeh S,
 3329 Ardeshiryajimi A. In vitro fibroblast migration by sustained release of PDGF-BB
 3330 loaded in chitosan nanoparticles incorporated in electrospun nanofibers for
 3331 wound dressing applications. *Artificial Cells, Nanomedicine, and Biotechnology*
 3332 2018;46:511–20. <https://doi.org/10.1080/21691401.2018.1430698>.
- 3333 [214] Mandapalli PK, Labala S, Jose A, Bhatnagar S, Janupally R, Sriram D, et al.
 3334 Layer-by-Layer Thin Films for Co-Delivery of TGF- β siRNA and Epidermal
 3335 Growth Factor to Improve Excisional Wound Healing. *AAPS PharmSciTech*
 3336 2017;18:809–20. <https://doi.org/10.1208/s12249-016-0571-6>.
- 3337 [215] Tellier LE, Treviño EA, Brimeyer AL, Reece DS, Willett NJ, Guldberg RE, et al.
 3338 Intra-articular TSG-6 delivery from heparin-based microparticles reduces
 3339 cartilage damage in a rat model of osteoarthritis. *Biomater Sci* 2018;6:1159–67.
 3340 <https://doi.org/10.1039/C8BM00010G>.
- 3341 [216] Cheng G, Ma X, Li J, Cheng Y, Cao Y, Wang Z, et al. Incorporating platelet-rich
 3342 plasma into coaxial electrospun nanofibers for bone tissue engineering.
 3343 *International Journal of Pharmaceutics* 2018;547:656–66.
 3344 <https://doi.org/10.1016/j.ijpharm.2018.06.020>.
- 3345 [217] Anitua E, Pino A, Troya M, Jaén P, Orive G. A novel personalized 3D injectable
 3346 protein scaffold for regenerative medicine. *J Mater Sci: Mater Med* 2017;29:7.
 3347 <https://doi.org/10.1007/s10856-017-6012-6>.
- 3348 [218] Waters R, Alam P, Pacelli S, Chakravarti AR, Ahmed RPH, Paul A. Stem cell-
 3349 inspired secretome-rich injectable hydrogel to repair injured cardiac tissue. *Acta*
 3350 *Biomaterialia* 2018;69:95–106. <https://doi.org/10.1016/j.actbio.2017.12.025>.
- 3351 [219] Pignatelli C, Perotto G, Nardini M, Cancedda R, Mastrogiacomo M,
 3352 Athanassiou A. Electrospun silk fibroin fibers for storage and controlled release
 3353 of human platelet lysate. *Acta Biomaterialia* 2018;73:365–76.
 3354 <https://doi.org/10.1016/j.actbio.2018.04.025>.
- 3355 [220] Tansathien K, Suriyaumporn P, Charoenputtakhun P, Ngawhirunpat T,
 3356 Opanasopit P, Rangsimawong W. Development of Sponge Microspicule Cream
 3357 as a Transdermal Delivery System for Protein and Growth Factors from Deer
 3358 Antler Velvet Extract. *Biological and Pharmaceutical Bulletin* 2019;42:1207–15.
 3359 <https://doi.org/10.1248/bpb.b19-00158>.

- 3360 [221] Davoodi P, P. Srinivasan M, Wang C-H. Effective co-delivery of nutlin-3a and
3361 p53 genes via core-shell microparticles for disruption of MDM2-p53 interaction
3362 and reactivation of p53 in hepatocellular carcinoma. *Journal of Materials*
3363 *Chemistry B* 2017;5:5816-34. <https://doi.org/10.1039/C7TB00481H>.
- 3364 [222] Grim JC, Brown TE, Aguado BA, Chapnick DA, Viert AL, Liu X, et al. A
3365 Reversible and Repeatable Thiol-Ene Bioconjugation for Dynamic Patterning
3366 of Signaling Proteins in Hydrogels. *ACS Cent Sci* 2018;4:909-16.
3367 <https://doi.org/10.1021/acscentsci.8b00325>.
- 3368 [223] Zhang C, Zhang T, Jin S, Xue X, Yang X, Gong N, et al. Virus-Inspired Self-
3369 Assembled Nanofibers with Aggregation-Induced Emission for Highly Efficient
3370 and Visible Gene Delivery. *ACS Appl Mater Interfaces* 2017;9:4425-32.
3371 <https://doi.org/10.1021/acsmi.6b11536>.
- 3372 [224] Pinese C, Lin J, Milbreta U, Li M, Wang Y, Leong KW, et al. Sustained delivery
3373 of siRNA/mesoporous silica nanoparticle complexes from nanofiber scaffolds
3374 for long-term gene silencing. *Acta Biomaterialia* 2018;76:164-77.
3375 <https://doi.org/10.1016/j.actbio.2018.05.054>.
- 3376 [225] Tenkumo T, Vanegas Sáenz JR, Nakamura K, Shimizu Y, Sokolova V, Epple
3377 M, et al. Prolonged release of bone morphogenetic protein-2 in vivo by gene
3378 transfection with DNA-functionalized calcium phosphate nanoparticle-loaded
3379 collagen scaffolds. *Materials Science and Engineering: C* 2018;92:172-83.
3380 <https://doi.org/10.1016/j.msec.2018.06.047>.
- 3381 [226] Raftery RM, Mencía-Castaño I, Sperger S, Chen G, Cavanagh B, Feichtinger
3382 GA, et al. Delivery of the improved BMP-2-Advanced plasmid DNA within a
3383 gene-activated scaffold accelerates mesenchymal stem cell osteogenesis and
3384 critical size defect repair. *Journal of Controlled Release* 2018;283:20-31.
3385 <https://doi.org/10.1016/j.jconrel.2018.05.022>.
- 3386 [227] McMillan A, Nguyen MK, Gonzalez-Fernandez T, Ge P, Yu X, Murphy WL, et
3387 al. Dual non-viral gene delivery from microparticles within 3D high-density stem
3388 cell constructs for enhanced bone tissue engineering. *Biomaterials*
3389 2018;161:240-55. <https://doi.org/10.1016/j.biomaterials.2018.01.006>.
- 3390 [228] Rinker TE, Philbrick BD, Hettiaratchi MH, Smalley DM, McDevitt TC, Temenoff
3391 JS. Microparticle-mediated sequestration of cell-secreted proteins to modulate
3392 chondrocytic differentiation. *Acta Biomaterialia* 2018;68:125-36.
3393 <https://doi.org/10.1016/j.actbio.2017.12.038>.
- 3394 [229] Delplace V, Ortin-Martinez A, Tsai ELS, Amin AN, Wallace V, Shoichet MS.
3395 Controlled release strategy designed for intravitreal protein delivery to the
3396 retina. *Journal of Controlled Release* 2019;293:10-20.
3397 <https://doi.org/10.1016/j.jconrel.2018.11.012>.
- 3398 [230] Dai J, Long W, Liang Z, Wen L, Yang F, Chen G. A novel vehicle for local
3399 protein delivery to the inner ear: injectable and biodegradable thermosensitive
3400 hydrogel loaded with PLGA nanoparticles. *Drug Development and Industrial*
3401 *Pharmacy* 2018;44:89-98. <https://doi.org/10.1080/03639045.2017.1373803>.
- 3402
- 3403